SANDIA NATIONAL LABORATORIES
WASTE ISOLATION PILOT PLANT

Recommendation for the Lower Limit of the Waste Shear Strength (Parameter BOREHOLE : TAUFAIL)

Author: Courtney G Herrick (6711)   _Courtney G Herrick_   5/1/07
          Print   Signature   Date

Author: Michael Riggins (6711)   _for Mike Riggins_   5/1/07
          Print   Signature   Date

Author: Byoung Yoon Park   _Y Park_   5/1/07
          Print   Signature   Date

Technical Review: T. William Thompson (CTAC)   _Courtney G Herrick for Bill Thompson_   5/1/07
          Print   Signature   Date

QA Review: Janis Trone (6710)   _(signature)_   5/1/07
          Print   Signature   Date

Management Review: Moo Y. Lee (6711)   _(signature)_   5/1/07
          Print   Signature   Date

WIPP:1.4.2.4:PA:QA-L:545750

Table of Contents

List of Tables

List of Figures

Executive Summary

This paper represents an assessment of the waste shear strength (TAUFAIL) as currently used in the computer program CUTTINGS_S. The current values as given in the performance assessment parameter database are as follows:

Material	Property	Distribution	Range	Description
Borehole	TAUFAIL	Loguniform	0.05 – 77.0 Pascals	Effective shear strength for erosion of waste.

Based on a reevaluation of San Francisco Bay mud, detailed literature review, additional data and analysis, and computer modeling we propose the following changes be made to TAUFAIL in the performance assessment parameter database:

Material	Property	Distribution	Range	Description
Borehole	TAUFAIL	Uniform	1.33 – 77.0 Pascals	Effective shear strength for erosion of waste.

1 Introduction

Waste Isolation Pilot Plant (WIPP) Performance Assessment (PA) scenarios include cases of human intrusion in which a future oil or gas exploratory borehole intersects the waste in the repository. Drilling mud flowing up the borehole will apply shearing stresses to the borehole wall. It is hypothesized that if the shear stresses in the drilling mud exceed the shear strength of the materials located at the borehole wall, erosion will occur and wall material will be eroded away (Berglund 1992). This erosion of the borehole wall is called "cavings." As a result, the borehole diameter may increase locally at the level of the repository. Due to cavings, the volume of waste removed from the repository can actually be larger than the volume of the borehole originally cut through the waste by the drill bit ("cuttings"). As the diameter of the borehole increases, the fluid shear stresses at the outer boundary decrease. If the failure strength of the wall material equals or exceeds the fluid shear stress at the outer boundary of the flow region, then the caving process will stop.

WIPP PA uses the parameter BOREHOLE : TAUFAIL to represent the shear strength of the waste in the numerical code CUTTINGS_S. (see WIPP PA 2004a, 2004b, 2005a, 2005b for a thorough description of the CUTTINGS_S code). It is officially called the "effective shear strength for erosion," but is more commonly known as the "waste shear strength." The parameter is treated as a sampled value in WIPP PA with a log-uniform distribution and range of 0.05 to 77 Pa. This range of values was derived by DOE from literature reviews of erosion of a bay mud and consideration of the mean particle size of WIPP waste as determined by an expert elicitation (Berglund 1996, CTAC 1997). The lower limit of this range of values was chosen to conform to what is hypothesized as an extreme case of degradation of the waste and waste containers.

This paper reexamines the lower limit value of BOREHOLE : TAUFAIL according to the manner outlined in the planning document AP-131, Rev. 0 (Kirkes and Herrick 2006). In Section 2, a brief history of how the lower limit of the waste shear strength was obtained is provided. Section 3 discusses concepts and definitions used in erosion studies of ocean and channel bed sediments. Section 4 revisits the findings of the expert panel on mean particle sizes in WIPP. Section 5 discusses the results of experiments performed on surrogate waste materials. Section 6 discusses the results of erosion tests performed on San Francisco Bay muds for the US Army Corps of Engineers, San Francisco District. In Section 7 we discuss the effects that compression will have on the strength of the waste. In Section 8 we briefly discuss the probability of stuck pipe or gas erosion occurring. Section 9 presents a summary, conclusions, and recommendation for the value of the lower limit of the waste shear strength.

2   *History of the Value of the Lower Limit of TAUFAIL*

J. Berglund performed the first analyses and created the original models for cuttings, cavings, and spalling for the WIPP purposes. This initial work is summarized in Berglund (1992). In that work, Berglund assumed that "In the absence of experimental data, the effective shear strength for erosion of the repository material is assumed to be similar to that of a montmorillonite clay, with an effective shear strength of 1 to 5 Pa (Sargunam et al., 1973)."

The values for the erosional strength of the waste were again examined by Butcher (1994). In his memorandum, he argued that from a mechanical standpoint, the degraded waste would be similar to a clay-sand mixture. Based on literature values, he estimated that the strength of such a mixture would range between 0.1 and 1 Pa, with a median value of 0.5 Pa.

In 1995, Butcher et al. changed the range again based on their literature review. The range of values they used was 0.1 to 10 Pa, with a median of 1 Pa in a constructed distribution.

For the CCA, the DOE assumed a uniform distribution of the waste shear strength with a range of 0.05 to 10 Pa and a median of 5.0 Pa (DOE 1996). Again, these ranges were based on soft bay mud studies. Selection of the values was based on a memorandum from Berglund (1996). The Berglund memorandum simply reports the range of data for an ocean-bay mud (Partheniades and Paaswell 1970) and montmorillonite clay (Sargunam et al. 1973).

The Conceptual Models Peer Review Report of July 1996 (DOE 1996, Appendix Peer, Peer 1, Conceptual Models Peer Review Report (July 1996)) states that they agreed with the assumptions made by the DOE and assessed that the Cuttings/Cavings Model was adequate. In Section 3.13.2.1 of that report concerning validity of model assumptions, they state, "Among the basic assumptions made for the fluid flow calculations is that, in the absence of experimental data, the effective shear resistance to erosion of the repository waste is similar to ocean bay mud or montmorillonite clay. In the absence of accurate waste characterization or knowledge of the form this waste is in as the time of intrusion, this assumption appears appropriate because of the low shear strengths of these substances." Furthermore, in Section 3.13.2.7 the panel states, "The parameters for calculations were checked as presented in the CUTTINGS_S User's Manual and found to be appropriate."

The sensitivity of the Cavings Model to changes in the waste shear strength was studied by the EPA as part of their evaluation for the Performance Assessment Validation Test (PAVT) (Trovato 1997a). They found that the cavings model demonstrated significant sensitivity to the values chosen for TAUFAIL. The lower limit was of particular interest because a weaker material would result in greater cavings releases. As a result, the EPA required the DOE to change its method for estimating the waste shear strength and use an estimation based on particle size distributions instead of analog experimental data as was done for the CCA (Trovato 1997b).

For the PAVT, the waste shear strength was estimated based on particle size distributions determined by an expert elicitation panel. The estimates used the Shield's parameter, which relies on a measure of the central point of a population of particles of different sizes, to determine the critical shear stress for an erodible, cohesionless sediment bed (Simon and Senturk 1992). With this approach, the calculated critical shear strength ranged from 0.64 to 77 Pa (Wang 1997, Wang and Larson 1997). For conservativism, the low value of the low value from the CCA was retained for the PAVT while the high value from the Shield's parameter method was used for the high value of the PAVT (EPA 1998). The decision to use 0.05 Pa for the low value was supported by information that indicated that very fine-grained cohesive materials may not act as a cohesionless soil assumed by the Shield's parameter calculation. The high end of the range was considered appropriate for cohesionless particles and was retained based on the expert elicitation results. A loguniform distribution for the waste was selected for the PAVT to provide equal weighting over the three orders of magnitude in the range.

This range is the current range, 0.05 to 77 Pa, in use in WIPP PA calculations.

3   Erosion of Soft Cohesive Sediments

3.1   Characteristics of Soft Cohesive Sediment Erosion

Mehta et al. (1982) and Parchure and Mehta (1985) discuss the erosional characteristics of soft cohesive sediments. They differentiate between two bed types commonly used in erosion testing of sediments: placed beds and deposited beds. Placed beds are mechanically placed in the flume's sample holder and are considered to be representative of fully consolidated deposits. Deposited beds are those that are emplaced in the flume by the deposition and settling of sediments out of the flow of a current. They are stratified with respect to their properties with depth. Both placed and deposited beds can exhibit two modes of failure. The first, known as "surface erosion," involves particle by particle or aggregate by aggregate entrainment of the surficial sediments. The second, known as "bed erosion," results from shear loading of the bed. In this case the plane of failure is deeper into the bed and erosion takes place by the removal of relatively large pieces of soil. This is the same observation made by Partheniades and Paaswell (1970, p 763) who refer to these two types of erosion as "surface erosion" and "mass erosion."

Resistance to erosion is characterized by the properties of the bed. The erosion or resuspension potential of a bed is dependent of the mode of formation of the bed before its erosion. In a natural environment, the bed forms as a result of deposition and settling. The degree of aggregation in a settling sediment influences the structure of the deposit. Aggregates in a freshly deposited bed are often composed of fluffy, weak units in comparison with settling aggregates.

As consolidation proceeds, the aggregates in layers below the surface are crushed, and comparatively stronger, more tightly packed units result. The bed becomes stratified and the aggregate shear strength and density typically increase monotonically with depth. When consolidation is complete after a period of several days to months (Mehta et al. 1982, Jepsen et al. 1997, Roberts et al. 1998), the shear strength and the density distributions become invariant, and the bed acquires more uniform properties. Placed beds, by virtue of the manner in which they are prepared, are representative of fully consolidated beds.

A common feature of placed beds is that the rate of surface erosion becomes constant or nearly constant after a short initial period of relatively more rapid erosion. The constant rate of erosion under a constant shear stress results because the shear strength of the bed varies little with depth. The erosion rate for deposited beds typically decreases as erosion proceeds, eventually reaching a constant value or even arresting. This resuspension behavior of deposited beds is explained when it is recognized that, by virtue of its manner of formation, the aggregate shear strength of the deposited bed increases measurably with depth due to settling of the sediments and consolidation of the sediments. The upper, surficial layer is soft with a high water content, often in excess of 100%, and low aggregate shear strength. Upon consolidation, the flocs or aggregates breakup and the particles undergo some rearrangement and settling causing the bed density and shear strength to increase with both depth and time. The increase in bulk density is associated with a decrease in porosity and water content.

In their erosion tests on kaolinite and lake mud deposited beds, Parchure and Mehta (1985) found and defined a number of characteristics of the beds that vary with depth and time. (The mud they tested was composed of montmorillonite, illite, kaolinite, and quartz.) Figure 3-1 shows an example of the variation of density, expressed in terms of concentration or weight of sediment solids per volume of sampled water, and shear strength with depth for kaolinite eroded in salt water. As expected from the foregoing discussion, both the density and shear strength increase with depth. They idealized the increase in shear strength with depth in Figure 3-2 in terms of three zones. The value of the shear strength, τ_s, at $z = 0$, τ_{so}, is for incipient motion of the bed. Incipient motion is the threshold condition between erosion and sedimentation of a single particle (Julien 1998). The Shield's Diagram is a nondimensional plot of incipient motion shear stress values. Zone 1 has a thickness z_c that is bounded by τ_{so} at $z = 0$ and τ_{sc} at $z = z_c$. Zone 2 has a thickness z_d and is bounded by τ_{sc} at $z = z_c$ and τ_{sm} at $z = z_c + z_d$. An important difference between Zones 1 and Zone 2 is that the gradient $\delta\tau_s/\delta_z$ is much larger in Zone 1 than that in Zone 2. Below z_d, in Zone 3, the shear strength of the bed is nearly constant, τ_{sm}.
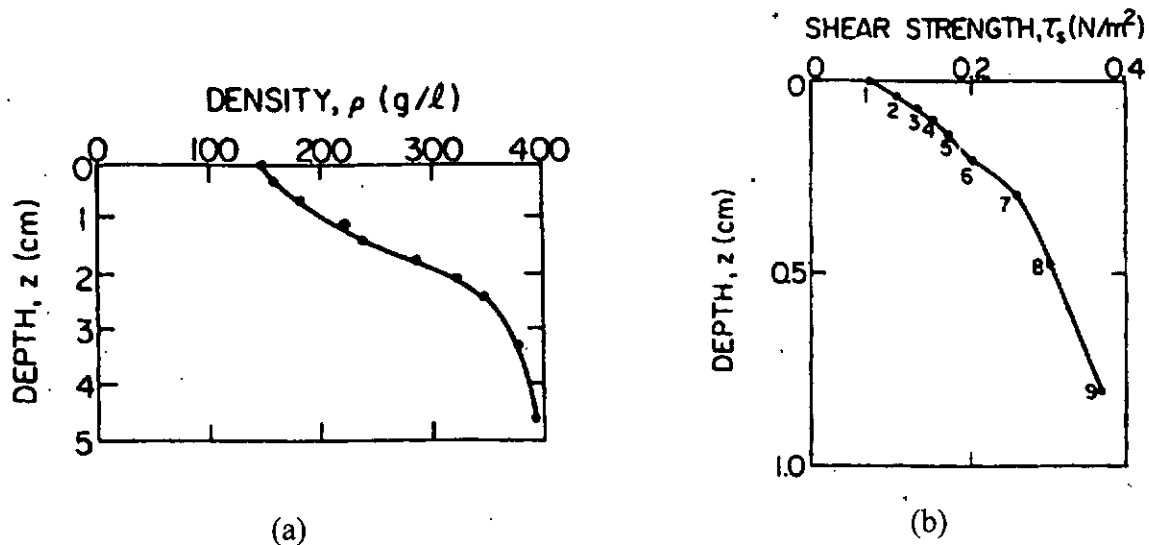
Figure 3-1. Variation of (a) density and (b) shear strength with depth of a kaolinite sediment bed in salt water. (Parchure and Mehta 1985, Figures 3 and 4.)
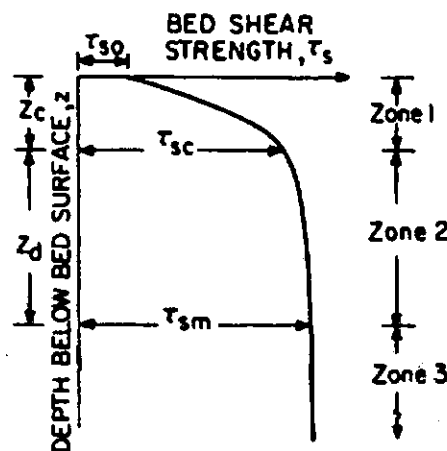
Figure 3-2. Schematic representation of three-zoned description of bed shear strength profile. (Parchure and Mehta 1985, Figure 5.)

Both τ_{so} and τ_{sc} can be estimated from a plot of the sediment concentration in the eroding fluid at the end of each incremental step in the testing process, $C(T)$, versus the bed shear stress, τ_b (Parchure and Mehta 1985); from a plot of suspended mass per unit surface area versus τ_b (Teeter 1987); or from plot of rate of erosion versus τ_b (Teeter 1987). Figure 3-3 shows a plot of $C(T)$ versus τ_b from Parchure and Mehta (1985) for three different consolidation times. It is typically possible to approximate the data by two linear segments. The first segment is extrapolated to intersect the $C(T) = 0$ axis. The point where the line crosses the axis is τ_{so}. The

point at which the two linear segments intersect corresponds to τ_{sc}. For all $\tau_b < \tau_{sc}$, the rate of erosion is low compared to that of $\tau_b > \tau_{sc}$. In most cases, investigators studying erosion of sediments are interested in τ_{so} and/or τ_{sc}, and not τ_{sm}. For instance, see Table 3-1 for the data for Zone 1 from Parchure and Mehta (1985).
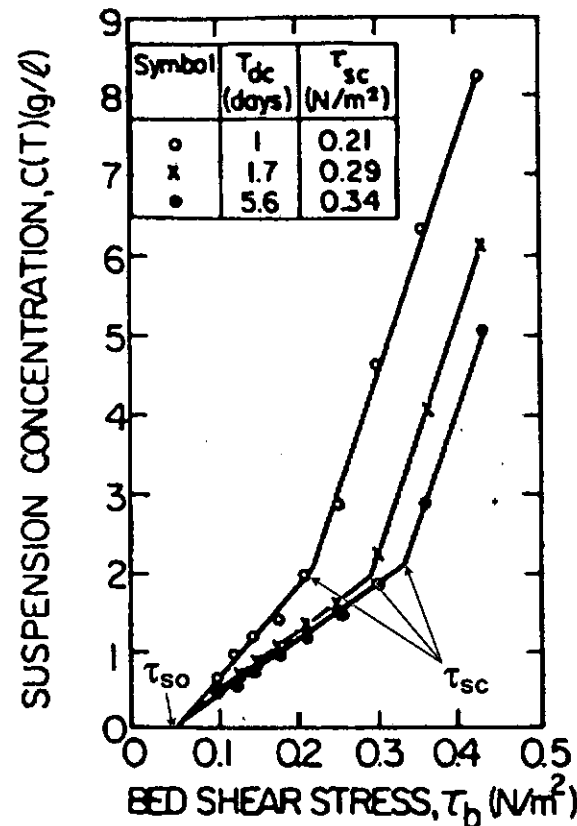
·Figure 3-3. Concentration *C(T)* at the end of each time step versus bed shear stress, τ_b, for a kaolinite sediment bed in salt water. Illustrated are the definitions of bed surface shear strength, τ_{so}, and characteristic shear strength of the bed, τ_{sc}. (Modified from Parchure and Mehta 1985, Figure 6)

A couple of observations can be made regarding the test results in Table 3-1. The first is that the present value of TAUFAIL chosen for San Francisco Bay mud is indeed on the conservative side of the range of values of other muds, but is still within the range typically found. Second, we see that Zone 1 is only a surface effect. It extends to a maximum depth of 0.40 cm (0.16 in). In tests conducted by Villaret and Paulic at the University of Florida on San Francisco Bay muds for the Army Corps of Engineers, the extent of Zone 1 is less than 0.2 cm (Figure 3-4). This is based on an estimate from the figures of that report (Teeter 1987, App. B, Figures 30 and 32) and applying the method described in Parchure and Mehta (1985) which involves iteratively solving

$$\Delta z = \frac{h}{\rho(z)} \Delta C \qquad (3\text{-}1)$$

for each increase in shear stress of the flume. In this equation Δz is the change in depth with each increase, h is the water flow depth in the flume, $\rho(z)$ is the bed dry density at depth z, and ΔC is the change in suspension concentration associated with each increase in shear stress. Again, Zone 1 only represents the shear strength of the top layer of the bed. It is for this reason Villaret and Paulic refer to τ_{so} as "bed surface shear strength" (Teeter 1987, App. B). The value of TAUFAIL = 0.05 Pa, in the present nomenclature is the surface bed shear strength, τ_{so}, as calculated by Partheniades and Paaswell (1970) using their expression. It is the value of incipient particle motion of this surficial layer. Mehta et al (1982) and Parchure and Mehta (1985) conclude that the thickness of Zone 1 is on the order of millimeters in their experiments and that "in moderate tidal environments, such as costal Florida, maximum bed erosion during typical tidal conditions is found to be limited to a few centimeters."

Table 3-1. Properties of Zone 1. (Parchure and Mehta 1985, Table 1).

Series [a]	Salinity (ppt)	T_{dc} (days)	τ_{so} (Pa)	τ_{sc} (Pa)	z_c (cm)	$\overline{\tau}_s$ (Pa)
LM	0.5	1.7	0.08	0.21	0.09	0.16
LM	1	1.7	0.12	0.27	0.07	0.24
LM	2	1.7	0.17	0.33	0.05	0.28
LM [b]	5	1.7	0.17	0.40	0.12	0.34
LM	10	1.7	0.17	0.62	0.17	0.39
KS	35	1.0	0.04	0.21	0.40	0.15
KS	35	1.7	0.04	0.29	0.30	0.22
KS	35	3.0	0.04	0.33	0.32	0.23
KS	35	5.6	0.04	0.34	0.26	0.33
KS	35	10.0	0.04	0.40	0.16	0.37
KT	0	1.0	0.10	0.30	0.16	0.23
KT	0	2.0	0.10	0.30	0.11	0.23
KT	0	3.0	0.10	0.35	0.03	0.26

where:
  T_{dc} is the time the beds were allowed to consolidate
  $\overline{\tau}_s$ is the shear stress averaged over the thickness of Zone 1, z_c

Notes:
  [a] Series defined as: LM – Lake Mud, KS – Kaolinite in Salt water, and KT – Kaolinite in Tap (fresh) water
  [b] Values were approximated due to insufficient data

The value τ_{sc} is called by Mehta et al (1982) and Villaret and Paulic (Teeter 1987, App. B) the "characteristic shear strength" of the bed. It is the shear strength of the bed at the beginning of Zone 2. Laboratory results presented in Partheniades and Paaswell (1970), Mehta et al. (1982), Parchure and Mehta (1985), Teeter (1987), and many other demonstrate that the critical shear stress increases rapidly through Zone 1, but below this layer the rate of increase of the critical shear stress decreases at a much slower rate until becoming almost invariant with depth at a level τ_{sm}. The value τ_{sc} demarks the lower value of that time in which the critical shear stress trends

toward becoming a constant (Figure 3-2). According to Mehta et al. (1982) and Parchure and Mehta (1985) the extent of Zones 1 and 2 is on the order of centimeters, so the extent Zone 2 is relatively quite small.
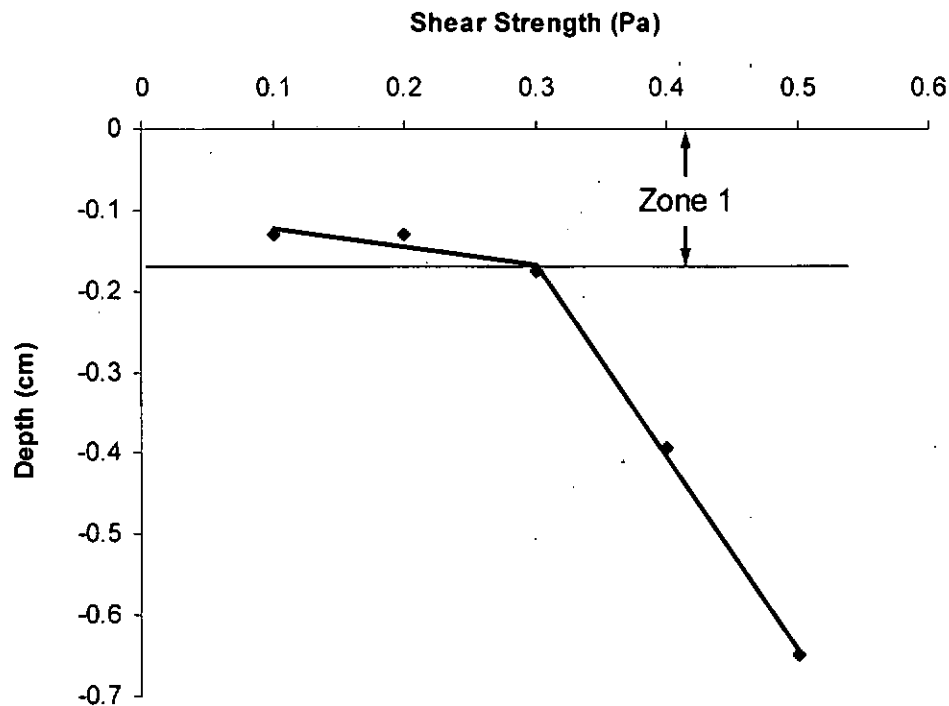
Figure 3-4 Variation of bed shear strength with depth for SF Bay mud (Teeter 1987, App. B, Fig. 32) based on the procedure in Parchure and Mehta (1985). The large initial concentration at the beginning of step one appears to be explained by Mehta et al. (1982) as the rather rapid resuspension of deposited sediment in the return pipe and other parts of the system, so the calculated depth of Zone 1 is probably an overestimate.

3.2 Analysis of Partheniades (1965) Erosion Tests

The experimental work performed by Parthenaides (1962, 1965) formed the bases for the Partheniades and Paaswell (1970) paper. Partheniades conducted erosion and deposition studies on a bed of clay which was referred to as "San Francisco Bay Mud." The mud is described as:

1. Classification: bluish-gray clay, high plasticity with some organics, falls between CH and OH in Unified Soil Classification System, principal mineral is montmorillonite with some illite.

2. Grain size: Clay ($<2\mu$) ~60% by weight, Silt (2μ to 50μ) ~ 40% by weight, and fine sand small amount.

3. Atterburg limits: $w_{ll} = 99\%$, $w_{pl} = 44\%$, and $PI = 55\%$

4. Natural water content: $w_n = 110\%$

5. Natural dry density: 40 lbs/ft^3

6. Shear strength: Remolded laboratory vane ultimate shear strength was 26 lb/ft^2 (0.18 psi). Flocculated shear strength was estimated to be between 1/136 to 1/12 of remolded strength, with an average of not more the 1/100 of the remolded strength or $\sim$ 0.0018 psi.

Two types of test beds were considered. The first type was a 0.1 ft thick bed made of natural material (remolded mud) at the natural moisture content. This type of test bed was used for Series I and II tests. During the Series I tests a deep narrow grove of width b_m developed in the bed which ran the length of the flume. The rest of the test bed remained relatively flat but had a "crust" of possibly coarser grained material. Series II tests involved removing the crust and remolding the bed. In the process the moisture content of the bed increased slightly to 120%. For this Series II tests an erosion pattern similar to the Series I tests also formed, i.e., a narrow groove was formed in the bed that ran the length of the flume. However, a crust was not observed possibly because the flow rates were kept high in an attempt to prevent the deposition of the fine sand. The second type of test bed consisted of the same material used in the first type however the material was put into suspension and then allowed to settle out to create a "flocculated" bed. This test bed was 0.15 ft thick and was used for the Series III tests. It appears that the same erosion pattern as the Series I and II tests developed, however values for the width of the groove were not given.

Table 3-2. Summary of erosion rates from Partheniades (1965, Tables 1, 5, and 6).

Series I Erosion Rates

Run No.	Average Velocity (ft/sec)	Average Shear Stress lbs/ft^2	Average Shear Stress Pa	Estimated Rate of Erosion ((g/ft^2)/hour Initial	Estimated Rate of Erosion ((g/ft^2)/hour Final	Erosion width (b_m in feet)
2	0.80	0.0023	0.110	0.050	0.050	0.550
3	1.34	0.0103	0.492	0.338	0.338	0.550
4	1.13	0.0070	0.334	0.170	0.170	0.550
5	0.95	0.0045	0.215	0.096	0.096	0.550
6	0.80	0.0023	0.110	0.050	0.050	0.550
9	1.48	0.0125	0.538	—	0.720	0.195
10	1.90	0.0195	0.934	1.670	1.670	0.195
11	2.34	0.0278	1.330	2.820	1.670	0.195

Series II Erosion Rates

Run No.	Average Velocity (ft/sec)	Average Shear Stress lbs/ft^2	Average Shear Stress Pa	Rate of Erosion ((g/ft^2)/hour Initial	Rate of Erosion ((g/ft^2)/hour Final	Erosion width (b_m in feet)
22	1.32	0.0100	0.478	0.174	—	0.33
23	2.31	0.0272	1.300	0.674	—	0.33
24	2.80	0.0383	1.880	2.160	—	0.33
25	3.22	0.0592	2.830	6.250	—	0.33

Series III Erosion Rates

Run No.	Average Velocity (ft/sec)	Average Shear Stress lbs/ft^2	Average Shear Stress Pa	Rate of Erosion ((g/ft^2)/hour Initial	Rate of Erosion ((g/ft^2)/hour Final	Erosion width (b_m in feet)
26	0.87	0.0032	0.153	0.165	0.041	—
27	1.07	0.0060	0.286	0.750	0.138	—
28	1.27	0.0091	0.435	0.506	0.506	—
29	1.07	0.0060	0.286	0.156	0.046	—
30	1.27	0.0091	0.435	0.166	0.009	—
31	1.46	0.0120	0.574	—	0.252	—
32	1.46	0.0120	0.574	0.252	0.252	—

The Series I and II test results are reproduced in Figure 3-5. The Series III data, the settled or flocculated bed, were not plotted in the original papers. Subsequent analysis by the present authors showed data scatter.
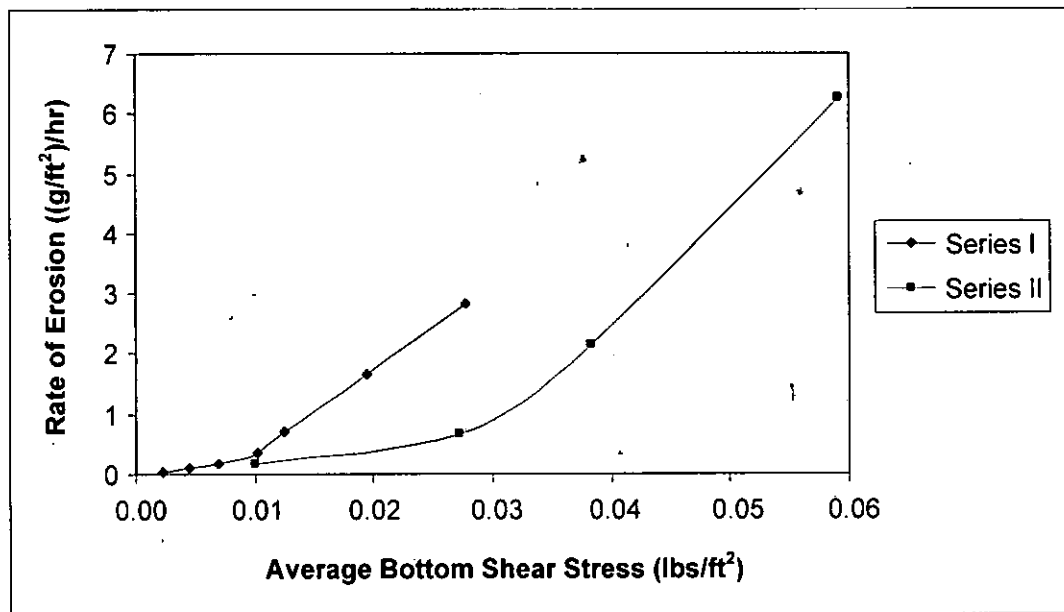
Figure 3-5. Shear stress versus rate of erosion plots for Series I and II tests (Partheniades 1965, Figure 7; Partheniades and Paaswell 1970, Figure 1).

Based on the test data and Figure 3-5, Partheniades (1965) made the following observations:

1. Initiation of scouring was first noticed at a velocity of 0.80 fps (which corresponds to a shear stress of 0.110 Pa) (pg. 112), [the author later states it is estimated to be the range of 0.65 to 0.80 fps. (pg. 122)]

2. There is a critical value of shear stress above which erosion rates increase much more rapidly with τ than below the critical value. For Series I this critical value was 0.010 lb per sq ft (0.48 Pa) and for Series II it was 0.028 lb per sq ft (1.34 Pa) (pg 124)

3. From a comparison of the results of Series I, II, and III it was found that the minimum scouring shear stress for dense and deposited bed were approximately the same and equal to 0.57 dynes per sq cm (0.057 Pa). (pg 127).

The data are plotted as average shear stress as a function of the erosion rates in order to better asses the shear stress parameters as discussed in the previous section. Figure 3-6 and Figure 3-7 represent the Series I and Series II data, respectively. A piecewise linear curve is fit to the data to determine the intercept (bed surface shear strength, τ_{so}) and intersection (characteristic shear strength, τ_{sc}) of the curves. The piecewise linear curve fits give a good representation of the Partheniades data in both figures. Using the above data and plots, a summary of the shear strength parameters are given in Table 3-3. These are compared with Partheniades' (1965) analysis. Differences between the present analysis and Partheniades results from the curve fitting methods used to analyze the data. In the present analysis the data were fit with a piecewise linear curve whereas Partheniades fit his data to a smooth function. Partheniades does not indicate how he chose his values for τ_{so} or τ_{sc}.
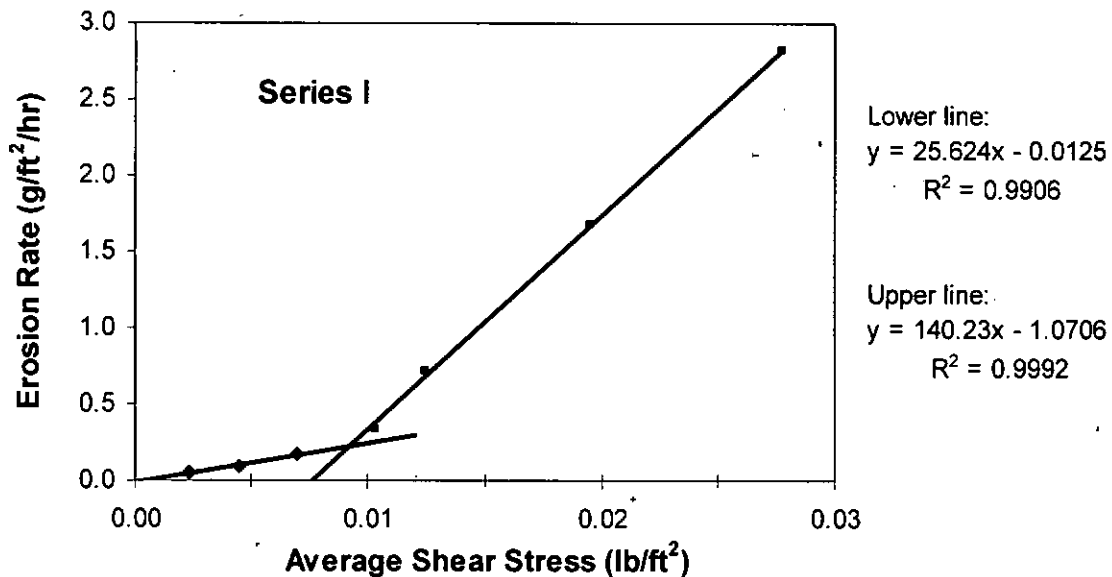
Figure 3-6. Plot of Series I rate of erosion versus average shear stress (data from Partheniades 1965).

Lower line:
y = 25.624x - 0.0125
R^2 = 0.9906

Upper line:
y = 140.23x - 1.0706
R^2 = 0.9992
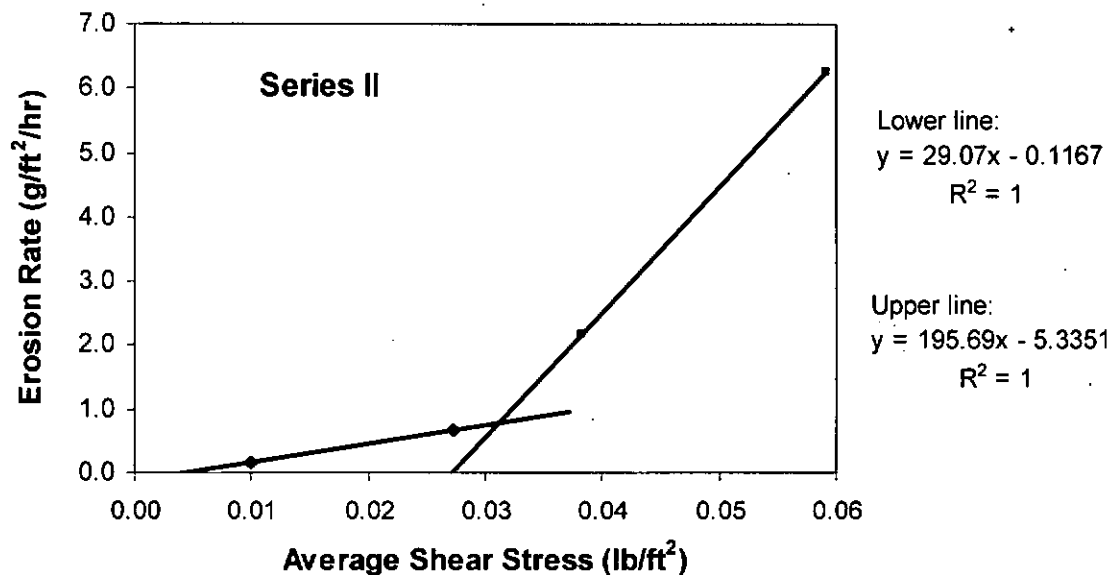
Figure 3-7. Plot of Series II rate of erosion versus average shear stress (data from Partheniades 1965).

Lower line:
y = 29.07x - 0.1167
R^2 = 1

Upper line:
y = 195.69x - 5.3351
R^2 = 1

The results for Series III tests are plotted in Figure 3-8. There is much data scatter in the original results and a linear fit does not represent the data very well (R^2 = 0.03). An improvement to the fit is obtained if the erosion rates are averaged over specified shear stress levels. No discernable "break" is apparent due to the scatter in the data. The results are also presented in Table 3-3.
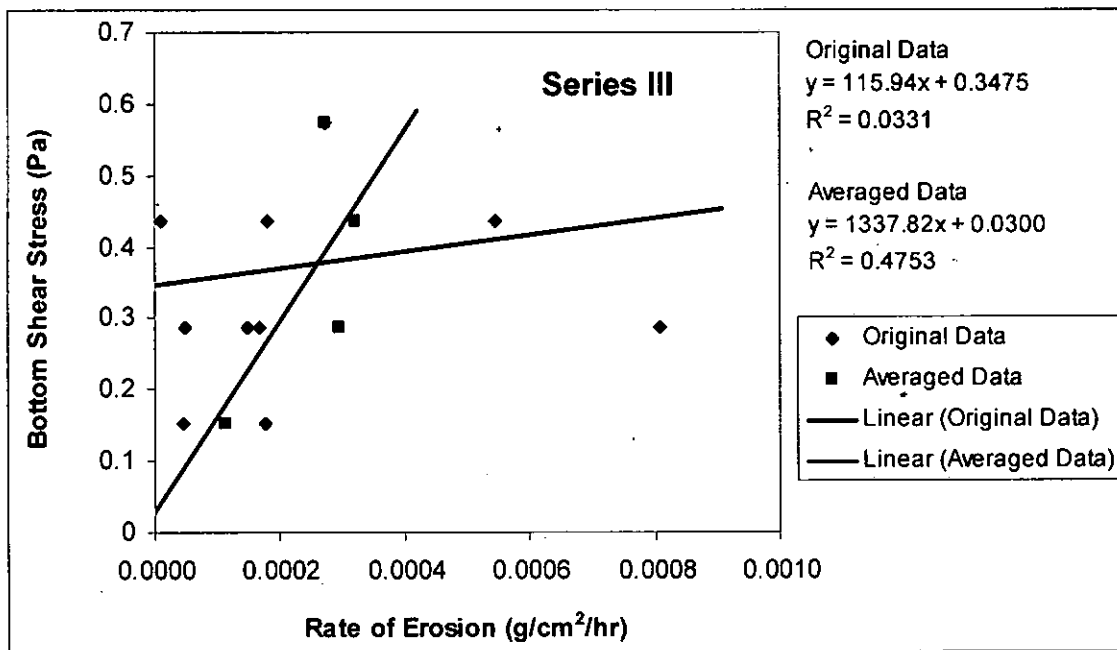
Figure 3-8. Plot of Series III data from Partheniades (1965) for bottom shear stress versus rate of erosion. Original data is shown by dark blue diamonds and average erosion rates at each bottom shear stress level are depicted by violet squares. The above figure does not represent a piecewise linear fit, but two separate linear fits.

Table 3-3. Summary of shear strengths from present analysis and Partheniades (1965).

Series	Bed surface shear strength, τ_{so}		Characteristic shear strength, τ_{sc}	
	Present analysis [Pa]	Partheniades 1965 [Pa]	Present analysis [Pa]	Partheniades 1965 [Pa]
I	0.0234		0.4421	0.4788
II	0.1922		1.4996	1.3405
III – original data	0.3475			
III – averaged data	0.0300			
average	0.1078 [a]	0.057 [b]	0.9708 [a]	0.9097 [a]

Notes
   a. Consists of Series I and II data only.
   b. Partheniades' average includes all three series.

3.3   Operational Critical Shear Stress

Another definition for shear strength is given by Villaret and Paulic (Teeter 1987, App. B). It is the "operational" or "design" critical shear stress for erosion and is designated τ_c. It is determined by extending the second line of a $C(T)$ or rate of erosion versus bed shear strength

plot, if there is one, to the ordinate = 0 axis (see Figure 3-9). If there is no piecewise linear fit, e.g., insufficient data, data scatter, author's preference, etc., then the operational shear strength is the shear stress value at y = 0 of the line fit through all the data.

Many investigators simply ignore or are unable to determine Zone 1 behavior and simply report τ_c or τ_{sc}. As Parthenaides and Paaswell (1970, pg. 761) remark:

> Most of the summarized work had the disadvantage of an arbitrary and subjective criterion for failure. In most cases, this criterion corresponded to a stage of very rapid scouring, i.e., a state of failure.

It can be seen that the value of τ_c is intermediate to τ_{so} and τ_{sc}, e.g., $\tau_{so} < \tau_c < \tau_{sc}$.

Symbol	T_{dc} (days)	τ_{sc} (N/m²)
o	1	0.21
x	1.7	0.29
●	5.6	0.34
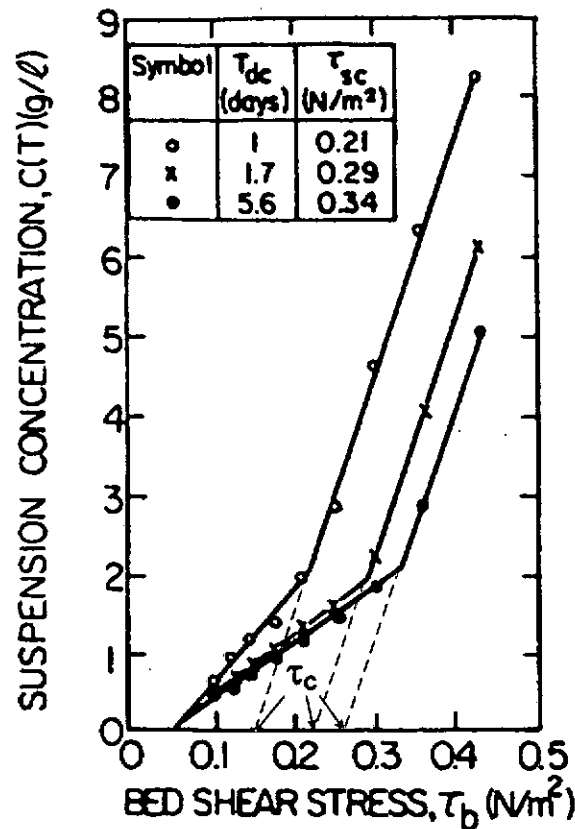
Figure 3-9. Concentration *C(T)* at the end of each time step versus bed shear stress, τ_b, for a kaolinite sediment bed in salt water. Illustrated is the definition of the operational or design shear strength of the bed, τ_c. (Modified from Parchure and Mehta 1985, Figure 6)

3.4   Recommendation for the Waste Shear Strength Value

In light of the above discussion, it is felt that this values τ_c or τ_{sc} are more representative of the shear strength of the waste than τ_{so}. The value τ_{so} is a surface phenomenon and would represent a

flow moving across the top of a sediment bed in a flume experiment or marine environment (Figure 3-10). However, in an intrusion event, drilling would cut down through the mass of degraded waste. The drilling mud would flow up the borehole in a direction perpendicular to the upper surface. The strength of the mass of the degraded waste is better represented by τ_c or τ_{sc}, the strength values of the entire mass. The value of τ_{sc} represents the minimum shear strength of the material in the bed. Theoretically, due to consolidation, the lower layers of the bed of degraded waste reach a maximum value of τ_{sm}, which is very nearly a constant. However, values of τ_{sm} seem to be rarely reported and it is probable that this idea is more applicable to experimental work rather than field conditions where much more pressure and much longer times are available. Therefore, use of τ_c or τ_{sc} as the shear strength of the waste is conservative.

Zone 1
Waste Mass or Zones 2 and 3
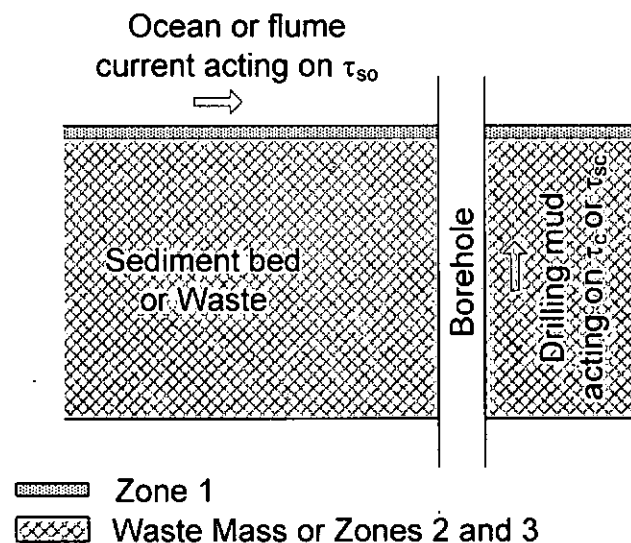
τ_{so} is the sediment bed surface shear strength
τ_c is the waste mass operational shear strength
τ_{sc} is the waste mass characteristic shear strength

Figure 3-10. Schematic of various shear strengths and the direction of the currents acting on them.

This idea of using the bed characteristic shear strength was substantiated in an e-mail from J. Buffington to C. Herrick (Buffington 2007). Dr. Buffington was the first author of a paper which cataloged more than 80 years of incipient motion data (Buffington and Montgomery 1997). In that e-mail Dr. Buffington states:

> However, I'm not sure how useful these data will be to your problem. Seems like you are interested in the shear strength, which is not quite the same as incipient motion from a streambed.

Incipient motion is a term for the beginning of surface erosion, which occurs at τ_{so}. Shear strength in this context refers to the characteristic shear strength of the bed.

4 Review of Analysis Based on Expert Panel's Particle Distribution

In this approach the critical shear stress of the waste (TAUFAIL) is hypothesized to depend on the waste particle size. A waste particle size distribution was constrained based on an expert panel elicitation mandated by the Environmental Protection Agency (EPA) for WIPP PAVT. The waste particle diameter was identified by the EPA as lacking supporting evidence (Trovato 1997a) and requiring derivation through expert judgment in Trovato (1997b). According to the second letter (Trovato 1997b):

> The one parameter remaining (#2, ID# 3246, Material BLOWOUT, Parameter PARTDIA, waste particle diameter in Cuttings Model for direct brine release) is considered "sensitive" but the value for that parameter is not supported by data. Therefore, the parameter value must be derived through "expert judgment" in accordance with EPA's WIPP Compliance Criteria at 40 C.F.R. §194.26 (expert judgment) and 40 C.F.R. §194.22(a)(2)(v) (quality assurance procedures for the implementation of expert judgment elicitation).

Furthermore in Enclosure 2 of that same letter it says:

ID#	Material ID	Parameter ID	Description	Parameter to be Used in Verification Test
2254	BOREHOLE	TAUFAIL	Waste Shear Strength	Dependent on Results of Particle Size Distribution Expert Elicitation. [1]

[1] The values for this parameter are dependent on the results of the expert elicitation for the particle size distribution. Once the particle size is established via the expert elicitation, TAUFAIL should be calculated based on Shields Parameter (see, for example, Simon, D.B. and Senturk, F., 1992, *Sediment Transport Technology: Water and Sediment Dynamics*) as a function of particle diameter.

Based on an analysis of the expert elicitation results (CTAC 1997), the lower limit of the mean particle size of WIPP waste was estimated to be 1 mm, while the upper limit was determined to be either 10 cm assuming no cementation or approaching room size when cementation occurs (Wang 1997). This range was determined by converting the expert elicitation panel's particle size distribution to a volume fraction basis and considering complete waste degradation. For the purposes of calculating the critical shear stress in the waste, Wang and Larson (1997) assumed a range of 1 mm to 10 cm and a minimum mean particle density of 2.5 g/cm^3. The Department of Energy's (DOE) approach was to use the Shield's parameter following the method in Simon and Senturk (1992) as suggested by the EPA (Trovato, 1997b) and as outlined in a facsimile to DOE by T. Peake (1997).

The Shields parameter is a measure of threshold condition between erosion and sedimentation of a single particle. This condition is usually referred to as incipient motion, a term for the beginning of surface erosion. Fluid flow around sediment particles exerts forces that tend to initiate particle motion (τ_{so}). The resisting force of non-cohesive material relates to particle weight. Threshold conditions occur when the hydrodynamic moment of forces acting on a single

particle balances the resisting moment of force. The Shields diagram remains the most widely used criterion for incipient motion of sediment (Coa et al. 2006). The critical value of the Shield's parameter, ψ_c, corresponding to the beginning of motion depends on whether laminar or turbulent flow conditions prevail around the particle. The mean particle sizes averaged on volume fractions were used to calculate the parameter TAUFAIL since the Shields parameter is a dimensionless measure of τ_{so}.

Wang and Larson's Table 2 is reproduced below as Table 4-1. The range of mean particle diameters of interest is 1 mm to 10 cm (Wang, 1997), which yields values for the critical shear stress of WIPP waste as 0.64 Pa for 1 mm particles and 76.52 Pa for 10 cm particles. The DOE chose not to use the lower limit for TAUFAIL and recommended using the CCA value of 0.05 Pa to be conservative and as directed by Kruger (1997). The EPA accepted the lower value of 0.05 Pa "for conservativism" (EPA, 1998).

The particle size distribution as determined by the Expert Panel Elicitation fills one of the gaps mentioned by the Conceptual Model Peer Review (DOE 1996, Appendix Peer, Peer 1, Conceptual Models Peer Review Report (July 1996)) in that it provides knowledge of the future state of the waste.

Table 4-1. Critical shear stress of WIPP waste calculated as a function of waste mean particle diameter (Wang and Larson 1997, Table 2).

Particle diameter d_g (m)	Grain scale Re	Shields parameter ψ_c	TAUFAIL (Pa)
1.00E-04	17	0.033	0.04
1.00E-03	170	0.05	0.64
5.00E-03	850	0.06	3.83
1.00E-02	1700	0.06	7.65
2.00E-02	3400	0.06	15.30
5.00E-02	8500	0.06	38.26
6.00E-02	10200	0.06	45.91
8.00E-02	13600	0.06	61.21
1.00E-01	17000	0.06	76.52
2.00E-01	34000	0.06	153.04

5 Tests on Surrogate Waste Materials

Jepsen et al. (1998b) performed erosional shear testing on a highly degraded surrogate waste samples developed by Hansen et al. (1997). The degraded waste material properties were summarized for the spallings model review panel by Hansen et al (2003). The material was developed in a logical, systematic manner based on consideration of the anticipated future state of the waste considering inventory, evolution of the underground environment, and experimental results. Hansen et al. (1997, 2003) developed their model material from the estimated inventory

of standard waste drums. The surrogate waste comprised a mixture of raw materials including iron, glass, cellulosics, rubber, plastic, solidification cements, soil, and WIPP salt. They considered degradation of each waste constituent. The authors asserted that the degraded waste material properties represented the lowest plausible realm of the future waste state because no strengthening processes were included such as compaction, cementation, mineral precipitation, more durable packaging and compressed waste, and less corrosion. It is believed that the samples used by Jepsen et al. (1998b) represent an unobtainable degraded state and are thus far weaker than any possible future state of the waste (Hansen et al 1997, 2003; Hansen 2005). It is therefore believed that this represents a very conservative approach.

5.1   Analysis of Shear Strengths of Surrogate Waste Material Samples

Jepsen et al. (1998b) performed their tests using an apparatus (Sedflume) developed at the University of California-Santa Barbara. The flume is 120 cm long by 10 cm wide by 2 cm high rectangular duct which is constructed of clear acrylic to allow sample-water interactions to be observed. Integrated into the end of the duct is the 10 cm wide by 15 cm long test section. During the test as the material erodes an operator continuously moves the sample upwards such that the sample-water interface remains level with the bottom of the flume. Erosion rate is recorded as the upward movement as a function of time.

Three types of waste materials were tested. The Chain of Custody (COC) records identifying the types of samples are found in RESPEC's laboratory notebook (Mellegard, 1998).

1. Category I consists of five samples of 50% degraded surrogate material designated B2 thru B6.   .

B1	no COC found but there is a memo from RE/SPEC to UCSB dated 12/03/1997 describing the sample. This sample was not used as it would not fit into the sample holder.
B2 & B3	COC Ref. No. 325/1-98/45, RE/SPEC to UCSB dated 01/23/1998
B4, B5, & B6	COC Ref. No. 325/2-98/34, RE/SPEC to UCSB dated 02/12/1998

2. Category II consists of three samples of 100% degraded surrogate material designated B7 thru B9.

B7, B8, & B9	COC Ref. No. 325/5-98/28, RE/SPEC to UCSB dated 05/15/1998

3. Category III consists of five magnesium oxide (MgO) bricks designated B11 thru B15.

B10, B11, & B12	COC Ref. No. 325/5-98/37, RE/SPEC to UCSB dated 05/19/1998
B13, B14, & B15	COC Ref. No. 325/6-98/5, RE/SPEC to UCSB dated 06/29/1998

   Notes:
   1) Sample B10 description is 100% MgO – Air Dried. Sample B10 was received in a damaged state and was not tested.
   2) Samples B11 thru B15 descriptions are 100% MgO – Brine Saturated.

The Jepsen et al. data of average erosion rates for the calculated shear stresses for the samples tested are given in Table 5-1.

The measurement of critical shear stress for erosion is described in Jepsen, et al. (1998b, pg. 7) as follows:

> A critical shear stress can be quantitatively defined as the shear stress at which a very small, but accurately measurable, rate of erosion occurs. In the present study, this rate of erosion was chosen to be 10^{-4} cm/sec; this represents 1 mm of erosion in approximately 15 minutes. Since it would be difficult to measure all critical shear stresses at exactly 10^{-4} cm/sec, erosion rates were generally measured above and below 10^{-4} cm/sec at shear stress which differ by a factor of two. The critical shear stress was then linearly interpolated to an erosion rate of 10^{-4} cm/sec. This gave results with a 20% accuracy for the critical shear stress. Some of the samples could not be eroded at rates greater than 10^{-4} cm/sec within the range of shear stresses possible. For these samples, the test was run at a particular shear stress for several hours in order to obtain a measurable amount or erosion.

The shear stress was calculated using Prandtl's Universal Law of Friction for a pipe with a smooth wall, namely:

$$\frac{1}{\sqrt{\lambda}} = 2.0 \log\left[\frac{UD\sqrt{\lambda}}{v}\right] - 0.8 \tag{5-1}$$

where λ is the friction factor, U is the mean flow speed (cm/sec), D is the hydraulic radius (cm), and v is the kinematic viscosity (cm^2/sec).

The kinematic viscosity, v, is defined as η/ρ, where η is the dynamic viscosity (g/(cm sec)) and ρ is the mass density (g/cm^3).

For a pipe with a rectangular cross section, as in Sedflume, the hydraulic diameter is given as

$$D = \frac{2hw}{h+w} \tag{5-2}$$

where h is the duct height (cm) and w is the duct width (cm)

Table 5-1. Average erosion rates (cm/sec) for each shear stress (dyne/cm^2) (Jepsen et al. 1998b, Table 1)

Sample	Shear Stress (dynes/cm^2)											
	2	3	4	6	8	12	16	20	24	32	40	64
B1 [1]												
B2						5.5E-05	8.5E-05	1.7E-04	1.4E-03			
B3									2.0E-04	1.7E-03	2.2E-03	
B4						1.4E-04	2.3E-03	8.3E-03				
B5					1.7E-04							
B6							8.1E-03	8.3E-03				
B7	5.6E-05	3.3E-04	6.6E-04	5.0E-03	7.6E-03							
B8		1.0E-04	3.1E-04	8.3E-04	1.5E-03	4.4E-03						
B9		5.6E-05	2.1E-04	5.7E-04	1.8E-03							
B10 [2]												
B11												2.6E-05
B12												4.6E-06
B13S [3]												2.3E-05
B13F [3]												1.8E-05
B14S [3]							2.8E-05			3.7E-05		4.3E-05
B14F [3]							5.9E-05			5.5E-05		4.0E-05
B15S [3]			2.0E-04			4.3E-03						
B15F [3]			1.7E-04			3.3E-03						

Notes: [1] Sample B1 was too large to fit in tube.

[2] Sample B10 was received destroyed.

[3] *S* means tested in salt water conditions and *F* means tested under fresh water conditions.

The friction factor is defined as

$$\lambda = \frac{8\tau}{\rho U^2} \qquad (5\text{-}3)$$

where λ is the friction factor, τ is the wall shear stress, ρ is the density of water, and U is the mean flow speed.

Inserting Eqs. 5-2 and 5-3 into 5-1 the wall shear stress (τ) is given as an implicit function of the mean flow speed (U).

Table 5-2 contains the values of the critical shear strengths as obtained using the methodology described above, i.e., the shear stress evaluated at an erosion rate of 10^{-4} cm/sec.

Table 5-2. Critical shear stresses for each sample as determined by Jepsen et al. (1998b, Table 2)

Sample	Critical Shear Stress	
	dyne/cm^2	Pa
Category I		
B1	—	—
B2	16.7	1.67
B3	22.0	2.20
B4	10.6	1.06
B5	7.2	0.72
B6	14.0	1.40
Category II		
B7	2.2	0.22
B8	3.0	0.30
B9	3.4	0.34
Category III		
B10	—	—
B11	>64	>6.4
B12	>64	>6.4
B13	>64	>6.4
B14	>64	>6.4
B15	2.0	0.20

As discussed in Section 3.1, there are two types of erosion. The first is "surface erosion" in which erosion takes place by the removal of individual particles and/or small clusters (flocs) when hydrodynamic forces overcome the bonds formed between particles (Parchure and Mehta 1985, Partheniades and Paaswell 1970). Surface erosion takes place in Zone 1 which is on the order of centimeters or less. The bed surface shear strength (τ_{so}) can be quantitatively defined by extrapolating the first of the two linear segments that characterize an erosion rate versus shear stress plot to an erosion rate of zero.

The second is "bed erosion" (Parchure and Mehta 1985) or "mass erosion" (Partheniades and Paaswell 1970) in which erosion takes place by the removal of relatively large pieces of soil. Bed erosion is initiated when flow induced forces on the bed causes stresses within the sediment to exceed the shear strength along localized planes. It is usually defined as the break in the shear stress vs. erosion rate plot above which erosion rates increase more rapidly with shear stress than below the critical value. The onset of bed erosion is demarked by the bed's characteristic shear strength (τ_{sc}). This point can be quantitatively determined by fitting two piecewise linear curves to the data and evaluating the intersection.

Table 5-3 gives the values of τ_{so} and τ_{sc} based on piecewise linear curve fitting of the results from Jepsen et al (1998b) testing of surrogate waste material. The data for Category III waste (MgO bricks) is not included since they are not considered waste. An example of how τ_{so} and τ_{sc} values were obtained is shown in Figure 5-1 for Sample B2.

Table 5-3. Summary of shear strengths from present analysis and Jepsen et al (1998b).

Sample	Present Analysis Piecewise Linear Fit		Present Analysis Operational shear strength (τ_c) [Pa]	Jepsen et al. (1998b) reported shear strength values [Pa]
	Bed surface shear strength (τ_{so}) [Pa]	Bed characteristic shear strength (τ_{sc}) [Pa]		
Category I				
B2	0.47	1.98	1.94	1.67
B3 [1]	—	—	2.19	2.20
B4 [1]	—	—	1.27	1.06
B5 [2]	—	—	—	0.72
B6 [2]	—	—	—	1.40
Category II				
B7	0.18	0.38	0.35	0.22
B8	0.27	0.76	0.59	0.30
B9	0.26	0.59	0.51	0.34

Notes:
1. Insufficient data for piecewise linear curve fit.
2. Insufficient data for piecewise linear or linear curve fit.

B2 Data

Lower line:
y = 7E-05x - 3E-05
$R^2 = 1$

Upper line:
y = 0.0031x - 0.006
$R^2 = 1$
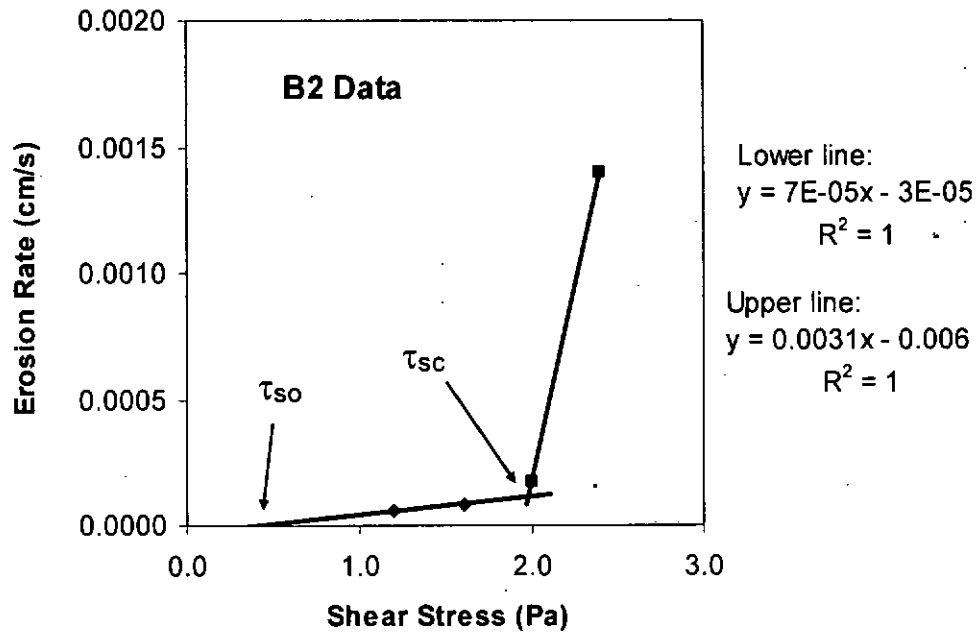
Figure 5-1. Example of piecewise linear fit to data from Sample B2 to obtain bed surface shear strength (τ_{so}) and bed characteristic shear strength (τ_{sc}).

As also mentioned in Section 3.3, there is a third shear strength value that is used to characterize the strength of the bed, that is, the "operational shear strength" (τ_c). It is obtained by fitting a single line through the data after which the erosion rate increases at a much faster rate. The intercept of that line with the shear stress axis defines the operational shear strength. For samples B3 and B4, the data did not indicate an increase in erosion rate so a linear fit was used for all the data. Our evaluation of τ_c is also given in Table 5-3. An example of how our value was obtained is shown in Figure 5-2 for Sample B2.
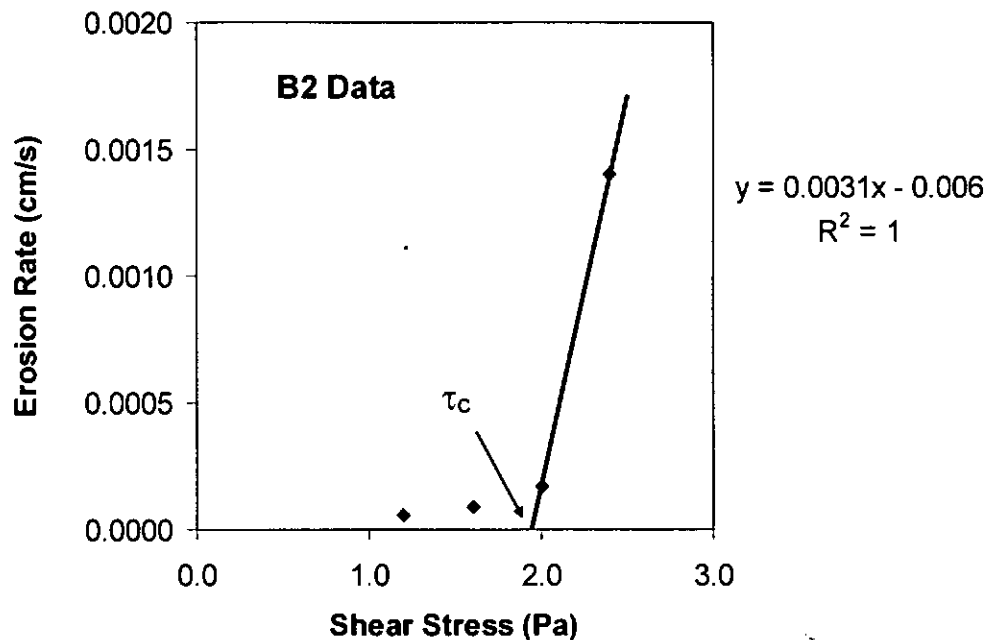
Figure 5-2. Example of linear fit to data of Sample B2 after which the erosion rate increases sharply to obtain the operational shear strength τ_c.

6 US Army Corp of Engineers Results on San Francisco Bay Muds

The US Army Corps of Engineers dredges materials in San Francisco Bay harbors and waterways to ensure clear, safe shipping lanes. The dredged materials are then disposed of at a disposal site near Alcatraz Island. Strong ebb currents at the Alcatraz disposal site prevent the accumulation of disposed muds from around the bay and transport them seaward past the Golden Gate Bridge.

Since the presently accepted model for the waste shear strength is that it behaves in a manner similar to San Francisco Bay mud, a better understanding of their general erosion behavior is important rather than relying on a single set of tests. The Alcatraz disposal site analyses provide that site specific information.

Sediments from a number of locations around San Francisco Bay were subject to erosion testing at two laboratories (Teeter 1987). The first was the Hydraulics Laboratory at the US Army Engineer Waterways Experimental Station (WES) in Vicksburg, Mississippi. The second set of tests was performed by C. Villaret and M. Paulic of the Coastal and Oceanographic Engineering Department, University of Florida (UF), Gainesville. Dr. Ashish J. Mehta was the principal investigator.

6.1 Waterways Experimental Station (WES) Erosion Testing

WES testing was conducted on two composite sediment materials. Both are fine-grained, cohesive sediments that make up the bulk of the materials deposited at the Alcatraz site. Sediments taken from the Alcatraz disposal site were combined into a single sample designated CL. Sediments obtain from the Redwood Harbor were combined into another sample designated CH-2. All samples were passed through a No. 200 sieve to remove coarse materials. Eighteen erosion tests were conducted on the two sediment materials. Tests were run with three levels of moisture content or bulk wet density (BWD) and three levels of sand content – 1, 15, and 40 percent. A tilting flume with recirculating saltwater was used for all testing with sediments molded into small recessed chambers in the floor of the flume.

The results of their tests are given in Table A2 (Teeter 1987). In that table and Table A1, the specific weight (mass) total or concentration is the dry density of the sample (ρ_{dry}). The mass density of the solids is taken to be $\rho_s = 2.650$ g/cm^3 and liquid density of the salt water is $\rho_w = 1.025$ g/cm^3. The porosity ϕ can be determined from:

$$\phi = 1 - \frac{\rho_{dry}}{\rho_s} \tag{6-1}$$

The water content w, which is defined as the ratio of the weight of water to the weight of solids, can be calculated from:

$$w = \frac{\phi \rho_w}{(1-\phi)\rho_s} = \frac{\phi \rho_w}{\rho_{dry}} \tag{6-2}$$

For a saturated sediment ($S = V_w/V_v = 1$), the saturated density (ρ_{sat}) is the same as the bulk wet density (BWD). It can be calculated from:

$$\rho_{sat} = \phi \rho_w + (1-\phi)\rho_s = \rho_{dry}(1+w) \tag{6-3}$$

The results from the WES erosion tests are given in Table 6-1. The reported shear strength values are the operation shear strengths (τ_c).

Table 6-1. Erosion results from WES tests based on Teeter 1987, Tables A1 and A2.

Sediment/ percent sand	Dry density or specific mass total [kg/m³]	Specific mass fines [kg/m³]	porosity	Water content [fraction]	BWD [kg/m³]	Terminal bed shear stress [N/m²]	Maximum excess shear stress [N/m²]	Erosion time [sec]	Erosion rate total [g/cm²/sec]	Erosion rate total [g/cm²/hr]	τ_c [N/m²]
CL/0	533	533	0.799	1.536	1352	2.13	0.32	3600	2.94E-05	0.106	1.98
	465	465	0.825	1.818	1310	1.62	1.38	3600	1.16E-05	0.042	1.57
	380	380	0.857	2.311	1258	0.68	0.33	1200	9.11E-05	0.328	0.56
CL/15	577	490	0.782	1.390	1379	2.13	0.32	1800	4.69E-05	0.169	1.90
	530	450	0.800	1.547	1350	0.68	0.33	3600	8.80E-05	0.317	0.56
	413	351	0.844	2.095	1278	0.68	0.33	1200	1.65E-04	0.594	0.48
CL/40	705	423	0.734	1.067	1457	1.62	1.38	1800	1.00E-04	0.360	1.29
	569	341	0.785	1.415	1374	0.68	0.33	900	1.58E-04	0.569	0.49
	460	276	0.826	1.841	1307	0.68	0.33	600	3.51E-04	1.264	0.36
CH-2/0	495	495	0.813	1.684	1329	1.62	1.38	300	2.37E-04	0.853	1.37
	403	403	0.848	2.157	1272	0.68	0.33	1200	8.09E-05	0.291	0.64
	333	333	0.874	2.691	1229	0.68	0.33	300	6.23E-04	2.243	0.46
CH-2/15	564	479	0.787	1.431	1371	2.13	0.32	2400	6.09E-05	0.219	2.03
	465	395	0.825	1.818	1310	0.68	0.33	3600	5.24E-05	0.189	0.65
	397	337	0.850	2.195	1268	0.68	0.33	300	6.09E-04	2.192	0.46
CH-2/40	771	463	0.709	0.943	1498	2.13	0.32	2700	4.00E-05	0.144	2.06
	605	363	0.772	1.307	1396	0.68	0.33	2820	8.51E-05	0.306	0.64
	491	295	0.815	1.701	1326	0.68	0.33	300	7.99E-04	2.876	0.42

Notes:

1. Values are given for a mass density of solids ρ_s = 2650 [kg/m³] and a mass density of salt water ρ_w = 1025 [kg/m³]
2. The maximum excess shear strength was calculated as $\tau_i - \tau_{i-1}$, where τ_i is the bed shear stress at the termination of step i and $i-1$ refers to the previous step (Teeter 1987, Table A2).

The critical shear stress for erosion (τ_c) [N/m^2] from the WES tests were correlated to the specific weight of the fines (γ_f) [g/cm^3] for both sample types using a power law fit as:

$$\tau_c = 17.26 \gamma_f^{3.29} \tag{6-4}$$

For our purposes, as needed for Section 7.2.3, we correlated the critical shear stress for erosion (τ_c) [N/m^2] with the BWD (Figure 6-1) and water content (Figure 6-2). Considering BWD first:

$$\tau_c = 8.887 \times 10^{-24} BWD^{7.3473} \tag{6-5}$$

where the units of τ_c are [Pa] and bulk wet density are [kg/m^3].
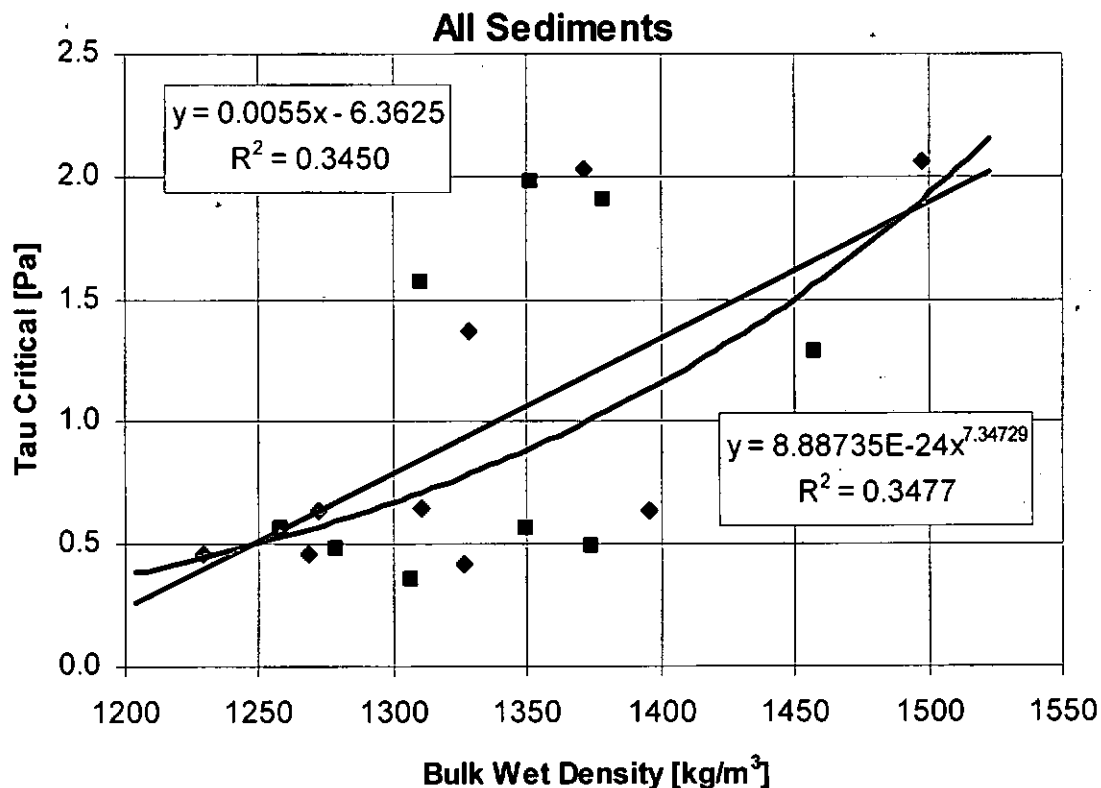
Figure 6-1. Power law and linear fits to the plot of critical shear stress for erosion versus the bulk wet density for the WES data (Teeter 1987, App. A). The blue squares represent the CL test results and the red diamonds represent the CH-2 results.

It is evident from Figure 6-1 that the shear strength of the sediments increases with bulk wet density. Based on the interspersion of the two data, the data can be appropriately fit with a single function. A power law function fits the data slightly better than a line even though neither correlation is very high. This agrees with the findings of other investigators such as Jepsen et al. (1997, 1998a, 2001) and Roberts et al. (1998) who also found a power law increase of shear strength with BWD.

In terms of water content, the relationship with τ_c is given by:

$$\tau_c = 1012.5 w^{-1.3923}$$

(6-6)

where the units of τ_c are [Pa] and water content w is in terms of percent.

All Sediments

$y = 1012.5x^{-1.3923}$

$R^2 = 0.3489$

$y = -0.0083x + 2.427$

$R^2 = 0.3340$
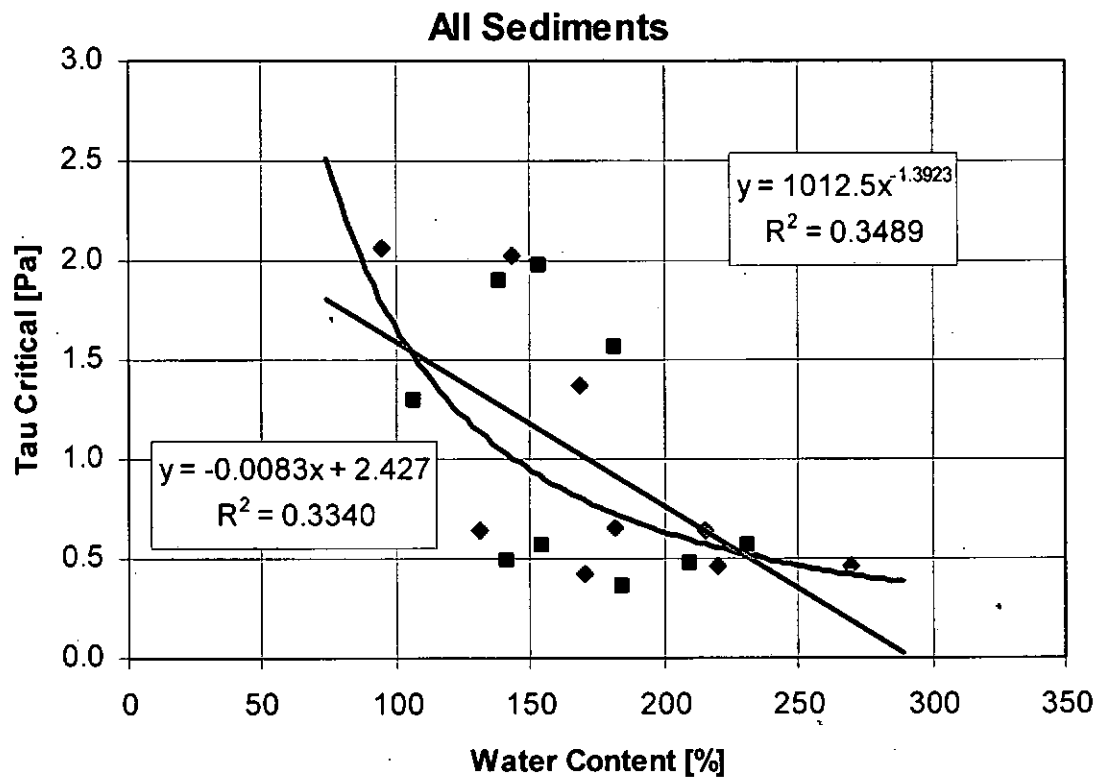
Figure 6-2. Power law and linear fits to the plot of critical shear stress for erosion versus the water content for the WES data (Teeter 1987, App. A). The blue squares represent the CL test results and the red diamonds represent the CH-2 results.

Again, both sets of data can be appropriately fit with a single function and a power law function fits the data slightly better than a line. As the water content of the sediment decreases, there is a rapid increase in the critical shear strength for erosion.

6.2 University of Florida (UF) Erosion Testing of San Francisco Bay Muds

The UF tests on San Francisco Bay mud were conducted on a third composite sample of fine-grained, cohesive sediment made from core sections from the Larkspur-Richmond Longwharf. Tests were performed on both placed (dense) and deposited from suspension (soft) beds. For tests on the deposited beds, the samples were allowed to consolidate for 0.5 and 3.8 days. In addition, two types of flumes were used, a rocking flume that produced oscillatory currents and

an annular flume that produced a steady, unidirectional current. The tests conditions are give in Table 6-2.

Table 6-2. San Francisco Bay mud conditions for the University of Florida tests (Teeter 1987, App. B Table 8).

Test No.	Apparatus	Bed Type Consolidation time	Dry Density (ρ_{dry})	Bulk wet density (BWD)	Moisture Content (w) [2]
1	Annular Flume	Placed (dense) —	0.96	1.63	70%
2	Annular Flume	Deposited (soft) 0.5 days	0.22	1.17	432%
3	Rocking Flume	Deposited (soft) 0.5 days	0.22	1.17	432%
4	Annular Flume	Deposited (soft) 3.8 days	0.40	1.28	220%
5	Rocking Flume	Deposited (soft) 3.8 days	0.40	1.28	220%
P1 [1]	Straight Flume	Placed (dense) 40 days	0.61 [2]	1.36	123% [3]
P2 [1]	Straight Flume	Placed (dense) 15 days	0.57	1.34	135% [3]

Notes:
1. Series I and II from Partheniades 1965
2. Partheniades 1965 for reported a value of $40 \frac{lb}{ft^3} * \frac{ft^3}{(12in)^3} * \frac{in^3}{(2.54cm)^3} * \frac{454gm}{lb} = 0.64 \frac{gm}{cm^3}$ for P1 (pg. 109), but no value was found for P2.
3. Partheniades 1965 for reported values of 110% for P1 (pg. 109) and 120% for P2 (pg. 121)

Villaret and Paulic also include in their analysis the data from Series I and II of Parthenaides (1962, 1965), which were conducted on remolded, placed beds. Their justification reads

> Since Partheniades also used sediment from the San Francisco Bay which is spatially well mixed (Krone, 1978), results from these tests are included in the subsequent analysis.

The authors compared the erosion rate versus bed shear stress plots for their tests against Partheniades Series I and II and found that the data agreed with Series I up to $\tau_b = 0.8$ Pa, attributing differences between the two at larger values of τ_b to different methods of bed preparation. Concerning Series II, Villaret and Paulic state that iron oxide from rust in the return pipe of the flume used by Partheniades enhanced resistance of the bed to erosion due to cementing of aggregates. In all three cases of erosion of placed beds, incipient erosion was considered to have begun at approximately the same bed shear stress $\tau_{so} = 0.1$ Pa.

Analysis of the data was performed by Villaret and Paulic (Teeter 1987, App. B). A piecewise linear curve was used to determine the bed shear stress for "incipient erosion" (τ_{so}, which is

referred to τ_{co} in the original paper) and the "operational" or "design" value of the critical bed shear stress (τ_c) which is taken as the intercept of the second line extended down to the bed shear stress axis (Figure 6-3). Two methods were used to determine τ_c, Method A is the standard plot of erosion rate versus bed shear stress and Method B involves a change in sediment concentration over a 90 minute interval (C_{90}) versus bed shear stress. Method B was only used for deposited or soft beds. The results are given below in Table 6-3.

Table 6-3 San Francisco Bay mud shear strength values as determined by Villaret and Paulic at the University of Florida (Teeter 1987, App. B, Table 9)

Test No.	τ_{so} [a] (Pa)	τ_c Method A (Pa)	Method B (Pa)	M [b] (g/cm^2-min)
1	0.12	0.65	— [c]	2.8×10^{-4}
2	0.16	0.35	0.23	2.8×10^{-4}
3	— [d]	0.12	0.05	2.8×10^{-4}
4	0.10	0.26	0.30	2.8×10^{-4}
5	0.10	0.28	0.20	2.8×10^{-4}
P1	0.12 [e]	0.38 [f]	— [c]	2.8×10^{-4}
P2	0.12 [e]	1.20 [f]	— [c]	2.8×10^{-4}

Notes:
  a. In original, τ_{so} is referred to as τ_{co}.
  b. M is the erosion rate constant.
  c. Method B not applied as it yields the same value as Method A (see text of Teeter 1987, App. B, p. B20)
  d. Insufficient data.
  e. Partheniades 1965, pg. 127, gives these values as 0.57 dynes = 0.057 Pa. He also estimates the initiation of scouring to begin at ~0.80 fps (0.110 Pa) (pg. 112).
  f. Partheniades 1965, pg. 124, gives these critical shear stress values; for Series I = 0.010 lb/ft^2 (0.48 Pa) and Series II = 0.028 lb/ft^2 (1.34 Pa).
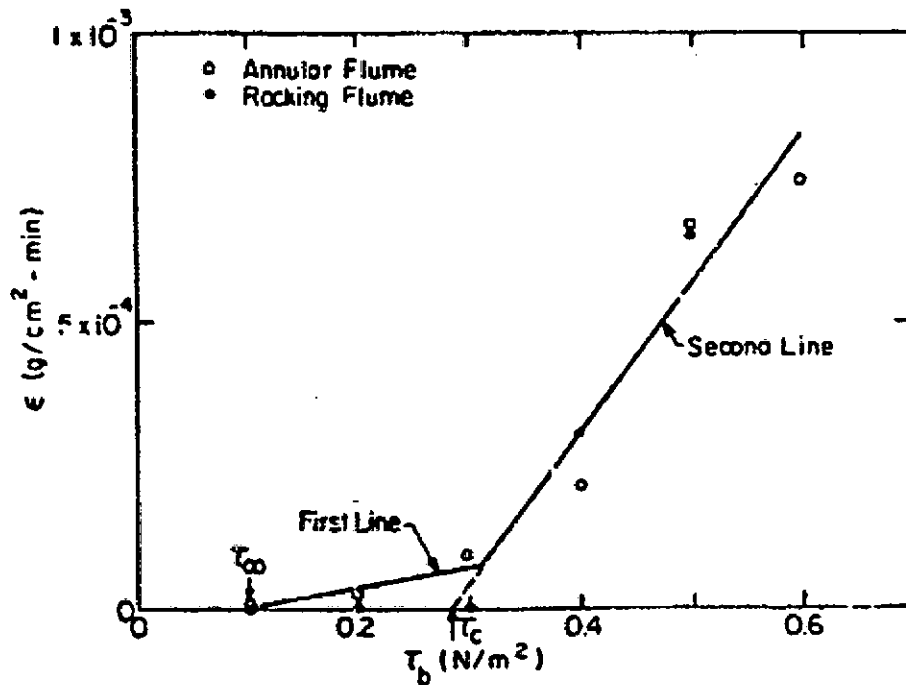
Figure 6-3. Example of San Francisco Bay mud erosion rate versus bed shear stress plot for deposited (soft) bed after 3.8 days of consolidation. Also shown are how the values $\tau_{co} = \tau_{so}$ and τ_c are determined (Teeter 1987, App. B, Figure 39).

In Table 6-3, it is noticed that the bed surface shear strength, τ_{so}, values are close to each other with a mean of 0.12 Pa. As explained by Villaret and Paulic, for the same sediment, incipient motion occurs at the same shear stress level because the surface shear strength is unaffected by the overburden. Therefore, neither the bed preparation procedure nor the bed density significantly influences τ_{so}.

The operational (τ_c) or characteristic shear strength (τ_{sc}) of the bed, on the other hand, is influenced by the density of the material being eroded. Villaret and Paulic were able to correlate their data into a single linear relationship:

$$\tau_c = 1.04(BWD - 1) \tag{6-7}$$

where τ_c has units of Pa and BWD is the bulk wet density in units of g/cm^3.

The waste has a porosity of 68% as emplaced. If it were saturated, it would have a bulk wet density of 1388 kg/m^3. Using this value in Eq 6-5 and 6-7 would give operational shear strength values of 1.09 and 0.40 Pa for the WES and UF results, respectively.

7 Compression Effects on Waste Shear Strength Behavior

7.1 Compression

Compression and consolidation of a soil, which is presently conceived of as the model for the waste, occurs by a decrease in pore volume. According to Das (2006) the deformation of a soil for a given load increment can be divided into three stages (Figure 7-1). We will consider two of stages – loading compression and secondary compression (or secondary consolidation).

The first stage is caused by stresses from salt creeping into the repository and compressing the waste. According to Lambe and Whitman (1979, pg 19)

> .... the soil will normally decrease in volume as the load is increased. This volume decrease comes about because individual particles nestle closer and closer together. There are shear failures (sliding) at the many individual contact points, but there is no overall shear failure of the soil mass. The vertical load can be increased without limit. Such a process is volumetric *compression*.
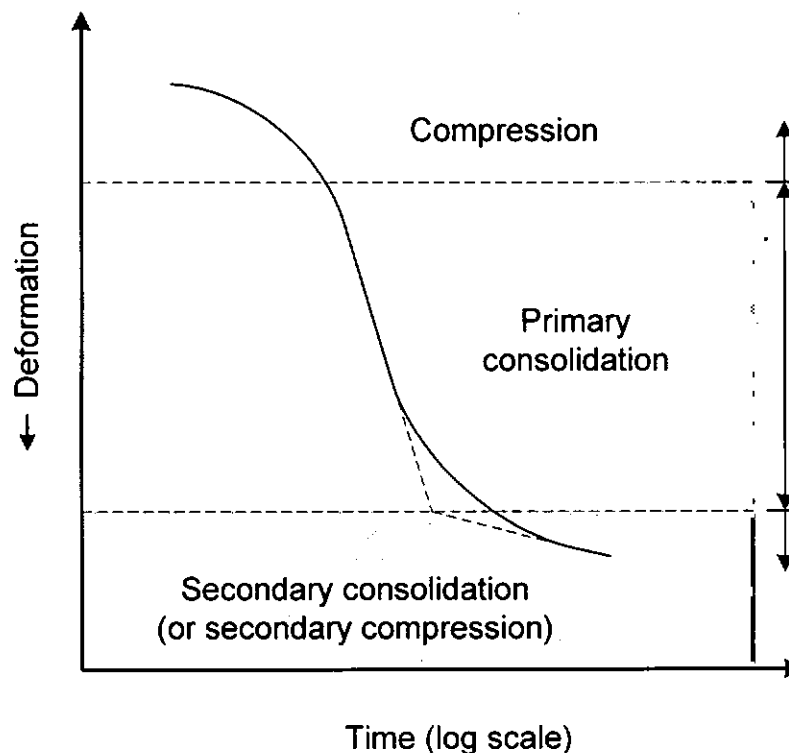
Figure 7-1. Time – deformation plot in a soil for a given load increment (Das 2006, Fig. 10.10). Lambe and Whitman (1979) refer to secondary consolidation settlement as secondary compression, which was added to the figure.

Lambe and Whitman (1979, Sec 27.7) noted that time-dependent deviations from predicted results occur in the soil (Figure 7-2), which they referred to as secondary compression. (Das refers to it as secondary consolidation settlement.) Secondary compression occurs with time as

plastic readjustments occur in the soil fabric. It occurs because mineral skeleton has time-dependent properties.
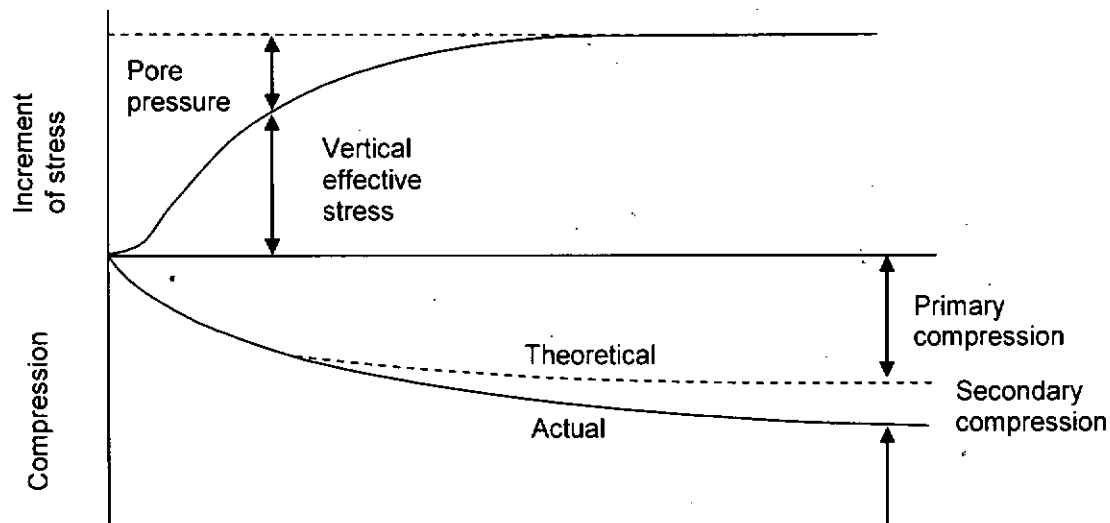
Figure 7-2. Primary and secondary compression for a soil with time (Lambe and Whitman 1979, Figure 27.14, pg 420).

We will not consider the effect of primary consolidation on the waste is this analysis.

7.2   Loading Compression

7.2.1   SANTOS Modeling to Determine the Porosity Change in the Waste with Time

The waste is in the underground where the salt creeps into each room over time. In addition, gases are being generated due to degradation of metals and microbial activity. The geometry and the time history are too complicated to calculate the stresses on the waste by hand. Therefore loading compression calculations of the waste were performed using the structural code SANTOS as it is the only currently qualified numerical code.

SANTOS is finite element code capable of representing 2D planar or axisymmetric geometries. The solution strategy used to obtain the equilibrium states is based on a self-adaptive, dynamic-relaxation solution scheme incorporating proportional damping. The explicit nature of the code means that no stiffness matrix is formed or factorized, thereby reducing the amount of computer storage necessary for execution. The element used in SANTOS is a uniform-strain, 4-node, quadrilateral element with an hourglass control scheme to minimize the effects of spurious deformation modes. Constitutive models for many common engineering materials are available within the code. A robust master-slave contact surfaces algorithm for modeling arbitrary sliding

contact is implemented. The executable SANTOS version 2.1.7 is installed on Warthog, a Linux workstation, where it was qualified (Arguello and Holland 1996, WIPP PA 2003a).

The analysis of the waste was performed using a procedure identical to that used in the Stone (1997a) and Park and Holland (2003), using the mesh for the current horizon, with the exception that instead of calculating the porosity change of the entire room, only the porosity change of the waste was calculated. In order to accomplish this, the waste had to be identified by labeling it with side set 800. Other than the labeling the waste, this is the original mesh used in Stone (1997a) (Figure 7-3). The NUMBERS program was modified so that it reads the data in the region bound by the side set 800 instead of the entire room. Finally, the AWK file was modified so that it determines the porosity change in the waste with time. The modified input files for FASTQ, NUMBERS, and AWK are given in Appendix A. All other input parameters were kept the same as in Stone (1997a) and Park and Holland (2003). The multi-mechanism deformation (M-D) model (Munson and Dawson 1982, Munson et al 1989, Stone 1997b) was used for both argillaceous halite and pure halite. The soils and crushable foams model was used for both the anhydrite and the waste (Stone 1997b). Material parameters for the rocks are given in Table 7-1 and Table 7-2.

Table 7-1. Material properties of the WIPP salts used in the analyses.

	Parameters		Units	Clean Salt	Argillaceous Salt
Elastic Properties (Butcher 1997)	Shear modulus	G	MPa	12,400	
	Young's modulus	E	MPa	31,000	
	Poisson's ratio	v	–	0.25	
Salt Creep Properties (Munson et al. 1989)	Secondary creep constant	A_1	s^{-1}	8.386×10^{22}	1.407×10^{23}
		B_1		6.086×10^{6}	8.998×10^{6}
		A_2		9.672×10^{12}	1.314×10^{13}
		B_2		3.034×10^{-2}	4.289×10^{-2}
	Activation energies	Q_1	cal/mole	25,000	25,000
		Q_2	cal/mole	10,000	10,000
	Stress exponents	n_1	–	5.5	5.5
		n_2		5.0	5.0
	Stress limit of the dislocation slip mechanism	σ_0	MPa	20.57	20.57
	Stress constant	q	–	5,335	5,335
	Transient strain limit constants	M	–	3.0	3.0
		K_0	–	6.275×10^{5}	2.470×10^{6}
		c	K^{-1}	9.198×10^{-3}	9.198×10^{-3}
	Constants for work-hardening parameter	α	–	-17.37	-14.96
		β	–	-7.738	-7.738
	Recovery parameter	δ	–	0.58	0.58

Table 7-2. Material properties of the anhydrite used on the analyses (Butcher 1997)

Material Property		Units	Anhydrite
Young's modulus		MPa	75,100
Density		kg/m^3	2,300
Poisson's ratio			0.35
Drucker-Prager constants	C	MPa	1.35
	a	--	0.45
Bulk modulus		MPa	83,440
Two mu		MPa	55,630
SANTOS input constants	A_0	MPa	2.3
	A_1		2.338
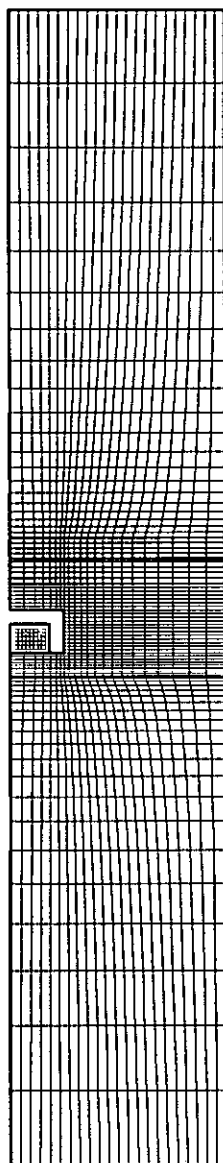
Figure 7-3. The discretized finite element mesh used in the present analyses. The mesh is from Stone (1997a).

7.2.1.1 Gas generation

Stone (1997a) used the user-supplied subroutines INITST to provide an initial stress state to the top of the mesh and FPRES to determine the gas pressure in the repository based on a constant rate of gas generation. The gas pressure in the disposal room was computed from the ideal gas law based on the current free volume in the room, V. The gas pressure, p_g, was computed with the following relationship:

$$p_g = f \cdot \frac{NRT}{V}$$

(7-1)

where N, R and T are the mass of gas in g-moles for the baseline case, the universal gas constant, and the absolute temperature in degrees Kelvin, respectively. Eight gas generation scenarios were used in SANTOS by multiplying a base gas generation potential and rate by a factor, f, as follows: f=0.0, 0.1, 0.2, 0.4, 0.6, 0.8, 1.0, and 1.2. These pressure histories envelop the pressure histories calculated by BRAGFLO on both a repository and panel scale (Clayton 2007) (see Appendix B). The base rate is given in Butcher (1997) as 1,050 moles/drum with a production rate of 1 mole/drum/year for gases produced from anoxic corrosion and 550 moles/drum with a production rate of 1 mole/drum/year for microbial activity. Both INITST and FPRES are used unchanged from the originals.

7.2.1.2 Waste characterization

The stress-strain behavior of the waste was represented by the soils and foams volumetric plasticity model (Stone 1997b) with a piecewise linear function defining the relationship between the mean stress and the volumetric strain. Compaction experiments on simulated waste were used to develop this relationship (Butcher et al. 1990).

The yield surface of the model in principal stress space is a surface of revolution with its axis centered about the hydrostat and the open end pointing into the compression direction (Figure 7-4). The open end is capped with a plane that is at right angles to the hydrostat. The deviatoric part is elastic-perfectly plastic so the surface of revolution is stationary in stress space. The volumetric part has variable strain hardening so the end plane moves outward during volumetric yielding. The volumetric hardening is defined by a set of pressure-volumetric strain relations. An associated flow rule is used such that deviatoric strains produce no volume change. The model is best broken into volumetric and deviatoric parts with the deviatoric part resembling conventional plasticity. The volumetric yield function is a product of two functions, ϕ_s and ϕ_p, describing the surface of revolution as a polynomial in pressure, p, and a cap normal to the pressure axis, respectively. These are given by

$$\phi_s = \frac{1}{2} s_{ij} s_{ij} - a_0 + a_1 p + a_2 p^2 \tag{7-2}$$

$$\phi_p = p - g(\varepsilon_v) \tag{7-3}$$

where a_0, a_1, a_2 are constants defining the deviatoric yield surface, p is the pressure, and ε_v is the volumetric strain. The form of $g(\varepsilon_v)$ is defined in this problem by a set of piecewise linear segments relating to pressure-volumetric strain. Table 7-3 lists the pressure-volumetric strain data used for the waste drum model and the data are plotted in Figure 7-5. The model material properties are given in Table 7-4.
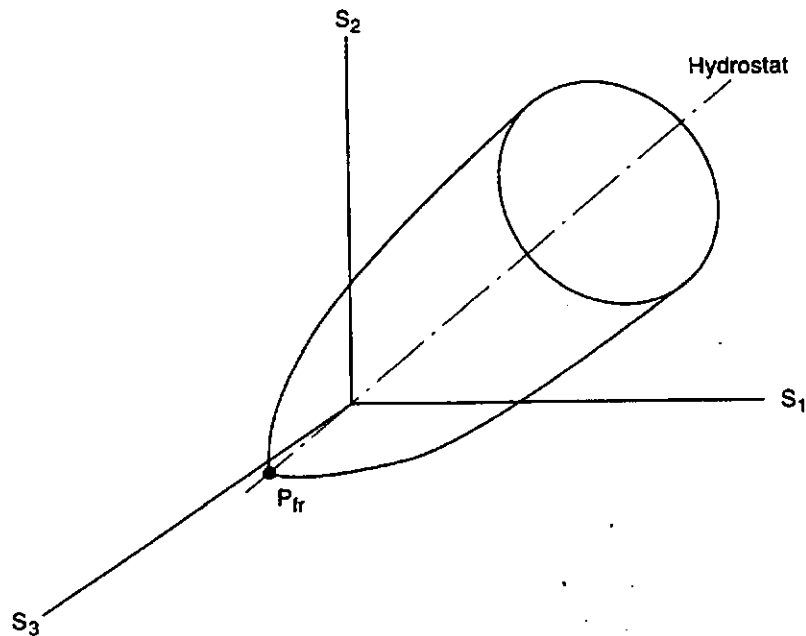
TRI-6346-13-0

Figure 7-4. Pressure dependent yield surface for the soils and foams material model for the waste (Stone 1997b, Figure 4.6.1)
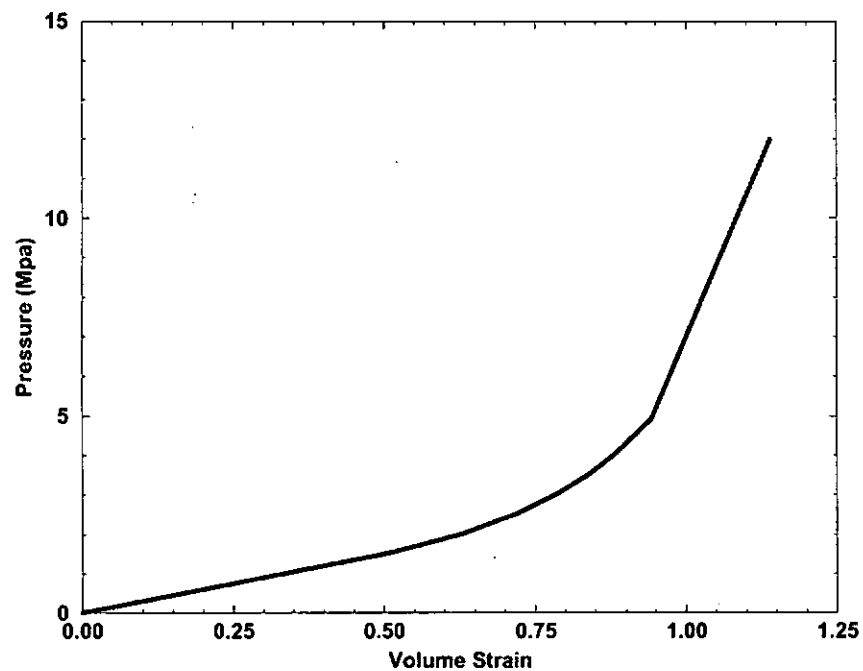
Figure 7-5. Curve of the pressure-bulk strain input to the volumetric plasticity model used to model the waste drums (Stone 1997a).

Table 7-3. Pressure and volumetric strain data used to define the volumetric plasticity model of the waste.

Pressure (MPa)	Volumetric Strain
1.53	0.510
2.03	0.631
2.53	0.719
3.03	0.786
3.53	0.838
4.03	0.881
4.93	0.942
12.0	1.14

Table 7-4. Material constants used with the volumetric plasticity model for the waste (Butcher, 1997)

Parameter	Unit	Value
G	MPa	333.0
K	MPa	222.0
a_0	MPa	1.0
a_1	—	3.0
a_2	—	0.

The physical properties of the waste are due to it being a combination of metallics, sorbents, cellulose, rubber and plastics, and sludges. The waste is modeled as an average mixture of these components. Table 7-5 summarizes the data used in the CCA for characterizing the waste (Butcher 1997). The initial waste dry density, ρ_{dry}, is 559.5 kg/m^3 and the solid waste density, ρ_s, is 1757 kg/ m^3. The initial waste density is the sum of the densities of the constituent waste forms. The corresponding initial waste porosity, ϕ_0, is calculated to be 0.681. For comparison sake, since the San Francisco Bay mud tested by Partheniades (1962) was used to determine the lower limit of TAUFAIL in CRA-2004, its physical properties are given in Table 7-5 also. The density of WIPP brine is from Brush (2005). It should be noted that if the WIPP waste prior to being compressed by the creeping salt were saturated, it would have physical properties that are quite similar to San Francisco Bay mud in its uncompacted state as tested in the aforementioned experiments.

Table 7-5. Physical properties of WIPP waste if fully saturated with brine and San Francisco Bay mud.

	WIPP waste (Butcher 1997, Brush 2005)	San Francisco Bay mud (Partheniades 1962, Teeter 1987)
solid density [kg/m^3]	1757	2650 (assumed)
dry density [kg/m^3]	559.5	640.7
porosity [%]	68.2	75.8
water content [%]	148	110
pore fluid density [kg/m^3]	1217 (WIPP brine)	1025 (salt water)
saturated density [kg/m^3]	1389	1345.6

7.2.2 Effect of Salt Creep with Time on Waste Properties

The numerical simulations were allowed to run out for 10,000 years. During that time, the salt crept into the room and began to crush the waste stack under all gas generation factors. Since the

- water content, $w = \dfrac{W_w}{W_s}$ (W_w is the weight of the water and W_s is the weight of the solids),

- and bulk wet density, $BWD = \rho_b = \dfrac{W_t}{V_t}$ (W_t is the total or wet weight and V_t is the total volume)

of the waste are both related to the its porosity, ϕ, it is important to understand the change in porosity with time. Figure 7-6 is a plot of the porosity of the waste with time for the different gas generation factors, f. In all cases, the most rapid change in porosity of the waste occurs early on, within the first century when institutional controls are in place. After that time the gas pressures have a smaller effect on the creep. The greatest change in waste porosity occurs when there is no gas pressure in the repository, and the least occurs at the highest gas generation rate of $f = 1.2$.

The porosities for these two extremes are listed in Table 7-6 for times 100 years and 10,000 years. For the case of $f = 1.2$, there is virtually no change in the porosity or any other parameter after 100 yrs.

Table 7-6. Porosity, water content, and bulk wet density of the waste for the extreme gas generation rates $f = 0.0$ and 1.2 at 100 years and 10,000 years. Calculation of the water content and bulk wet density assume that the waste has become fully saturated with brine.

	Porosity		Water content		Bulk wet density (kg/m³)	
	100 yrs	10000 yrs	100 yrs	10000 yrs	100 yrs	10000 yrs
f = 0.0	0.54	0.21	0.82	0.18	1463	1646
f = 1.2	0.62	0.62	1.13	1.12	1422	1423
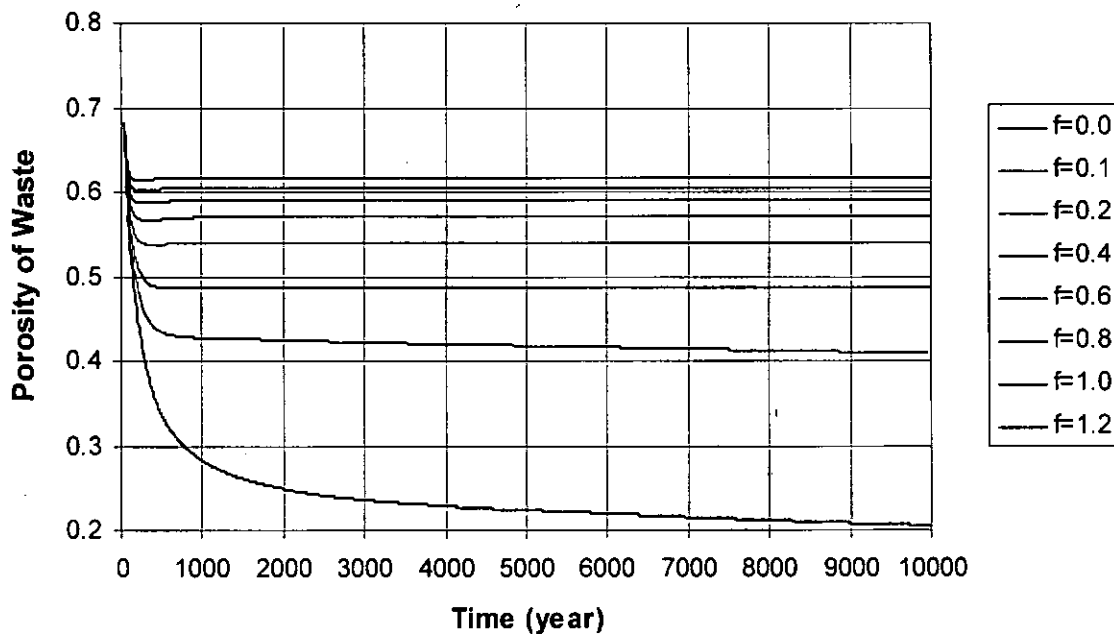
Figure 7-6. Variation of waste porosity with time for the various gas generation factors, f.

We have seen throughout this paper that the critical shear strength is a function of the bulk wet density. As the bulk wet density of the material increases, so does the shear strength. Assuming that the waste is saturated, which is its weakest condition, the bulk wet density is given in terms of the porosity as:

$$BWD = \phi\rho_w + (1-\phi)\rho_s \qquad (7\text{-}4)$$

where ρ_w is the density of the water, which in WIPP is brine ($\rho_w = 1217$ kg/m^3, Brush 2005), and ρ_s is the density of the solids, which is the density of the waste solids ($\rho_s = 1757$ kg/m^3, Butcher 1997).

We will also relate the critical shear strength to the water content. The relationship between water content, also known as moisture content, and porosity is given by:

$$w = \frac{\phi\rho_w}{(1-\phi)\rho_s} \qquad (7\text{-}5)$$

Plots of the bulk wet density and water content with time in a room of the repository are given in Figure 7-7 and Figure 7-8. In a manner similar to the porosity versus time plot (Figure 7-6) the biggest change in the bulk wet density and water content occurs in the gas where there is no gas being generated in the room. For the highest gas generation factor, $f = 1.2$, there are only minor changes occurring after 100 years.
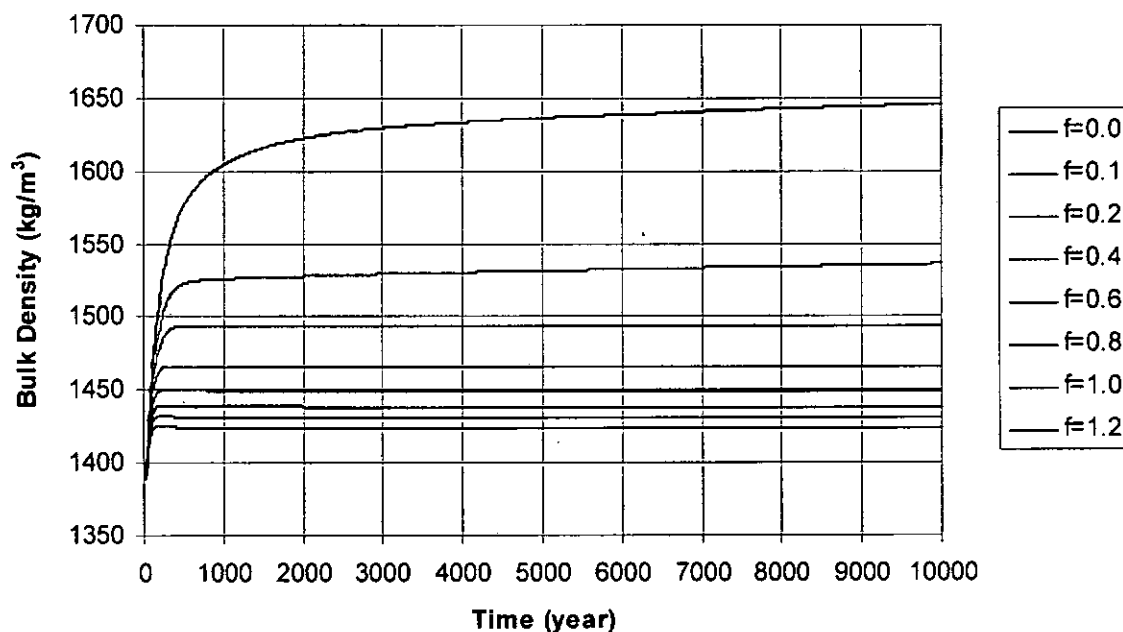
Figure 7-7. Plot of the bulk wet density of the waste with time for various gas generation factors f. For WIPP, the density of brine $\rho_w = 1217$ kg/m^3 (Brush 2005) and the solid density of the waste $\rho_s = 1757$ kg/m^3 (Butcher 1997).
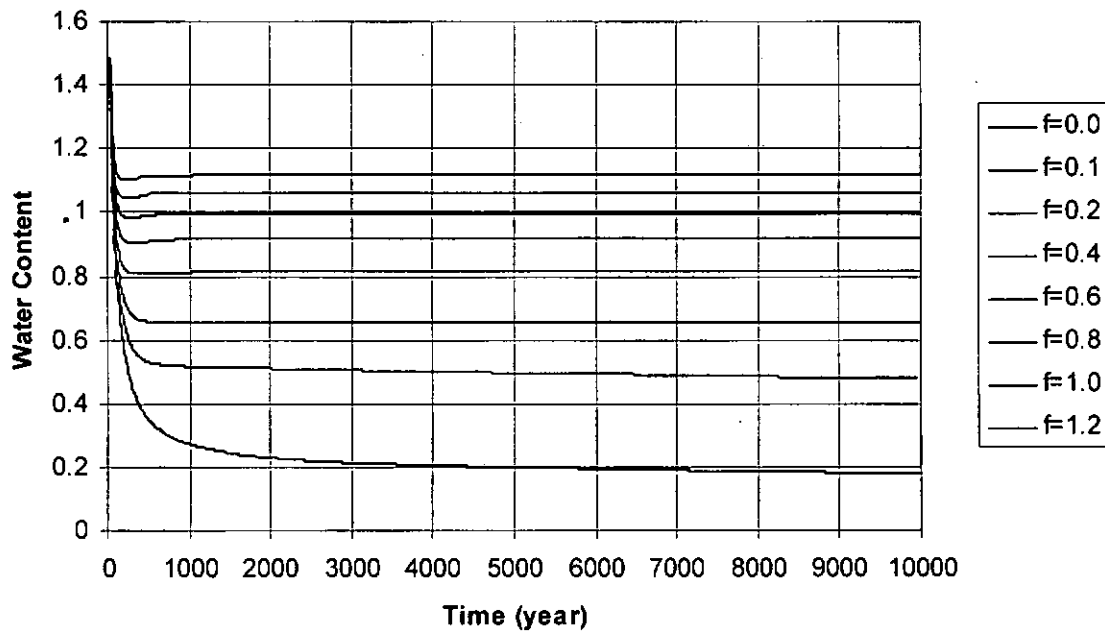
Figure 7-8. Plot of the water content of the waste with time for various gas generation factors f. For WIPP, the density of brine $\rho_w = 1217$ kg/m^3 (Brush 2005) and the solid density of the waste $\rho_s = 1757$ kg/m^3 (Butcher 1997).

The SANTOS input files are in the CVS library /nfs/data/CVSLIB/SANTOS_Analysis/Tests /Input/ClaySeamG. The SANTOS output files and Excel files used to generate the plots are in the CVS library /nfs/data/CVSLIB/SANTOS_Analysis/Tests/Output/ClaySeamG. Log files of the computer runs are found in the CVS library /nfs/data/CVSLIB/SANTOS_Analysis/ Tests/RunControl/ClaySeamG. CVS libraries are stored on the workstation elo. The entire Tests directory can be checked out of CVS using

```
cvs -d $CVSLIB/SANTOS_Analysis co Tests
```

This will create a directory Tests with all the subdirectories in the current directory you are in. A list of the input and output files is given in App. A. See Park and Holland (2003) and Park and Kirchner (2004) for a more complete discussion of run control procedures used for this analysis.

Use of SANTOS and its ancillary codes were not listed in the software codes that were going to be used for this analysis according to AP-131. When AP-131 was written, it was thought that the compression analysis could be kept to a one dimensional case for which there is an analytical solution. Once the analysis was begun, it was determined that a one dimensional analysis would not would not be sufficient because of the complex manner in which the creeping salt compresses the waste. SANTOS was invoked as the only presently qualified code accepted by the EPA.

7.2.3 Effect of Loading Compression on Waste Shear Strength

The creeping of the salt causes loading compression in the waste, which we expressed by the change in porosity. The change in porosity will result in a change in both the bulk wet density and water content of the waste if it is saturated. In this section we consider the effect that a change in bulk wet density or water content has on the shear strength of the waste. We will accomplish this first by using the shear strength versus bulk wet density relationship discussed in Section 6 specifically for San Francisco Bay muds, viz., WES Eq. 6-5 and U F Eq. 6-7. After that, we will use a generalized relationship that relates the critical shear strength to the water content of a fairly large number of sediments.

7.2.3.1 Effect of Loading Compression on the Waste Shear Strength if it Behaves in a Manner Similar to San Francisco Bay Muds

In Section 6 we discussed the results on a number of test performed by the US Army Corps of Engineers Waterways Experimental Station (WES) and the University of Florida (UF) on San Francisco Bay muds (Teeter 1987). In their analyses, the tests of Partheniades (1965) were also included. These analyses, therefore, yield a site specific erosional response of San Francisco Bay mud to bulk wet density changes. San Francisco Bay mud represents the current model for the erosional behavior of degraded waste.

Two relationships between operational shear strength and bulk wet density were found by the two investigative teams. The first relationship was determined from the WES results. It is best represented by a power-law fit (Eq 6-5) and is repeated here for convenience.

$$\tau_c = 8.887 \times 10^{-24} \, BWD^{7.3473} \tag{7-6}$$

The second relationship was determined by UF. Their data was best fit by a line (Eq 6-7). Again it is repeated here for convenience.

$$\tau_c = 1.04(BWD - 1) \tag{7-7}$$

These two relationships were used in the waste loading compression analysis above to estimate the operational shear strength of the waste if it behaves as San Francisco Bay mud.

Applying the WES results to the data of Figure 7-7, the variation of waste shear strength is given in Figure 7-9 below.
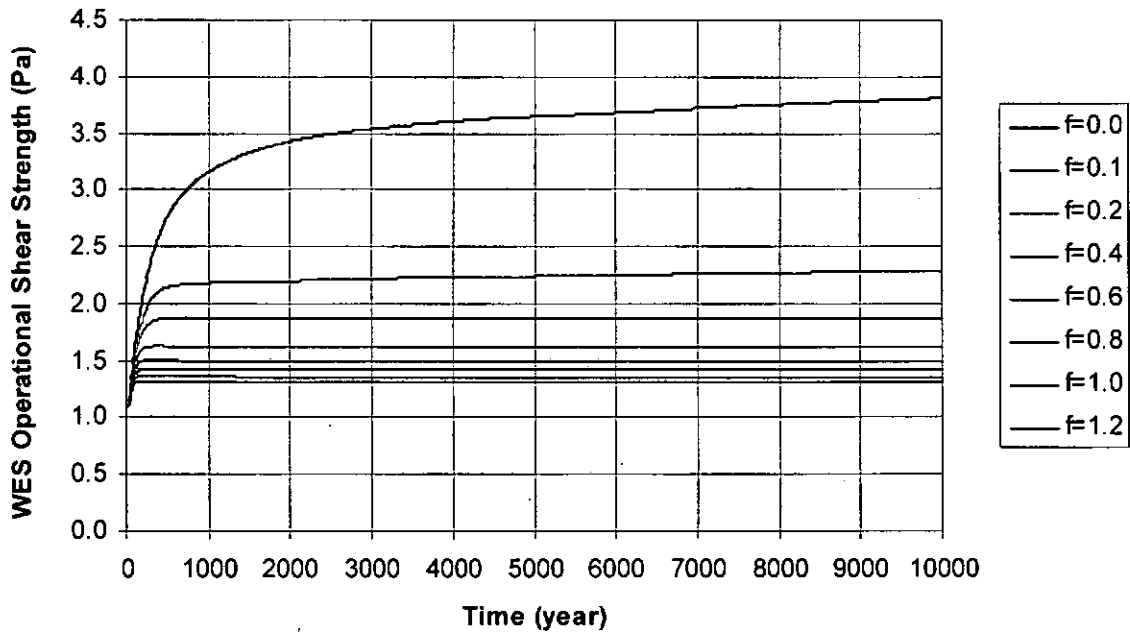
Figure 7-9. Variation of operational shear strength of the waste with time using WES erosion test results (Eq 7-12).

The UF relationship (Eq 7-13) was applied to the loading compression analyses also. The variation of waste shear strength with time is given in Figure 7-10 below.
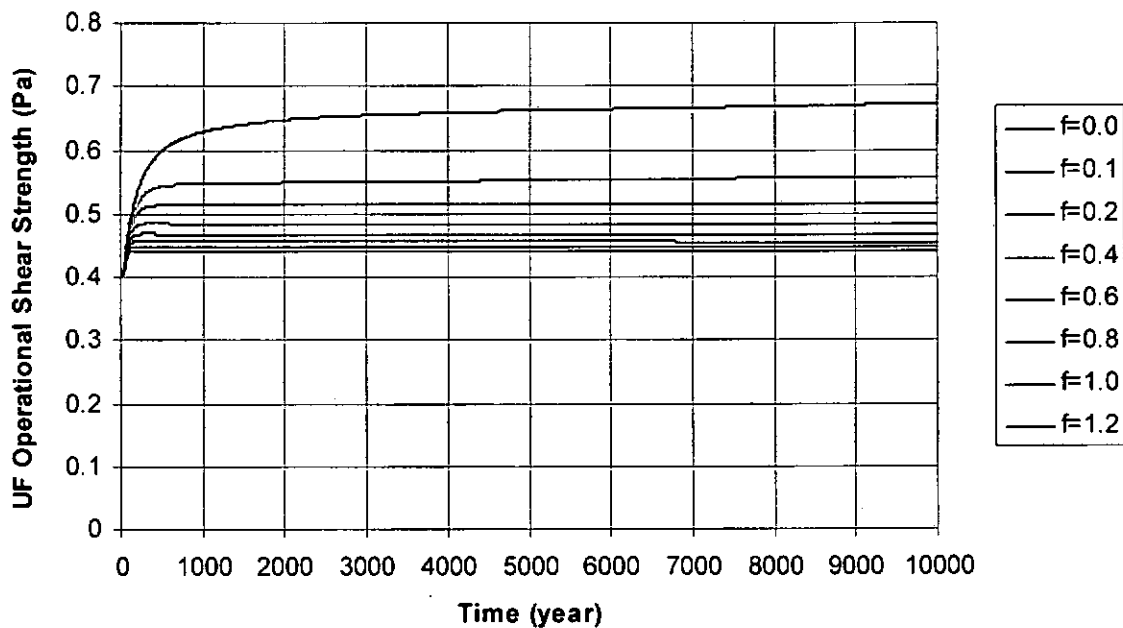
Figure 7-10. Variation of operational shear strength of the waste with time using UF erosion test results (Eq 7-13).

In both cases the waste shear strength varies with time in association with the change in porosity of the waste. The least change in occurs for a gas generation factor of $f = 1.2$. This is therefore the most conservative value. It is again seen that after 100 years $f = 1.2$ results are practically invariant with time. As acknowledged by Teeter (1987), the UF results give lower values of the operational shear strength for the same bulk wet density. This is apparent in a comparison of Figure 7-9 and Figure 7-10. The value of τ_c according to the WES and UF results at certain key times is given in Table 7-7.

Table 7-7. Operational shear strength values according to the application of erosional testing results obtained by WES and UF on San Francisco Bay muds at key times

time [years]	Operational Shear Strength, τ_c [Pa]					
	WES		UF		average	
	f = 0.0	f = 1.2	f = 0.0	f = 1.2	f = 0.0	f = 1.2
0	1.09	1.09	0.40	0.40	0.75	0.75
100	1.60	1.30	0.48	0.44	1.04	0.87
10,000	3.81	1.31	0.67	0.44	2.24	0.88

7.2.3.2 Effect of Loading Compression on the Waste Shear Strength if it Behaves in a Manner Similar to Sediments in General

Based on a detailed study of the literature and as discussed throughout this analysis, there are basically two different measures of shear stress, namely:

- Surface – erosion takes place by the removal of individual clay particles and small clay clusters.

- Mass – erosion takes place by the removal of relatively large pieces of soil.

The first type, "surface" erosion, represents the initiation of movement of individual clay particles or flocs when hydrodynamic forces overcome the bonds formed by interparticle forces. It is usually quantitatively defined by extrapolating the best-fit to the first line of the erosion rate versus shear stress to an erosion rate of zero to obtain the stress were erosion just initiates, τ_{so} (see Figure 7-11).

The second type, "characteristic" or "mass" erosion, represents the movement of larger clay particles and is initiated when flow induced forces on the bed causes stresses within the clay which may exceed the shear strength along localized planes. It is usually defined as the break in the shear stress versus erosion rate plot above which erosion rates increase more rapidly with shear stress than below the critical value, τ_{sc} (Partheniades 1965, Parchure and Mehta 1985). This point can be quantitatively determined by fitting two piecewise linear curves to the data, equating the two linear equations, and evaluating the intersection (see Figure 7-11).

In practice, however, no standard testing procedure exists for erodibility testing of marine or channel bed sediments. As pointed out by Teeter (1987), differences may arise due to a number of reasons such as:

1. Different sediments tested, even from the same general location
2. Different methods of bed preparation
3. Type of flume used
4. Recirculation or not of the eroded sediment
5. Whether or not uniform shear stresses are applied to the bed
6. How the erosion rates are calculated.

In addition, the two types of erosion are not always distinct and may overlap as is the case when the water velocity initiates movement, but may not have sufficient energy to keep the particles in suspension.

Thus, there seems to be confusion regarding the term "critical" shear stress. This paper uses τ_{so} to represent the shear stress for initiation of surface erosion (incipient motion) and τ_{sc} to represent the shear stress for initiation of mass erosion. The determination of τ_{so} and τ_{sc} is based on having sufficient data to create the piecewise linear curve fit, the fit requires at least two points per line segment. There are numerous instances where the reported value of τ_{sc} is based on a single linear fit, as there might be insufficient data or just the author's preference. This single linear fit may include all the data or it may be an extension of the second line of a piecewise linear fit. Examples of evaluating τ_{so} and τ_{sc} are shown in Figure 7-11. The operational shear strength τ_c lies within the range of values reported for mass erosion.
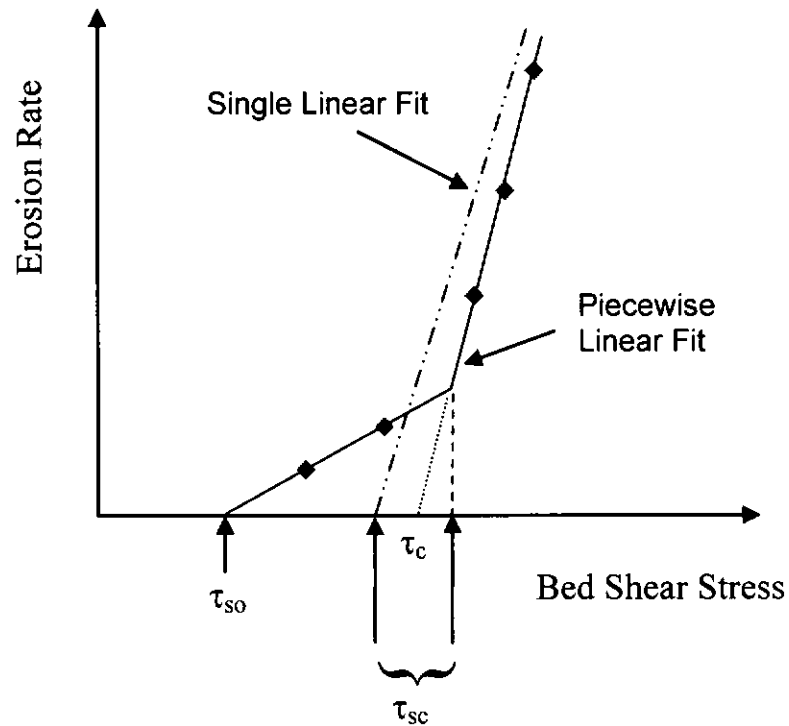
Figure 7-11. Determination of surface, τ_{so}, and characteristic, τ_{sc}, shear stress values as reported in practice. The operation shear strength, τ_c, lies within the range of τ_{sc} values typically reported by practitioners.

With this confusing terminology acknowledged, Table 7-8 gives a summary of results for the bottom shear stresses from our literature review. The characteristic shear strength includes single line and piecewise linear fits, including operation shear strength values (see Figure 7-11).

Table 7-8. Summary of critical shear stresses found in literature.

Test No. or Description	Initiation Stress τ_{so} (Pa)	Critical Stress τ_{sc} (Pa)	Moisture content w (%)	Reference
SF Bay Mud Series I	0.057	0.48	110	Partheniades 1965
SF Bay Mud Series II	0.057	1.34	120	Partheniades 1965
		0.04		Partheniades and Paaswell 1970 using Kennedy's Eq.
		0.51		Partheniades and Paaswell 1970 using Kennedy's Eq.
		19.15		USBR 1953 (Partheniades and Paaswell 1970)
		28.72		USBR 1953 (Partheniades and Paaswell 1970)
		57.45	.	USBR 1953 (Partheniades and Paaswell 1970)
		9.58		Flaxman 1963 (Partheniades and Paaswell 1970)
		28.72		Flaxman 1963 (Partheniades and Paaswell 1970)
		1.44		Dunn 1959 (Partheniades and Paaswell 1970)
		23.94		Dunn 1959 (Partheniades and Paaswell 1970)
		8.62		Espey 1963 (Partheniades and Paaswell 1970)
		95.75		Espey 1963 (Partheniades and Paaswell 1970)
		14.36		Rectoric 1964 (Partheniades and Paaswell 1970)
		95.75		Rectoric 1964 (Partheniades and Paaswell 1970)
		0.72		Rahman 1962 (Partheniades and Paaswell 1970)
		4.31		Rahman 1962 (Partheniades and Paaswell 1970)
		1.92		Grissinger 1966 (Partheniades and Paaswell 1970)
B2		1.67		Jepsen et. al. 1998b
B3		2.20		Jepsen et. al. 1998b
B4		1.06		Jepsen et. al. 1998b
B5		0.72		Jepsen et. al. 1998b
B6		1.40		Jepsen et. al. 1998b
B7		0.22		Jepsen et. al. 1998b
B8		0.30		Jepsen et. al. 1998b
B9		0.34		Jepsen et. al. 1998b
B2	0.47	1.98		Present analysis using Jepsen et al 1998b data
B7	0.18	0.38		Present analysis using Jepsen et al 1998b data
B8	0.27	0.76		Present analysis using Jepsen et al 1998b data
B9	0.26	0.59		Present analysis using Jepsen et al 1998b data
Sand	1.03	2.91		Uniform sand, SP (Navarro 2004)
Peachtree		2.18		Clayey or Silty Sand, SC-SM (Navarro 2004)
Murray	4.05	5.33	35	Silty Sand, SM (Navarro 2004)
Towns		17.21	34	Sandy Silt, ML (Navarro 2004)
Towns	11.31	15.62	34	Sandy Silt, ML (Navarro 2004)
Towns		6.82	31	Poorly Graded Sand, SP (Navarro 2004)
Habersham		17.35	30	Sandy Silt, ML (Navarro 2004)

Test No. or Description	Initiation Stress τ_{so} (Pa)	Critical Stress τ_{sc} (Pa)	Moisture content w (%)	Reference
Habersham		3.29	23	Silty Sand, SM (Navarro 2004)
Habersham		4.54	29	Silty Sand, SM (Navarro 2004)
Haralson	5.77	8.68	24	Silty Sand, SM (Navarro 2004)
Wilkinson		0.44	30	Poorly Graded Sand w Silt, SP-SM, Navarro (2004)
Bibb		9.68	39	Lean Clay w Sand, CL, Navarro (2004)
Bibb		3.32	30	Poorly Graded Sand w Silt, SP-SM, Navarro (2004)
Bibb	5.11	9.45	30	Sandy Silt, ML, Navarro (2004)
Effingham		3.24	21	Poorly Graded Sand, SP, Navarro (2004)
Decatur	7.90	9.88	20	Clayey Sand, SC, Navarro (2004)
McIntosh		17.17	33	Clayey Sand w Gravel (shells), SC, Navarro (2004)
SF Bay Mud-CL/0		1.98	155 [1]	Appendix A, WES (Teeter 1987)
SF Bay Mud-CL/0		1.57	183 [1]	Appendix A, WES (Teeter 1987)
SF Bay Mud-CL/0		0.56	232 [1]	Appendix A, WES (Teeter 1987)
SF Bay Mud-CL/15		1.90	140 [1]	Appendix A, WES (Teeter 1987)
SF Bay Mud-CL/15		0.56	156 [1]	Appendix A, WES (Teeter 1987)
SF Bay Mud-CL/15		0.48	210 [1]	Appendix A, WES (Teeter 1987)
SF Bay Mud-CL/40		1.29	108 [1]	Appendix A, WES (Teeter 1987)
SF Bay Mud-CL/40		0.49	142 [1]	Appendix A, WES(Teeter 1987)
SF Bay Mud-CL/40		0.36	185 [1]	Appendix A, WES (Teeter 1987)
SF Bay Mud-CH-2/0		1.37	169 [1]	Appendix A, WES (Teeter 1987)
SF Bay Mud-CH-2/0		0.64	217 [1]	Appendix A, WES (Teeter 1987)
SF Bay Mud-CH-2/0		0.46	270 [1]	Appendix A, WES (Teeter 1987)
SF Bay Mud-CH-2/15		2.03	144 [1]	Appendix A, WES(Teeter 1987)
SF Bay Mud-CH-2/15		0.65	183 [1]	Appendix A, WES (Teeter 1987)
SF Bay Mud-CH-2/15		0.46	220 [1]	Appendix A, WES(Teeter 1987)
SF Bay Mud-CH-2/40		2.06	95 [1]	Appendix A, WES(Teeter 1987)
SF Bay Mud-CH-2/40		0.64	132 [1]	Appendix A, WES (Teeter 1987)
SF Bay Mud-CH-2/40		0.42	171 [1]	Appendix A, WES (Teeter 1987)
Deposited Kaolinite	0.08	0.25	390 [2]	Annular Flume, App. B, Part 1, UF (Teeter 1987)
Deposited Kaolinite	0.08	0.25	390 [2]	Rocking Flume, App. B, Part 1, UF (Teeter 1987)
Deposited Mud	0.18	0.40	773 [2]	Annular Flume, App. B, Part 1, UF (Teeter 1987)
Deposited Mud	0.03	0.20	773 [2]	Rocking Flume, Appendix B, Part 1, UF (Teeter 1987)
Placed Kaolinite		0.25	202 [2]	Annular Flume, App. B, Part 1, UF (Teeter 1987)
Placed Kaolinite		0.28	202 [2]	Rocking Flume, App. B, Part 1, UF (Teeter 1987)
Placed Mud		0.22	200 [2]	Annular Flume, App. B, Part 1, UF (Teeter 1987)
Placed Mud		0.40	200 [2]	Rocking Flume, App. B, Part 1, UF (Teeter 1987)
Placed SF Bay Mud	0.12	0.65	70	Annular Flume, App. B, Part 2, UF (Teeter 1987)

Test No. or Description	Initiation Stress τ_{so} (Pa)	Critical Stress τ_{sc} (Pa)	Moisture content w (%)	Reference
Deposited SF Bay Mud	0.16	0.35	432	Annular Flume, App. B, Part 2, UF (Teeter 1987)
Deposited SF Bay Mud		0.12	432	Rocking Flume, App. B, Part 2, UF (Teeter 1987)
Deposited SF Bay Mud	0.10	0.26	220	Annular Flume, App. B, Part 2, UF (Teeter 1987)
Deposited SF Bay Mud	0.10	0.28	220	Rocking Flume, App. B, Part 2, UF (Teeter 1987)

Notes:
1. Moisture contents calculated based on data given in the paper.
2. Moisture contents calculated based on data given in the paper and an assumed specific gravity of the clay solids (Gs) of 2.65.

Using the values given in Table 7-8 a plot is made of the incipient motion and characteristic bed shear strength values as a function of moisture content as shown in Figure 7-12.
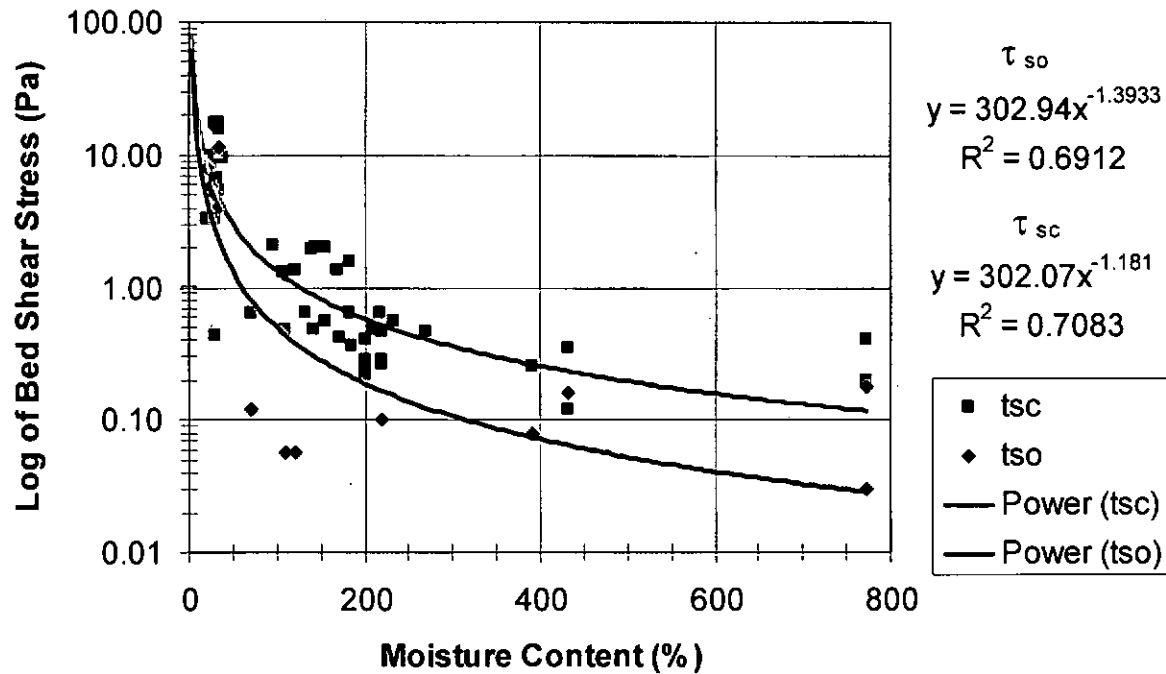
Figure 7-12. Plot of all incipient motion (τ_{so}) and characteristic bed shear strength (τ_{sc}) values from Table 7-8.

One observes from this figure that the critical shear stress values decrease significantly with increasing moisture content. Using standard Excel regression methods, a power law curve fit appears to best match the data. The "best" fits shown in Figure 7-12 give the following relationships:

Bed surface shear strength:

$$\tau_{so} = 302.94(w)^{-1.3933} \tag{7-8}$$

Characteristic bed shear strength:

$$\tau_{sc} = 302.07(w)^{-1.181} \tag{7-9}$$

where the shear stresses τ_{so} and τ_{sc} are in pascals and the moisture content w is in percent.

Applying these generalized relationships (Eq 7-8 and 7-9) to the loading compression analysis of Section 7.2.2, we obtain the following variations of τ_{so} and τ_{sc} for the waste with time in a room (Figure 7-13 and Figure 7-14).
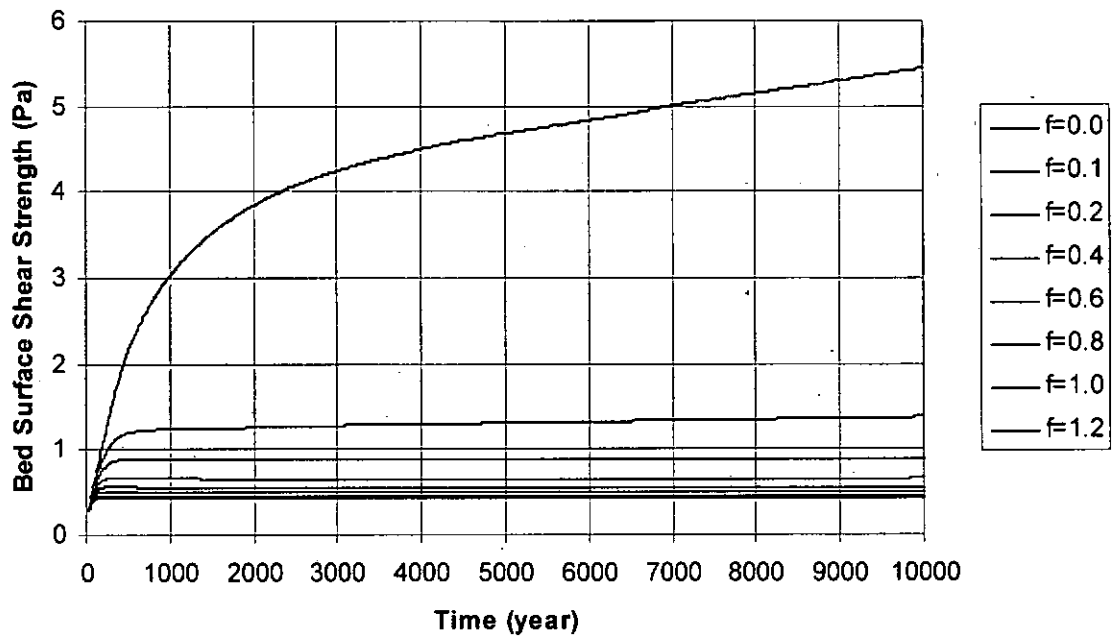
Figure 7-13. Variation of the bed surface shear strength (incipient motion) τ_{so} with time for all the sediment data listed in Table 7-8.
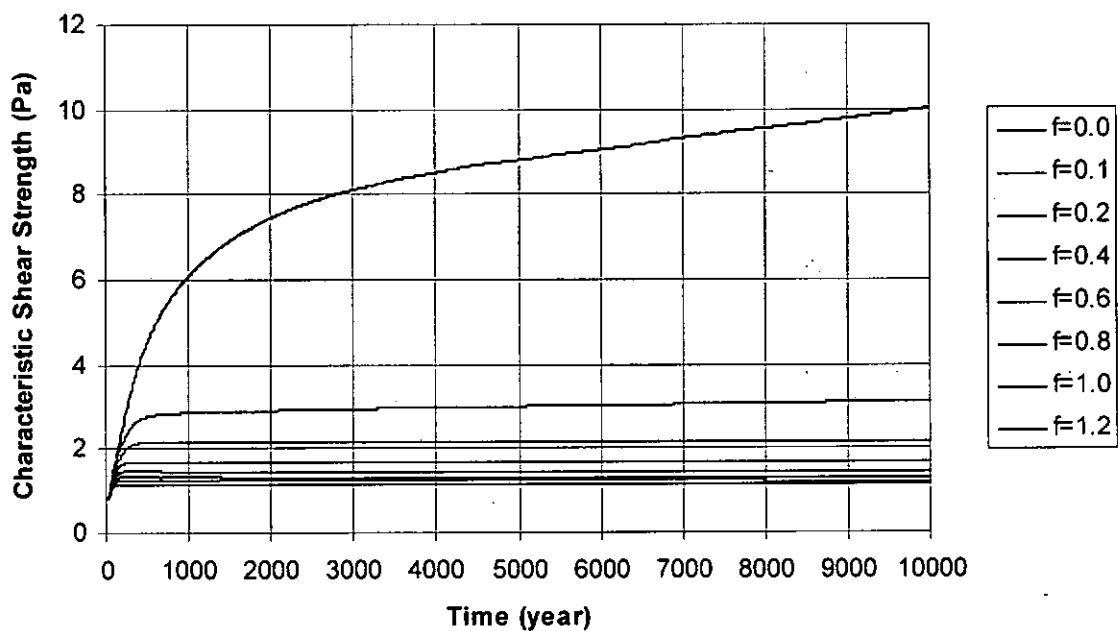
Figure 7-14. Variation of the bed characteristic shear strength τ_{sc} with time for all the sediment data listed in Table 7-8.

A table of values at key times is given in Table 7-9.

Table 7-9. Calculated fit values of bed surface shear strength (τ_{so}) and characteristic bed strength (τ_{sc}) at certain key times for all sediment data in Table 7-8.

time [years]	τ_{so} [Pa]		τ_{sc} [Pa]	
	f = 0.0	f = 1.2	f = 0.0	f = 1.2
0	0.29	0.29	0.82	0.82
100	0.64	0.42	1.63	1.13
10,000	5.45	0.42	10.02	1.15

Comparing the shear strengths between the San Francisco Bay mud erosion tests (Figure 7-9, Figure 7-10, and Table 7-7) with the combined results of all the sediments in our literature review (Figure 7-13, Figure 7-14, and Table 7-9) it is seen that the bay mud data are in all cases slightly less than the general case. The lowest strength values are obtained for the highest gas generation rate case $f = 1.2$. For this case, the gases generated by microbial activity and by anoxic corrosion resist the ability of the salt to creep into the room and compress the waste stack. Therefore, there is less primary compression of the waste which would lower its porosity or void ratio.

Concerning the key times chosen in Table 7-7 and Table 7-9, time = 0 years is not of interest because no degradation of the waste is expected to have occurred. However, it does represent the lowest possible value the waste shear strengths could have since it assumes no compression. It is worthy to note that the lowest value of the characteristic bed strength is $\tau_{sc} = 0.40$ Pa, which is about eight times the presently used value of 0.05 Pa. One hundred years is of great interest because that is the end of institutional control of WIPP. It is not expected that the waste at that time will have completely degraded to the point that its characteristics resemble a mud or clay, however some unknown degree of degradation will have taken place. Ten thousand years represents the end of the regulatory period of WIPP. The greatest degree of compression and degradation of the waste will have taken place by this time. With no gas generation, the only resistance to the creeping salt is from the waste stack. With gas generation, the salt is resisted by both the waste and the gas pressure. For $f = 1.2$, there is virtually no difference between the shear strength values at 100 years and those at 10,000 years.

7.3 Effect of Secondary Compression on the Physical Properties of the Waste if Modeled as a Sediment

For secondary compression of soils, the magnitude is found from the following relationship (Das 1983, Eq. 5.87)

$$\frac{\Delta H_t}{H_t} = C_\alpha \left(\log_{10} t_2 - \log_{10} t_1 \right) \tag{7-10}$$

Where, C_α is the secondary compression index. It is the slope line as shown below in Figure 7-15.
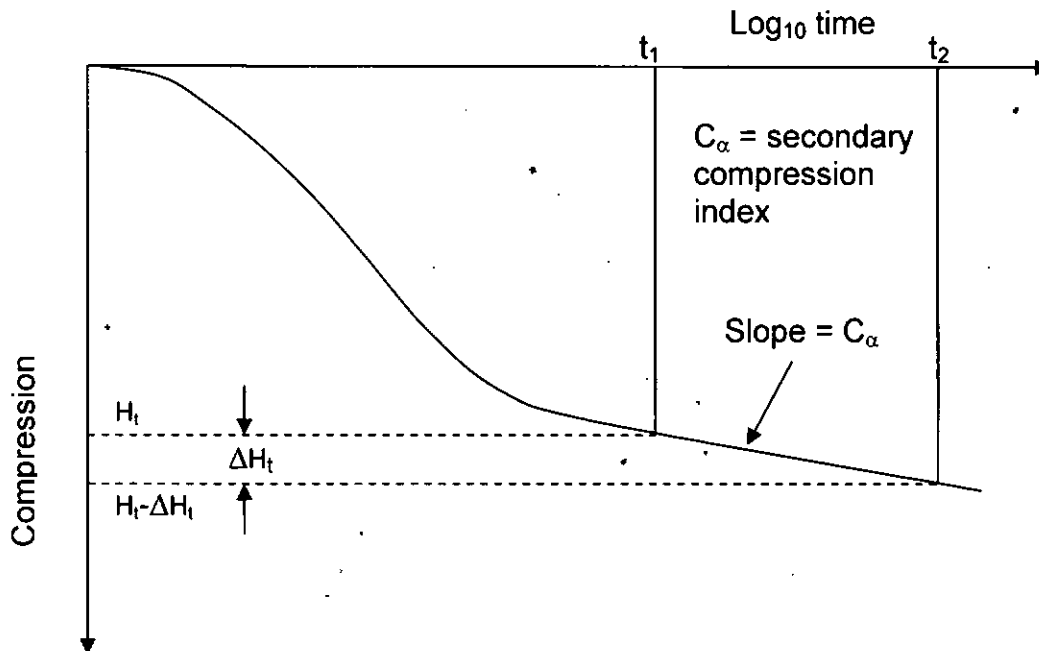
Figure 7-15. Schematic of soil behavior for secondary compression.

Eq. 7-10 can be simplified and expressed in terms of the void ratio as:

$$\Delta e = C_\alpha \left(1 + e_o \right) \log_{10} \frac{t_2}{t_1} \tag{7-11}$$

where Δe is the change in void ratio and e_o is the initial void ratio at t_1. Typical values for C_α are given below in Table 7-10.

For purposes of calculation, we assume that secondary compression begins at time $t_o = 1$ and continues through the repository life of 10,000. For illustrative purposes, we will model the waste with the extreme values for Lambe and Whitman Case 1 and Das Case 6 from Table 7-10. The initial porosity (ϕ_o) of the emplaced waste is 68.2% (Butcher 1997). One can convert porosity to void ratio using Eq 7-9 giving an initial void volume of the waste would be $e_o = 2.14$. Table 7-11 lists the void ratio and porosities based on secondary compression of the waste at certain times. The void ratio values are plotted in Figure 7-16. There is only a small change in the void ratio (3%) over the life of the repository for $C_\alpha = 0.005$, but a fairly significant change

(37%) for $C_\alpha = 0.064$. When transformed to porosities, the changes are much smaller. The change in porosity for $C_\alpha = 0.005$ is 0.95% and for $C_\alpha = 0.064$ is 16%.

Table 7-10. Typical secondary compression index values, C_α.

Lambe and Whitman 1979, Table 27.2, p. 420		
Case	C_α	Soil description
1	0.005 to 0.02	Normally consolidated clays
2	0.03 or higher	Very plastic soils, organic soils
3	Less than 0.001	Precompressed clays with OCR > 2
Das 1983, Table 5.3, p. 296 [1]		
Case	C_α	Secondary compressibility
1	< 0.002	Very low
2	0.004	Low
3	0.008	Medium
4	0.016	High
5	0.032	Very high
6	0.064	Extremely high

1. Das also presents a figure of C_α vs. moisture content.

Table 7-11. Void ratios and porosities calculated for secondary compression index values of $C_\alpha = 0.005$, 0.02, and 0.064 over the 10,000 repository period.

Time (years)	Void Ratio, e Secondary Compression Index			Porosity, ϕ Secondary Compression Index		
	$C_\alpha = 0.005$	$C_\alpha = 0.02$	$C_\alpha = 0.064$	$C_\alpha = 0.005$	$C_\alpha = 0.02$	$C_\alpha = 0.064$
1	2.14	2.14	2.14	0.682	0.682	0.682
10	2.12	2.08	1.94	0.680	0.675	0.660
100	2.11	2.01	1.74	0.678	0.668	0.635
1000	2.09	1.95	1.54	0.677	0.661	0.606
2000	2.09	1.93	1.48	0.676	0.659	0.596
5000	2.08	1.91	1.40	0.676	0.656	0.583
10000	2.08	1.89	1.34	0.675	0.654	0.572
% change from $t_o = 1$ yr	2.93	11.74	37.56	0.95	4.06	16.08
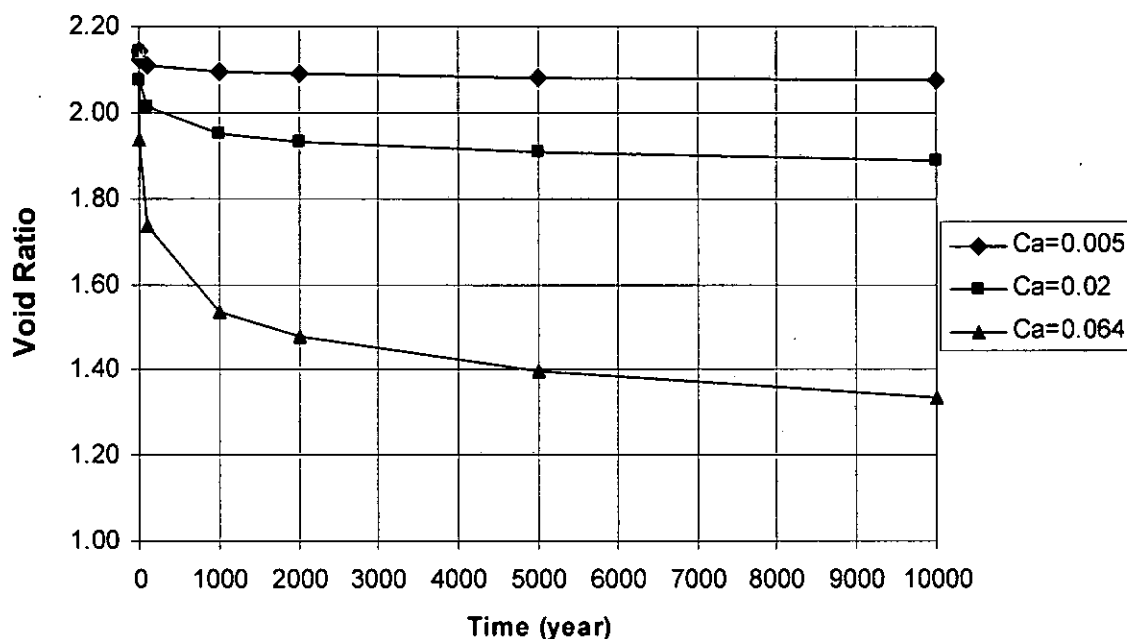
Figure 7-16. Void ratios given in Table 7-11 plotted as a function of time.

For our purposes, the change in bulk wet density (BWD) and water content (w) of the waste over time is more important. From the porosity, the bulk wet density and water content of the material can be calculated from Eq 7-4 and Eq 7-5, respectively. Table 7-12 lists the changes that would occur in the waste for these two parameters over the 10,000 year span of the repository for the three values of C_α.

Table 7-12. Water contents and bulk wet densities of the waste calculated for secondary compression index values of $C_\alpha = 0.005$, 0.02, and 0.064 over the 10,000 repository period.

Time (years)	Moisture Content, w			Bulk wet density, BWD [kg/m³]		
	Secondary Compression Index			Secondary Compression Index		
	$C_\alpha = 0.005$	$C_\alpha = 0.02$	$C_\alpha = 0.064$	$C_\alpha = 0.005$	$C_\alpha = 0.02$	$C_\alpha = 0.064$
1	1.482	1.482	1.482	1389.0	1389.0	1389.0
10	1.472	1.439	1.343	1389.8	1392.5	1400.7
100	1.461	1.395	1.204	1390.7	1396.1	1414.2
1000	1.450	1.352	1.065	1391.6	1399.9	1429.8
2000	1.447	1.339	1.023	1391.8	1401.1	1435.0
5000	1.442	1.322	0.968	1392.2	1402.7	1442.3
10000	1.439	1.308	0.926	1392.5	1403.9	1448.1
% change from t_o = 1 yr	2.93	11.74	37.56	-0.25	-1.08	-4.26

7.4 Combined Effect of Loading and Secondary Compression on Waste Shear Strength

The combined effect of loading and secondary compression of the waste if it is modeled as behaving as a sediment was determined for the extreme gas generation cases of $f = 0.0$ and 1.2. The effect of loading compression was determined in Section 7.2 based on the creep of salt. Secondary compression occurs with time due to plastic adjustment of the soil fabrics. It is determined by the secondary compression index and the time which passes. How secondary compression affects the physical properties of the waste was considered in Section 7-3.

In order to determine the combined effects of loading and secondary compression on the muds, the porosity was calculated at each time step used in SANTOS. The degree of loading compression changes with the stress condition in the room due to creeping salt and gas generation. To that was superimposed the change in porosity due to secondary compression as determined by the method outlined in Section 7.3. The porosity of the waste was determined from the total porosity change due to both loading and secondary compression. From the porosity, density of the brine, and density of the solids the bulk wet density of the waste can be calculated.

It was seen in Section 7.2 that the most conservative choice for loading compression occurred for the case of $f = 1.2$. At this gas generation factor, according to our SANTOS modeling, the least compression of the waste stack has occurs.

The question is what to use for C_α. Das (2006) gives the relationship of C'_α and water content in Figure 7-17 where

$$C'_\alpha = \frac{C_\alpha}{1 + e_p} \tag{7-12}$$

where e_p is the void ratio at the beginning of secondary compression. We assume that the waste behaves similar to ocean bay mud or montmorillonite clay and so secondary compression is superimposed on the effect of loading compression over the entire regulatory span of the repository. Using that model, the initial void ratio is $e_p = 2.14$, porosity $\phi = 68.2\%$, water content $w = 148\%$ (based on brine with fluid density $\rho_w = 1217$ kg/m^3 and waste with solid density $\rho_s = 1757$ kg/m^3), and $t_l = 1$.
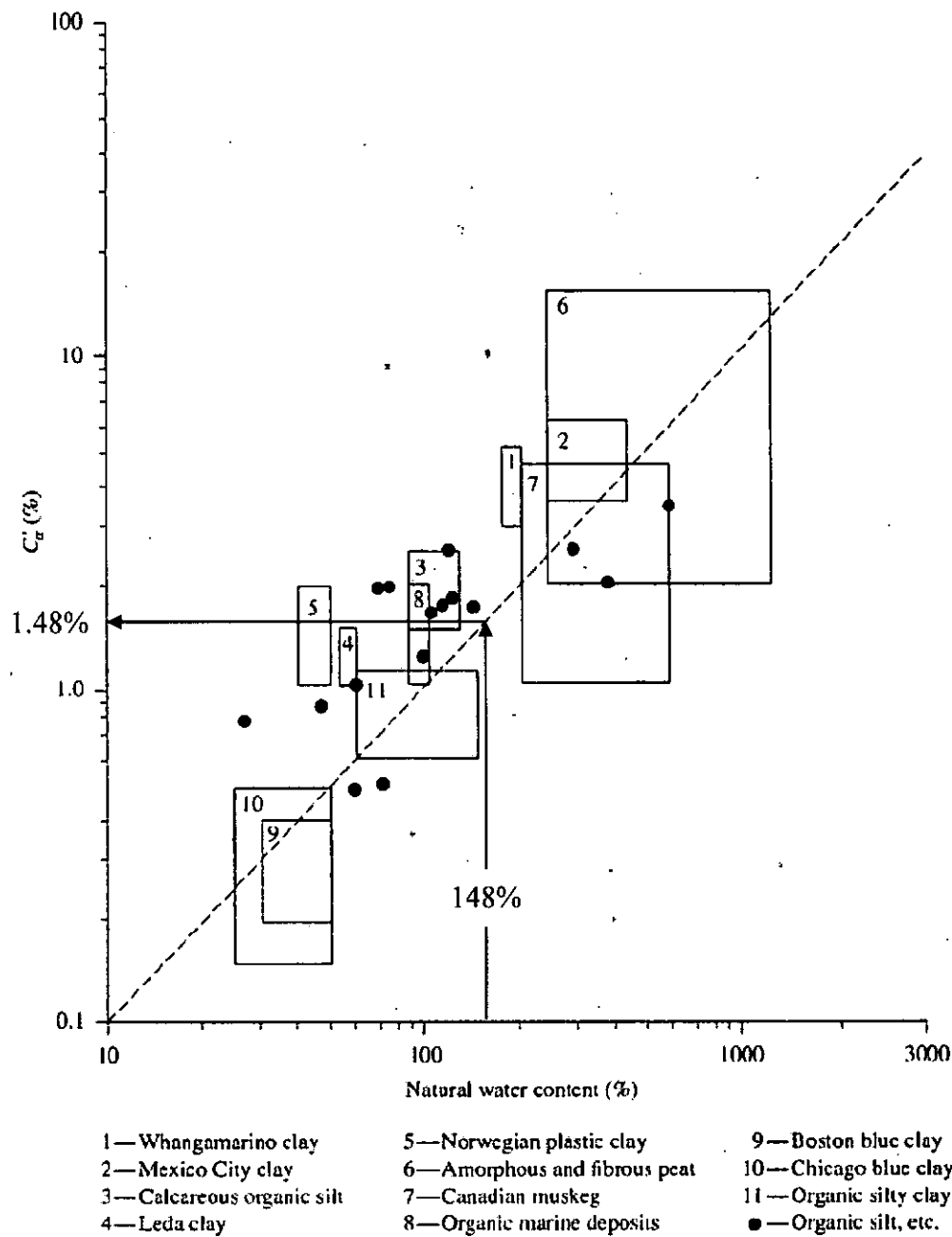
Figure 7-17. Relationship between C_α' and water content (Das 2006 Figure 10.27).

The relationship between C_α' and w is very well represented by

$$C_\alpha' = 0.01w \qquad (7\text{-}13)$$

where both C_α' and w are in percent. Using the values listed above, namely $w = 148\%$, Eq. 7-13 gives $C_\alpha' = 1.48\%$ and thus from Eq. 7-12 $C_\alpha = 0.046$.

The combined effects of loading and secondary compression were applied to the case where $f =$ 1.2. Below are plots of the various shear strength relationships we have used throughout this paper. These include the two material specific relationships between τ_c and BWD as determined in Teeter (1987) for San Francisco Bay muds and the general relationships derived in this paper between τ_{so} and w and τ_{sc} and w based on our literature survey. For reference, also shown on the plots are the curves for loading compression due to the salt creep only ("Salt creep").

In general, the effect of secondary compression on the shear strength can be quite large over the 10,000 year regulatory period. The controlling factor in the secondary compression is the relatively high initial porosity or void ratio of the waste.
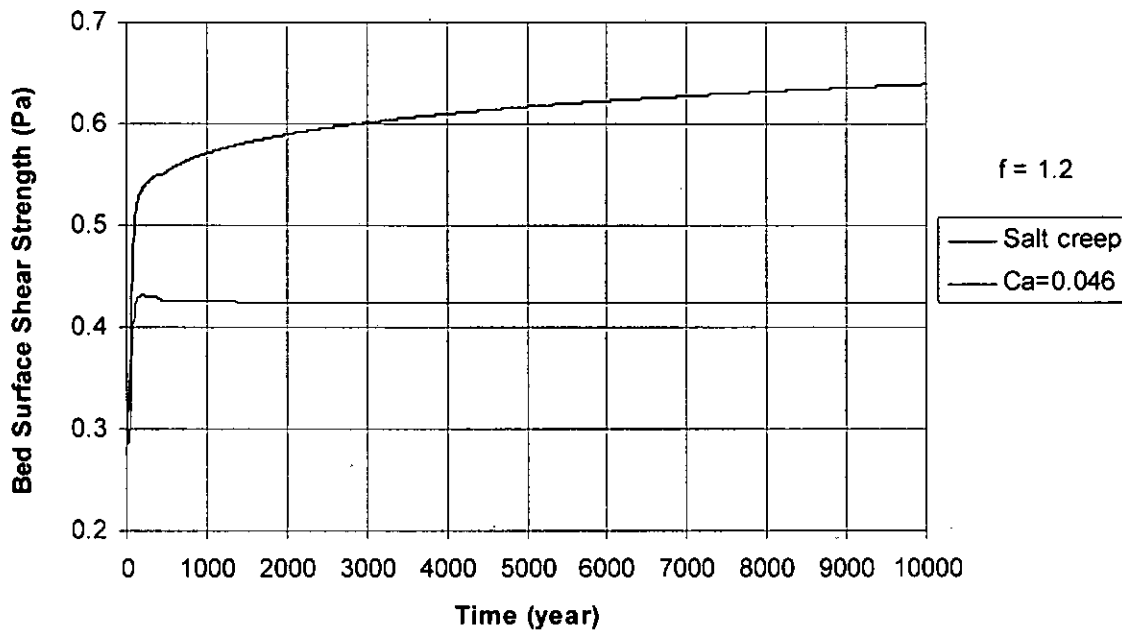
Figure 7-18. Variation of bed surface shear strength, τ_{so}, for all sediments (Table 7-8) when loading and secondary compression are both considered for the case of f = 1.2. Loading compression due to the salt creep only ("Salt creep") is shown for reference.
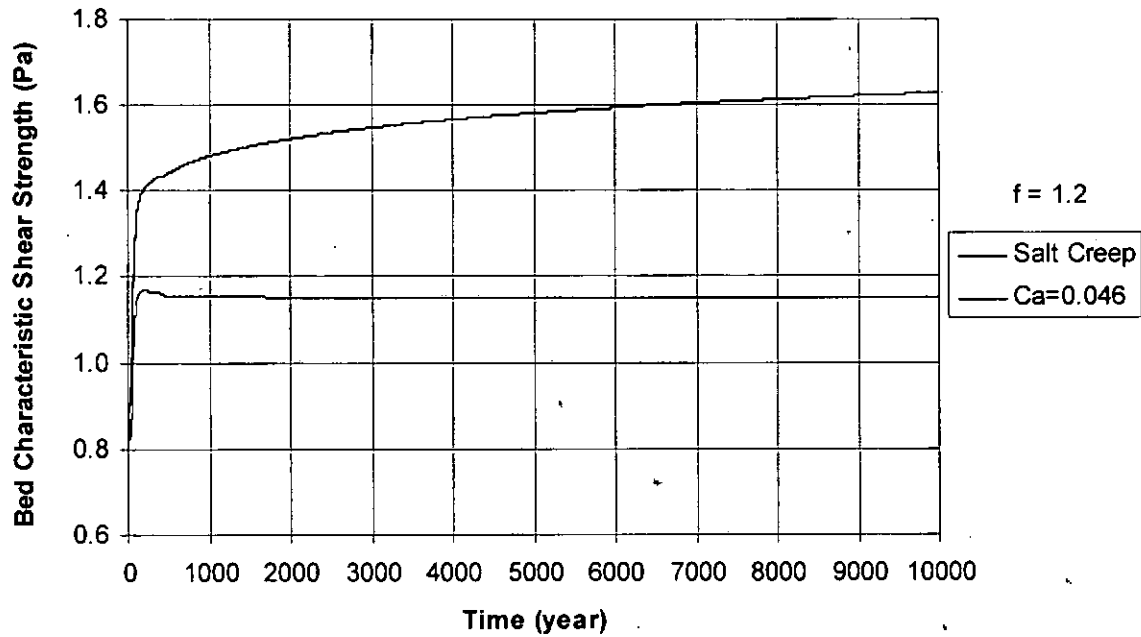
Figure 7-19. Variation of bed characteristic shear strength, τ_{sc}, for all sediments (Table 7-8) when loading and secondary compression are both considered for the case of $f = 1.2$. Loading compression only due to salt creep ("Salt creep") is shown for reference.
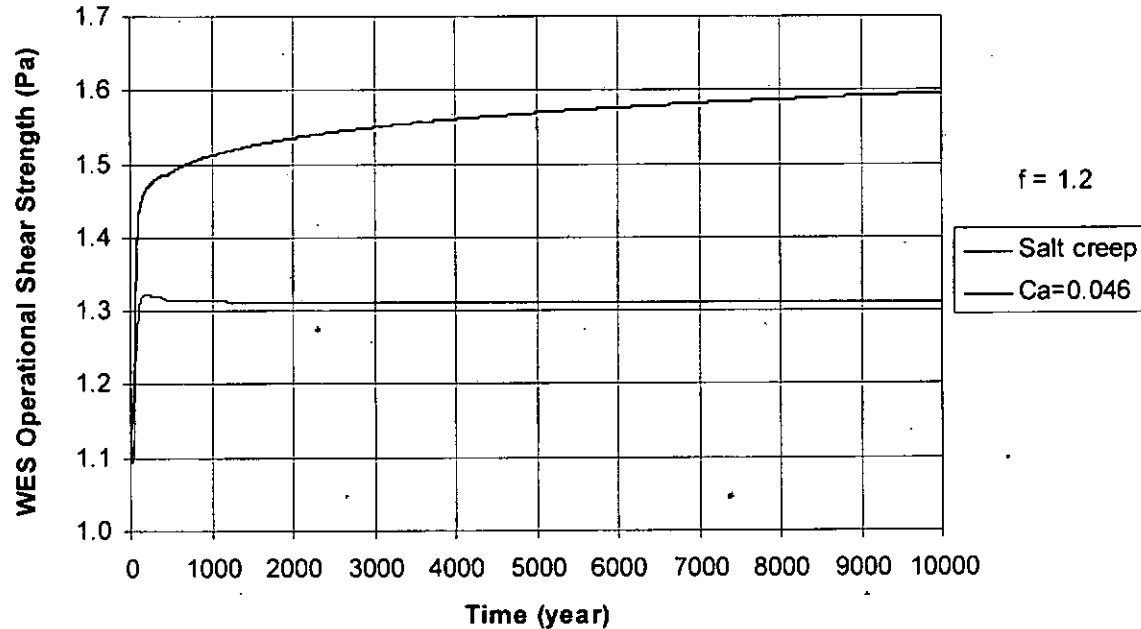
Figure 7-20. Variation of operational shear strength, τ_c, using relationship derived from WES experiments when loading and secondary compression are both considered for the case of $f = 1.2$. Loading compression only ("Salt Creep") is shown for reference.
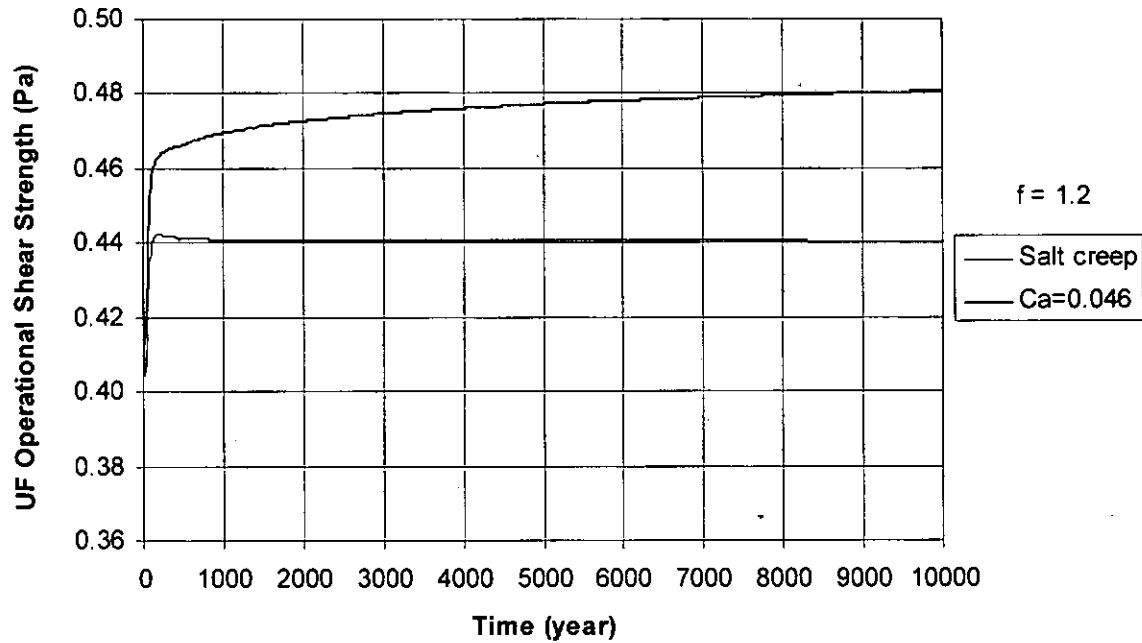
Figure 7-21. Variation of operational shear strength, τ_c, using UF derived relationship when loading and secondary compression are both considered for the case of $f = 1.2$. Loading compression due to salt creep only ("Salt creep") is shown for reference.

8 Waste Permeability the Probability of Stuck Pipe / Gas Erosion

Stuck pipe and gas erosion are postulated to occur if the waste permeability is less than 10^{-16} m^2 and if gas pressure conditions are met: if the gas pressure exceeds 8 MPa, gas erosion can occur and if it exceeds 10 MPa, stuck pipe can occur (Butcher 1995). In the CCA, the DOE assigned a value of 1.7×10^{-13} m^2 for the permeability of the waste based on the permeabilities of the waste components (DOE 1996, App. WCA, Sec. WCA.5.2.3). Since this value is greater than that which would cause gas erosion or stuck pipe to occur, the DOE did not model these processes. The results of the CCA showed that total releases are dominated by short term releases associated with inadvertent drilling intrusions into the waste and attention was shifted to examining these by Hansen et al. (1997).

9   Summary and Recommendation

9.1   Summary

This paper has reexamined the lower limit of the waste shear strength as it is applied in the cavings model of the code CUTTINGS_S. The shear strength parameter used in WIPP PA is BOREHOLE : TAUFAIL. The lower limit of the range of values used for TAUFAIL is presently set at 0.05 Pa. It was based on the shear stress required to cause incipient motion in a San Francisco Bay mud (Partheniades and Paaswell 1970). This paper has looked at this value from a number of different view points and found this value to be too.

In the time of the CCA, it was recognized that the particle size of the degraded waste was unknown. The particle size is known to influence the ability of sediment to erode – the greater the particle size, the more resistant the sediment is to erosion. The EPA required the DOE to conduct an expert panel evaluation of the anticipated particle based on the best available knowledge (Trovato 1997a, b). The EPA also accepted the findings of the expert panel, and therefore accepted the objective of the elicitation: to provide knowledge of the future state of the waste. The DOE applied the results in a Shield's diagram to determine the shear strength for incipient motion, another term for the beginning of surface erosion, and obtained a range 0.64 to 77 Pa. However, only the upper bound was accepted. The lower bound was rejected in favor of the more conservative value based on San Francisco Bay mud (EPA 1998).

The paper also examines the use of applying erosion test results to the waste. It was noted that the use of the values obtained for incipient motion are not the values that should be used for the waste. The value of shear strength for incipient motion, which is denoted by τ_{so} in this paper, is a surface phenomenon that concerns only the first few millimeters or centimeters of the sediment. The flow direction that gives rise to this value is across the surface, which is why τ_{so} is often referred to as the bed surface shear strength. On the other hand, a drill penetrating the waste will drill in a direction that penetrates the depths of the waste. In this case, the erosion will be occurring on a more dense material within the waste mass which is more able to resist erosion. In erosion experiments, Partheniades (1965) and Parchure and Mehta (1985) noted that there is a specific bed shear stress beyond which erosion of the bed at depth takes place. They refer to this as the characteristic shear strength of the bed (τ_{sc}) as it represents the behavior of the bed material, not a few loose grains on the bed surface. Typical erosion test results can be well represented by two lines (a piecewise linear fit) where the intersection of the two lines represents τ_{sc} (see Figure 3-3). The characteristic shear strength of the bed is a minimum value for the bed mass as a whole. Deeper into the bed, the density increases and the ability of the bed to resist erosion continues to increase. In laboratory experiments, the bed seems to reach a maximum value. This maximum value is thought to be an experimental remnant rather than something found in the field. The value of the shear strength proposed for the waste in this paper should be represented by the bed characteristic shear strength value, not the value of incipient motion of the surface.

Since the currently accepted model for the erosion behavior of the waste is based on San Francisco Bay mud, more data was obtained rather than the one test set upon which the parameter was initially based. The US Army Corp of Engineers had performed a much more

extensive study of San Francisco Bay muds (Teeter 1987). For this study, two laboratories were used to perform the work, one at the Waterways Experimental Station (WES) and the other at the University of Florida (UF). The investigators included the initial experiments in their analysis. They suggested the use of yet another shear strength measure which they called the operational shear strength. We use their notation and denote this value by τ_c. The data from WES showed a much greater dependence of τ_c on the bulk wet density of the material, but both the WES and UF results confirmed that the shear strength of sediment is dependent on its bulk wet density. It has been confirmed many times that as the bulk wet density increases, or the water content decreases, the shear strength of a material goes up. In general, the best fitting type of curve is a power law fit. The results of the USACE investigation are given in Eqs 6-5 and 6-7. The operational shear strengths are 1.09 and 0.40 Pa for WES and UF, respectively.

In this paper we also present the results of some erosion experiments performed on surrogate waste materials developed for the spallings model. This material was developed in a logical and systematic fashion based on the expected WIPP waste inventory and consistent with future repository conditions. The analyses of Jepsen et al (1998b) and this paper are in Table 5-3. The 100% degraded waste was weaker than the 50% degraded, however in neither case was the value of τ_{so}, which we do not recommend using, less than 0.2 Pa. The best measure of the surrogate waste material shear strength is the operational shear strength. On average, as reported by Jepsen et al. (1998b), $\tau_c = 0.29$ and 1.41 Pa for the 100% and 50% degraded wastes, respectively.

This paper looked at the results from a fairly large body of data found in the literature. The results were divided into those for incipient motion (surface erosion) and those for the bed characteristic shear strength. In practice there is no standard for running erosion tests or reporting their results. In Section 7.2.3.2 we simply labeled any results that were not reported as incipient motion (τ_{so}) as under the broad category characteristic shear strength (τ_{sc}). This is conservative in that all methods of analysis of erosion data will yield results less than or equal to the τ_{sc} as defined by Partheniades (1965) and Parchure and Mehta (1985). The results of this generalization can be described by two power law curves, one for τ_{so} (Eq 7-8) and one for τ_{sc} (Eq 7-9). Using these relationships we obtain $\tau_{so} = 0.29$ Pa and $\tau_{sc} = 0.82$ Pa for the natural water content of the waste of $w = 148\%$.

A summary of the results of different studies for waste in its uncompressed condition is given in Table 9-1.

Table 9-1. Compilation of results from various analyses conducted in this paper on WIPP waste in an uncompressed state if its erosion behavior is similar to a bay mud or montmorillonite clay.

	τ_{so} [Pa]	τ_c [Pa]	τ_{sc} [Pa]
Expert elicitation	0.64		
SF Bay mud – WES		1.09	
SF Bay mud – UF		0.40	
Surrogate material 100% degraded	0.24	0.29 (Jepsen et al. 1998b)	0.58
Surrogate material 50% degraded	0.47	1.41 (Jepsen et al. 1998b)	1.98
Literature review	0.29		0.82

In the repository, however, the salt will creep into a room and compress the waste. In addition, the degraded waste will also undergo a time-dependent secondary compression. The creep of the salt will be resisted by gas pressure generated from microbial activity and anoxic corrosion.

In order to assess the impact of loading compression, we used the structural code SANTOS to determine the change of porosity of the waste with time. The waste is modeled as deforming in accordance to the experimental relationship determined by Butcher et al (1990). The time-dependent effects of secondary compression were superimposed on the loading compression results.

The most conservative case is for the gas generation factor f = 1.2. This is the maximum gas generation factor ever obtained in BRAGFLO based on the PABC analysis. In this case, the waste undergoes the least amount of compression from the creeping salt. The results of how compression affect the waste shear strength is summarized in Table 9-2 below for the key times of 0, 100, and 10000 years. The results were fit to the relationships from the USACE (Teeter 1987) for San Francisco Bay mud and our literature review.

Table 9-2. Effects of compression on waste shear strength according to the relationships given by the US Army Corps of Engineers for San Francisco Bay mud and our literature survey at certain key times.

	t = 0 years		t = 100 years		t = 10,000 years	
	τ_{so} [Pa]	τ_c or τ_{sc} [Pa]	τ_{so} [Pa]	τ_c or τ_{sc} [Pa]	τ_{so} [Pa]	τ_c or τ_{sc} [Pa]
Loading compression only						
SF Bay mud – WES		1.09		1.30		1.31
SF Bay mud – UF		0.40		0.44		0.44
Lit total	0.29	0.82	0.42	1.14	0.42	1.15
Loading and secondary compression						
SF Bay mud – WES		1.09		1.42		1.60
SF Bay mud – UF		0.40		0.46		0.48
Lit total	0.29	0.82	0.51	1.33	0.63	1.63

9.2 Recommendation

The Conceptual Models Peer Review Panel (DOE 1996, Appendix Peer, Peer 1, Conceptual Models Peer Review Report (July 1996)) said that,

> Among the basic assumptions made for the fluid flow calculations is that, in the absence of experimental data, the effective shear resistance to erosion of the repository waste is similar to ocean bay mud or montmorillonite clay.

Since that time the erosional model for the waste has been San Francisco Bay mud in spite of an expert panel providing what was believed to be knowledge of the future state of the waste.

For our recommendation we will remain in accord with modeling the waste as "similar to ocean bay mud or montmorillonite clay." In so doing, since these materials will undergo both loading and secondary compression, we recommend including those effects. In addition, we recommend using the bed characteristic shear strength (τ_{sc}) as it is more representative of the repository situation in which a drill penetrates through the degraded material thickness. We also recommend using the entirety of the experimental data for erosional tests covered in our literature review as this is more representative of general soil behavior rather than a specific site such as San Francisco Bay. We also recommend that the case of $f = 1.2$ be used as it represents the most conservative case in that the least amount of loading compression occurs.

Finally, we also recommend using the state of the material as it would be found at 100 years, the end of institutional controls. For any time after that, the waste will under go further compression and the shear strength will increase.

We therefore recommend a lower limit value for BOREHOLE : TAUFAIL of 1.33 Pa as given in the last line of Table 9-2 for τ_{sc} "Lit total" at 100 years.

In addition, we recommend changing the distribution from loguniform to uniform. The new distribution spans less than two orders of magnitude, i.e.

$$\log_{10}\left(\frac{77}{1.33}\right) = 1.76$$

(9-1)

The use of a uniform distribution is appropriate when all that is known about a parameter is its range, as is the case here for TAUFAIL. The uniform distribution is the maximum entropy distribution under these circumstances. Loguniform distributions are appropriate for parameters that span many orders of magnitudes (Tierney 1996).

10 References

Arguello, J. G. and J. F. Holland, 1996. *SANTOS – Verification and Qualification Document*, Sandia National Laboratories, Carlsbad, NM. ERMS 235675.

Berglund, J.W. 1992. *Mechanisms Governing the Direct Removal of Wastes from the Waste Isolation Pilot Plant Repository Caused by Exploratory Drilling.* Sandia National Laboratories, Albuquerque, NM. SAND92-7295.

Berglund, J.W. 1996. *Parameters required for the CUTTINGS_S code for use in WIPP Performance Assessment.* Sandia National Laboratories, Carlsbad, NM. ERMS 236766.

Brush, L.H. 2005 *Results of Calculations of Actinide Solubilities for the WIPP Performance Assessment Baseline Calculations.* Sandia National Laboratories, Carlsbad, NM. ERMS 539800.

Buffington, J.M. 2007. Re: Critical shear strengths. E-mail sent to C. Herrick, February 22, 2007. ERMS 545763.

Buffington, J.M. and D.R. Montgomery. 1997. A systematic analysis of eight decades of incipient motion studies, with special reference to gravel-bedded rivers. *Water Resources Research,* vol. 33, no. 8, pages 1993-2029. ERMS 545812.

Butcher, B.M. 1994. *A Model for Cuttings Release Waste Properties.* Memorandum to distribution. January 6, 1994. Sandia National Laboratories, Albuquerque, NM. ERMS 309846.

Butcher, B.M. 1997. *A Summary of the Sources of Input Parameter Values for the WIPP Final Porosity Surface Calculations.* Sandia National Laboratories, Albuquerque, NM SAND97-0796.

Butcher, B. M., T. W. Thompson, R. G. van Buskirk, and N. C. Patti. 1990. *Mechanical Compaction of WIPP Simulated Waste.* Sandia National Laboratories, Albuquerque, NM. SAND90-1206.

Butcher, B.M., S.W. Webb, J.W. Berglund, and P.R. Johnson. 1995. *Systems Prioritization Method – Iteration 2. Baseline Position Paper: Disposal Room and Cuttings Models, Vol. 1*. Sandia National Laboratories, Carlsbad, NM. ERMS 228729.

Cao, Z., G. Pender, and J. Meng. 2006. Explicit formulation of the Shields diagram for incipient motion of sediment. *Journal of Hydraulic Engineering,* vol. 132, iss. 10, pp. 1097-1099. ERMS 545813.

Clayton, D. 2007. Maximum moles of gas produced in the PABC results. Memo to C. Herrick. Sandia National Laboratories, Carlsbad, NM. ERMS 545480.

CTAC (Carlsbad Area Office Technical Assistance Contractor). 1997. *Expert Elicitation on WIPP Waste Particle Diameter Size Distribution(s) During the 10,000-year Regulatory Post-closure Period: Final Report.* U.S. Department of Energy – Carlsbad Area Office, Carlsbad, NM. ERMS 541365.

Das, B.M. 1983. *Advanced Soil Mechanics.* McGraw-Hill Book Company, New York.

Das, B.M. 2006. *Principles of Geotechnical Engineering, 6th ed.* Thomson (Publisher), Ontario, Canada.

DOE (U.S. Department of Energy). 1996. *Title 40 CFR Part 191 Compliance Certification Application for the Waste Isolation Pilot Plant.* DOE/CAO-1996-2184. October 1996.

EPA (U.S. Environmental Protection Agency), 1998. *Technical Support Document for Section 194.23: Parameter Justification Report.* Docket A-93-02, V-B-14. ERMS 525159.

Hansen, F.D. 2005. A Revisit of Waste Shear Strength. Sandia National Laboratories, Carlsbad, NM. ERMS 541354.

Hansen, F.D., M.K. Knowles, T.W. Thompson, M. Gross, J.D. McLennan, J.F. Schatz. 1997. *Description and Evaluation of a Mechanistically Based Conceptual Model for Spall.* Sandia National Laboratories, Albuquerque, NM. SAND97-1369.

Hansen, F.D., T.W. Pfeifle, and D.L. Lord. 2003. *Parameter Justification Report for DRSPALL.* Sandia National Laboratories, Albuquerque, NM. SAND2003-2930.

Jepsen, R., J. Roberts, and W. Lick. 1997. Effects of bulk density on sediment erosion rates. *Water, Air, and Soil Pollution,* vol. 99, pp. 21-31. ERMS 252718.

Jepsen, R., J. Roberts, and W. Lick. 1998a. Long Beach harbor sediment study. US Army Corps of Engineers, Los Angeles District, Los Angeles, CA. Report DACW09-97-M-0068. ERMS 545814.

Jepsen, R., J. Roberts, and W. Lick. 1998b. Development and Testing of Waste Surrogate Materials for Critical Shear Stress. Sandia Contract AX-9022. Dept. of Mechanical and Environmental Engineering, University of California-Santa Barbara. ERMS 533809.

Jepsen, R., J. Roberts, A. Lucero, and M. Chapin. 2001. Canaveral ODMDS Dredged Material Erosion Rate Analysis. Sandia National Laboratories, Albuquerque, NM. SAND2001-1989.

Julien, P.Y. 1998. *Erosion and Sedimentation.* Cambridge University Press, Cambridge, U.K.

Kirkes, R. and C.G. Herrick. 2006. Analysis plan for the modification of the waste shear strength parameter and direct brine release parameters: AP-131, rev. 0. Sandia National Laboratories, Carlsbad, NM. ERMS 545130.

Kruger, M. 1997. Performance assessment parameter values identified in EPA letters, dated April 17 and 25, 1997, to DOE. Docket A-93-02, II-I-33.

Lambe, T.W. and R.V. Whitman. 1979. *Soil Mechanics, SI Version.* John Wiley and Sons, New York.

Mehta, A.J., T.M. Parchure, J.G. Dixit, and R. Ariathurai. 1982. Resuspension potential of deposited cohesive sediment beds. *Estuarine Comparisons.* V.S. Kenedy, ed. Academic Press, New York, N.Y. pp. 591-609. ERMS 545815.

Mellegard, K. 1998. Fabrication of Surrogate Waste Bricks for Erosion Studies: Laboratory Notebook (Volume 1 of 1). RSI Job 325 Task 20.1. Sandia National Laboratories Contract No. AG-4911. RESPEC, Rapid City, SD. ERMS 251625.

Munson, D.E. and P.R. Dawson. 1982. A Transient Creep Model for Salt During Stress Loading and Unloading. Sandia National Laboratories, Albuquerque, NM. SAND82-0962.

Munson, D.E., A.F. Fossum, and P.E. Senseny. 1989. *Advances in Resolution of Discrepancies between Predicted and Measured, In Situ Room Closures.* Sandia National Laboratories, Albuquerque, NM. SAND88-2948.

Navarro, H.R. 2004. *Flume Measurements of Erosion Characteristics of Soils at Bridge Foundations in Georgia.* MS Thesis, Civil Engineering. Georgia Institute of Technology. ERMS 545816.

Parchure, T.M. and A.J. Mehta. 1985. Erosion of soft sediment deposits. *Journal of Hydraulic Engineering,* vol. 111, no. 10, 1308-1326. ERMS 545817.

Park, B.Y. and J.F. Holland. 2003. *Structural Evaluation of WIPP Disposal Room Raised to Clay Seam G.* Sandia National Laboratories, Albuquerque, NM. SAND2003-3409. An associated document is: Park, B.Y. and J.F. Holland. 2006. *Error in DRZ calculation in the Clay Seam G analysis.* Sandia National Laboratories, Carlsbad, NM. ERMS 545053.

Park, B.Y. and T.B. Kirchner. 2004, *PA Run Control Summary for Porosity Surface Calculations of the Disposal Room using SANTOS.* Sandia National Laboratories, Carlsbad, NM. ERMS 536847.

Partheniades, E. 1962. *A Study of Erosion and Deposition of Cohesive Soils in Salt Water.* PhD thesis. University of California, Berkeley, California. ERMS 545818.

Partheniades, E. 1965. Erosion and deposition of cohesive soils. *Journal of the Hydraulics Division, Proceedings of the American Society of Civil Engineers,* vol. 91. no. HY1, pp. 105-139. ERMS 545819.

Partheniades, E. and R. E. Paaswell. 1970. Erodibility of Channels with Cohesive Boundary. *Journal of the Hydraulics Division, Proceedings of the American Society of Civil Engineers,* vol. 96. no.HY3, pp. 755-771. ERMS 241125.

Peake, T. 1997. Shear resistance to erosion (TAUFAIL). Facsimile to G. Basabilvazo. April 28, 1997. ERMS 545768.

Roberts, J., R. Jepsen, D. Gotthard, and W. Lick. 1998. Effects of particle size and bulk density on erosion on quartz particles. *Journal of Hydraulic Engineering,* vol. 124, no. 12, pp. 1261-1267. ERMS 252966.

Sargunam, A., P. Riley, K. Arulanandan, and R.B. Krone. 1973. Physico-chemical factors in erosion of cohesive soils. *Journal of the Hydraulics Division, Proceedings of the American Society of Civil Engineers,* vol. 99, no. HY3, 555-558. ERMS 241126

Simon, D.B. and F. Senturk. 1992. *Sediment Transport Technology: Water and Sediment Dynamics.* Sedimentation Engineering Manual No. 54. American Society of Civil Engineers, Water Resources Publication.

Stone. C.M. 1997a. *Final Disposal Room Structural Response Calculations.* Sandia National Laboratories, Albuquerque, NM. SAND97-0795.

Stone, C.M. 1997b. *SANTOS-A Two-Dimensional Finite Element Program for the Quasistatic, Large Deormation, Inelastic Response of Solids.* Sandia National Laboratories, Albuquerque, NM. SAND90-0543.

Teeter, A.M. 1987. *Alcatraz Disposal Site Investigation. Report 3: San Francisco Bay-Alcatraz Disposal Site Erodibility.* Miscellaneous Paper HL-86-1. Department of the Army. Waterways Experimental Station, Corps of Engineers, Vicksburg, MS. AD Number A181837. ERMS 545820.

Tierney, M.S. 1996. Distributions. Sandia National Laboratories, Carlsbad, NM. ERMS 235268.

Trovato, E.R. 1997a. Letter to G. Dials (DOE), April 17. Office of Air and Radiation, U.S. Environmental Protection Agency, Washington, D.C. Docket A-93-02, II-I-25.

Trovato, E.R. 1997b. Letter to G. Dials (DOE), April 25. Office of Air and Radiation, U.S. Environmental Protection Agency, Washington, D.C. Docket A-93-02, II-I-27.

Wang, Y. 1997. Estimate WIPP waste particle sizes based on expert elicitation results: revision 1. Memorandum to M.S.Y. Chu and M.G. Marietta, Aug 5, 1997. Sandia National Laboratories, Albuquerque, NM. ERMS 246936.

Wang, Y. and K.W. Larson. 1997. Estimate waste critical shear stress for WIPP PA caving model. Sandia Memorandum to M.S.Y. Chu and M.G. Marietta, June 27, 1997. Sandia National Laboratories, Albuquerque, NM. ERMS 246696.

WIPP PA (WIPP Performance Assessment). 2003a. *Verification and Validation Plan/Validation Document for SANTOS 2.1.7.* Sandia National Laboratories, Carlsbad, NM. ERMS 530091.

WIPP PA (WIPP Performance Assessment). 2003b. *Design Document for BRAGFLO Version 5.0.* Sandia National Laboratories, Carlsbad, NM. ERMS 525700.

WIPP PA (WIPP Performance Assessment). 2004a. *Design Document for CUTTINGS_S (Version 6.00).* Sandia National Laboratories, Carlsbad, NM. ERMS 537038.

WIPP PA (WIPP Performance Assessment). 2004b. *User's Manual for CUTTINGS_S (Version 6.00).* Sandia National Laboratories, Carlsbad, NM. ERMS 537039.

WIPP PA (WIPP Performance Assessment). 2005a. *Addendum to the Design Document for CUTTINGS_S (Version 6.00).* Sandia National Laboratories, Carlsbad, NM. ERMS 539236.

WIPP PA (WIPP Performance Assessment). 2005b. *Addendum to the User's Manual for CUTTINGS_S (Version 6.00).* Sandia National Laboratories, Carlsbad, NM. ERMS 539238.

APPENDIX A: SANTOS Input Files

A-1   FASTQ Input file

```
TITLE
DISPOSAL ROOM MODEL - Volume Change of Waste with Time
POINT    1      0.00      -54.19
POINT    2     20.27      -54.19
POINT    3      0.00       -8.63
POINT    4     20.27       -8.63
POINT    5      0.00       -8.63
POINT    6     20.27       -8.63
POINT    7      0.00       -7.77
POINT    8     20.27       -7.77
POINT    9      0.00       -6.39
POINT   10      5.03       -6.39
POINT   11      0.00       -6.39
POINT   12      3.675      -6.39
POINT   13      0.00       -3.71
POINT   14      3.675      -3.71
POINT   15      5.03       -2.43
POINT   16      0.00       -2.43
POINT   17      0.00        0.00
POINT   18     20.27        0.00
POINT   19      0.00        4.27
POINT   20     20.27        4.27
POINT   21      0.00       52.87
POINT   22     20.27       52.87
POINT   23     20.27       -2.43
POINT   24     20.27       -6.39
POINT   25      5.03        0.00
POINT   26      5.03       -7.77
POINT   27      5.03        4.27
POINT   28      5.03       -8.63
POINT   29      0.0         2.10
POINT   30      5.03        2.10
POINT   31     20.27        2.10
POINT   32      0.0         2.31
POINT   33      5.03        2.31
POINT   34     20.27        2.31
LINE     1      STR    1     2    0    22    1.0
LINE     2      STR    1     5    0    20    0.85
LINE     3      STR    2     6    0    20    0.85
$LINE    4      STR    5     6    0    15
LINE     5      STR   28     6    0    15    1.1
LINE     6      STR    5     7    0     4
LINE     7      STR    6     8    0     4
LINE     8      STR    7     9    0     5
LINE     9      STR   26     8    0    15    1.1
LINE    10      STR   24     8    0     5
LINE    11      STR   10    24    0    15    1.1
LINE    12      STR    9    10    0     7    0.8
LINE    13      STR   11    12    0    10
LINE    14      STR   12    14    0     7
LINE    15      STR   13    14    0    10
LINE    16      STR   11    13    0     7
```

```
LINE    17      STR   10    15    0    12
LINE    18      STR   24    23    0    12
LINE    19      STR    8    18    0    12
LINE    20      STR   16    17    0     7
LINE    21      STR   16    15    0     7    0.8
LINE    22      STR   15    23    0    15    1.1
LINE    23      STR   18    23    0     7
LINE    24      STR   25    18    0    15    1.1
LINE    25      STR   17    19    0     8
LINE    26      STR   18    20    0     8
LINE    27      STR   27    20    0    15    1.1
$LINE   28      STR   25    20    0     8
LINE    29      STR   19    21    0    20    1.15
LINE    30      STR   20    22    0    20    1.15
LINE    31      STR   21    22    0    22    1.0
LINE    32      STR   17    25    0     7    0.8
LINE    33      STR   19    27    0     7    0.8
LINE    34      STR    7    26    0     7    0.8
LINE    35      STR    5    28    0     7    0.8
LINE    36      STR   17    29    0     4
LINE    37      STR   18    31    0     4
LINE    38      STR   29    30    0     7    0.8
LINE    39      STR   30    31    0    15    1.1
LINE    40      STR   29    32    0     1
LINE    41      STR   31    34    0     1
LINE    42      STR   32    33    0     7    0.8
LINE    43      STR   33    34    0    15    1.1
LINE    44      STR   32    19    0     4
LINE    45      STR   34    20    0     4
SIDE   100      11    12
SIDE   101      21    22
SIDE   102      32    24
SIDE   103      33    27
SIDE   104      35     5
SIDE   105      34     9
SIDE   106      38    39
SIDE   107      42    43
$ NODEBC CARDS
NODEBC   2      1
NODEBC   1      2     6     8    16    20    36    40    44    29
NODEBC   1      3     7    10    18    23    37    41    45    30
$ SIDEBC CARDS
SIDEBC  10     31
SIDEBC  20      1     $ added by B.Y. Park 9/25/2003
SIDEBC 100     12
SIDEBC 200     17
SIDEBC 300     21
SIDEBC 400     13
SIDEBC 500     14
SIDEBC 600     15
SIDEBC 700     12    17    21
SIDEBC 800     13    14    15 $ Added by B.Y. Park 2/6/2007
$ REGION CARDS
REGION   1      1    -1    -3   104    -2
REGION   2      2   104    -7   105    -6
REGION   3      1   105   -10   100    -8
REGION   4      1   -11   -18   -22   -17
```

```
REGION    5     1   101   -23   102   -20
REGION    6     3   102   -37   106   -36
REGION    7     1   103   -30   -31   -29
REGION    8     4   -13   -14   -15   -16
REGION    9     2   106   -41   107   -40
REGION   10     3   107   -45   103   -44
SCHEME    P
EXIT
```

A-2   Sample SANTOS Input File

```
TITLE
Volume Change Calculation for Waste: f=0.0
PLANE STRAIN
INITIAL STRESS = USER
GRAVITY = 1 = 0. = -9.79 = 0.
PLOT ELEMENT, STRESS, STRAIN, VONMISES, PRESSURE
PLOT NODAL, DISPLACEMENT, RESIDUAL
PLOT STATE, EQCS, EV
RESIDUAL TOLERANCE = 0.5
MAXIMUM ITERATIONS = 1000
MAXIMUM TOLERANCE = 100.
INTERMEDIATE PRINT = 100
ELASTIC SOLUTION
PREDICTOR SCALE FACTOR = 3
AUTO STEP .015 2.592E6 NOREDUCE 1.E-5
TIME STEP SCALE = 0.5
HOURGLASS STIFFENING = .005
STEP CONTROL
500 3.1536e7
2000 3.1536e9
36000 3.1536e11
END
OUTPUT TIME
1 3.1536e7
1 3.1536e9
200 3.1536e11
END
PLOT TIME
10 3.1536e7
100 3.1536e9
120 3.1536e11
END
MATERIAL, 1, M-D CREEP MODEL, 2300. $ ARGILLACEOUS HALITE
TWO MU = 24.8E9
BULK MODULUS = 20.66E9
A1 = 1.407E23
Q1/R = 41.94
N1 = 5.5
B1 = 8.998E6
A2 = 1.314E13
Q2/R = 16.776
N2 = 5.0
B2 = 4.289E-2
SIG0 = 20.57E6
QLC = 5335.
M = 3.0
K0 = 2.47E6
C = 2.759
ALPHA = -14.96
BETA = -7.738
DELTLC = .58
RN3 = 2.
AMULT = .95
```

```
END
MATERIAL, 2, SOIL N FOAMS, 2300. $ ANHYDRITE
TWO MU = 5.563E10
BULK MODULUS = 8.3444E10
A0 = 2.338e6
A1 = 2.338
A2 = 0.
PRESSURE CUTOFF = 0.0
FUNCTION ID = 0
END
MATERIAL, 3, M-D CREEP MODEL, 2300. $ PURE HALITE
TWO MU = 24.8E9
BULK MODULUS = 20.66E9
A1 = 8.386E22
Q1/R = 41.94
N1 = 5.5
B1 = 6.086E6
A2 = 9.672E12
Q2/R = 16.776
N2 = 5.0
B2 = 3.034E-2
SIG0 = 20.57E6
QLC = 5335.
M = 3.0
K0 = 6.275E5
C = 2.759
ALPHA = -17.37
BETA = -7.738
DELTLC = .58
RN3 = 2.
AMULT = .95
END
MATERIAL, 4, SOIL N FOAMS, 559.5
TWO MU = 6.666E8
BULK MODULUS = 2.223E8
A0 = 1.0e6
A1 = 3.
A2 = 0.
PRESSURE CUTOFF = 0.
FUNCTION ID = 2
END
NO DISPLACEMENT X = 1
NO DISPLACEMENT Y = 2
PRESSURE, 10, 1, 13.57E6
CONTACT SURFACE, 100, 400, 0., 1.E-3, 1.E40
CONTACT SURFACE, 200, 500, 0., 1.E-3, 1.E4
CONTACT SURFACE, 300, 600, 0., 1.E-3, 1.E4
CONTACT SURFACE, 300, 200, 0., 1.E-3, 1.E4
CONTACT SURFACE, 100, 200, 0., 1.E-3, 1.E4
ADAPTIVE PRESSURE, 700, 1.e-6, -6.4
FUNCTION,1 $ FUNCTION TO DEFINE PRESCRIBED PRESSURE
0., 1.
3.1536e11, 1.
END
FUNCTION,2
0.0000, 0.0000
0.5101, 1.5300E6
```

```
0.6314, 2.0307E6
0.7189, 2.5321E6
0.7855, 3.0312E6
0.8382, 3.5301E6
0.8808, 4.0258E6
0.9422, 4.9333E6
1.1400, 12.000E6
END
FUNCTION = 3
0.  0.5
3.1536E11 1.
END
EXIT
```

A-3   Sample Subroutine INITST

```
      SUBROUTINE INITST( SIG,COORD,LINK,DATMAT,KONMAT,SCREL )
C
C  ***********************************************************************
C
C   DESCRIPTION:
C     THIS ROUTINE PROVIDES AN INITIAL STRESS STATE TO SANTOS
C
C   FORMAL PARAMETERS:
C     SIG        REAL        ELEMENT STRESS ARRAY WHICH MUST BE RETURNED
C                            WITH THE REQUIRED STRESS VALUES
C     COORD      REAL        GLOBAL NODAL COORDINATE ARRAY
C     LINK       INTEGER     CONNECTIVITY ARRAY
C     DATMAT     REAL        MATERIAL PROPERTIES ARRAY
C     KONMAT     INTEGER     MATERIAL PROPERTIES INTEGER ARRAY
C
C   CALLED BY: INIT
C
C  ***********************************************************************
C
      INCLUDE 'precision.blk'
      INCLUDE 'params.blk'
      INCLUDE 'psize.blk'
      INCLUDE 'contrl.blk'
      INCLUDE 'bsize.blk'
      INCLUDE 'timer.blk'
C
      DIMENSION LINK(NELNS,NUMEL),KONMAT(10,NEMBLK),COORD(NNOD,NSPC),
     *          SIG(NSYMM,NUMEL),DATMAT(MCONS,*),SCREL(NEBLK,*)
C
      DO 1000 I = 1,NEMBLK
         MATID = KONMAT(1,I)
         MKIND = KONMAT(2,I)
         ISTRT = KONMAT(3,I)
         IEND = KONMAT(4,I)
            DO 500 J = ISTRT,IEND
               II = LINK( 1,J )
               JJ = LINK( 2,J )
               KK = LINK( 3,J )
               LL = LINK( 4,J )
               ZAVG = 0.25 * ( COORD(II,2) + COORD(JJ,2) + COORD(KK,2) +
     *               COORD(LL,2) )
               STRESS = - 2300. * 9.79 * ( 655. - ZAVG )
               IF( MATID .EQ. 4 )THEN
                   STRESS = 0.
               END IF
               SIG(1,J) = STRESS
               SIG(2,J) = STRESS
               SIG(3,J) = STRESS
               SIG(4,J) = 0.0

 500          CONTINUE
1000 CONTINUE
      RETURN
```

END

A-4 Sample Subroutine FPRES

```
      SUBROUTINE FPRES( VOLUME,TIME,PGAS )
C ....
C .... THE PRESSURE IS COMPUTED ON THE BASIS OF THE IDEAL GAS LAW,
C .... PV = NRT. THE TOTAL NUMBER OF MOLES OF GAS, N (EN), PRESENT
C .... AT ANY TIME IS DETERMINED ON THE BASIS OF A CONSTANT RATE OF GAS
C .... GENERATION. R IS THE UNIVERSAL GAS CONSTANT AND THETA IS THE ROOM
C .... TEMPERATURE, 300 K. V IS THE CURRENT VOLUME OF THE ROOM. THE VOLUME
C .... MUST BE CORRECTED BY MULTIPLYING BY 2 OR 4 TO ACCOUNT FOR THE USE OF
C .... HALF OR QUARTER-SYMMETRY MODELS. THE VOLUME MUST ALSO BE MULTIPLIED
C .... BY A FACTOR TO ACCOUNT FOR 3D LENGTH.
C ....
C
      INCLUDE 'precision.blk'
C
      R = 8.314
      THETA = 300.
C
      IF( TIME .LT. 1.7325E10 )THEN
          PVALUE = 0.0
          RATE = 4.32E-4
          TSTAR = 0.0
      ELSE IF( TIME .LT. 3.3075E10 )THEN
          PVALUE = 7.48E6
          RATE = 2.16E-4
          TSTAR = 1.7325E10
      ELSE
          PVALUE = 1.0886e7
          RATE = 0.0
          TSTAR = 0.0
      END IF
C
C .... CORRECT VOLUME AT THIS TIME TO GET VOLUME OF VOIDS
C
      EN = PVALUE + RATE * ( TIME - TSTAR )
C     SCALE = 0.0
      SCALE = 0.0
      SYMFAC = 2.
      XLENG = 91.44
C
C .... THIS MODIFICATION REMOVES THE BACKFILL FROM VSOLID
C
C VSOLID FOR WASTE AND DRUMS ONLY 551.2
      VSOLID = 551.2
      VOLUME = SYMFAC * VOLUME * XLENG - VSOLID
      IF( VOLUME .LE. 0.0 )VOLUME = 1.
C
      PGAS = SCALE * EN * R * THETA / VOLUME
C
      RETURN
      END
```

A-5   NUMBERS Input File

```
planar
cavity 800 center 0.0 -4.41
exit
```

A-6 AWK Script to Calculate the Porosity Change in the Waste with Time

```
#
# This awk script computes the porosity and void change in the waste
# as a function of time (Based upon SANTOS output)
#
BEGIN {
  length_wast = 87.85           # Park and Holland, 2003, App.A-4
  height_wast = 2.676           # Park and Holland, 2003, Fig.9
  width_half_wast = 3.675       # Park and Holland, 2003, Fig.9
  area_half_wast = height_wast * width_half_wast
  dens_ws = 1757.       # Solid waste density (SAND97-0795, p.11)
  dens_w  = 559.5       # Initial waste density (SAND97-0795, p.11)
  vol_wast = 1728.            # Initial waste volume (= 87.85*2.676*7.35
(L*H*W))
  mass_ws = dens_w*vol_wast
  ratio = dens_w/dens_ws
}
{
  if ( $1 ~/[0-9]/ ) {
    nor_fac = area_half_wast/-9.849E+00
    half_sec = $2*nor_fac
    vol_ratio = area_half_wast/half_sec   # = (initial waste area)/(deformed
wast area)
    poro = 1. - ratio*vol_ratio
    changed_vol_wast = 2.*half_sec*length_wast
    void = poro*changed_vol_wast
    tim_yrs = $1/31540000
    print $1, poro, tim_yrs, void, half_sec
  }
}
```

A-7 Lists of Files Used in SANTOS Calculations Under CVS Run Control

All files used in the present analysis are stored in a repository on the workstation elo.sandia.gov in /data/CVSLIB/SANTOS_Analysis/Tests. The present analysis is named "ClaySeamG."

A complete listing of the log files can be checked out from the CVS library /nfs/data/CVSLIB/ SANTOS_Analysis/ Tests/RunControl/LogFiles/ClaySeamG using the command:

```
cvs -d $CVSLIB/SANTOS_Analysis co Tests/RunControl
/LogFiles/ClaySeamG
```

Note that there is a space before /LogFiles/ClaySeamG which should not be included on the command line. It is only there for formatting in this document.

Similarly, the input and output files from this analysis can be checked out from the CVS library using the commands:

```
cvs -d $CVSLIB/SANTOS_Analysis co Tests/Input/ClaySeamG
```

```
cvs -d $CVSLIB/SANTOS_Analysis co Tests/Output/ClaySeamG
```

Summary of Files Used – Entire Analysis

Table A-1. The command input file used in the entire analysis was:

File	Repository	Comment
Tests/RunControl/ClaySeamG /RS_Santos_Compile.inp	ACCESS_Warthog	Input file to ReadScript.py

Table A-2. The input files used in the entire analysis were:

File	Repository	Comment
lib/libnemIf.a	ACCESS_Warthog	Library used in the compilation of SANTOS
lib/libexoIIv2c.a	ACCESS_Warthog	Library used in the compilation of SANTOS
ACCESS/analysis/santos.exe/bsize.blk	ACCESS_Warthog	Include file for SANTOS subroutine compilation
lib/libsuplib.a	ACCESS_Warthog	Library used in the compilation of SANTOS
lib/libnetcdf.a	ACCESS_Warthog	Library used in the compilation of SANTOS
lib/libexoIIv2for.a	ACCESS_Warthog	Library used in the compilation of SANTOS
ACCESS/analysis/santos.exe/psize.blk	ACCESS_Warthog	Include file for SANTOS subroutine compilation
Tests/Input/ClaySeamG/initst.f	SANTOS_Analysis	Initial pressure subroutine
ACCESS/analysis/santos.exe /precision.blk	ACCESS_Warthog	Include file for SANTOS subroutine compilation

lib/libsupesdp.a	ACCESS_Warthog	`Library used in the compilation of SANTOS`
lib/libnemIc.a	ACCESS_Warthog	`Library used in the compilation of SANTOS`
ACCESS/analysis/santos.exe/timer.blk	ACCESS_Warthog	`Include file for SANTOS subroutine compilation`
ACCESS/analysis/santos.exe/params.blk	ACCESS_Warthog	`Include file for SANTOS subroutine compilation`
etc/ex1ex2v2	ACCESS_Warthog	Script that converts Exodus I files to Exodus II files
bin/santos.exe.o	ACCESS_Warthog	Santos main program object file
lib/libsantos.exe.a	ACCESS_Warthog	`Library used in the compilation of SANTOS`
Tests/Input/ClaySeamG/0.00up.g	SANTOS_Analysis	The mesh file
ACCESS/analysis/santos.exe/contrl.blk	ACCESS_Warthog	`Include file for SANTOS subroutine compilation`

Table A-3. The libraries used in the entire analysis were:

File		Comment
ACCESS_Warthog		Santos code and utilities
SANTOS_Analysis		Results of the analyses

Table A-4. The log file used in the entire analysis was:

File	Repository	Comment
Tests/RunControl/LogFiles/ClaySeamG /RS_Santos_Compile.log	SANTOS_Analysis	ReadScript.py log file

Table A-5. The output files used in the entire analysis were:

File	Repository	Comment
Tests/Output/ClaySeamG/santos.exe	SANTOS_Analysis	SANTOS executable that uses subroutine supplied
Tests/RunControl/LogFiles/ClaySeamG /RS_Santos_Compile.rtf	SANTOS_Analysis	Formatted version of ReadScript.py log file
Tests/Output/ClaySeamG/clayg.g	SANTOS_Analysis	Converted mesh file

Table A-6. The executable files used in the entire analysis were:

File	Repository	Comment
None		

Summary of Files Used in Part 1

Table A-7. The command input file used in Part 1 was:

File	Repository	Comment
Tests/RunControl/ClaySeamG /RS_Santos_Part1.inp	SANTOS_Analysis	Input file to ReadScript.py

Table A-8. The input files used in Part 1 were:

File	Repository	Comment
Tests/Output/ClaySeamG/santos.exe	SANTOS_Analysis	Executable file
bin/numbers2	ACCESS_Warthog	Calculates properties of an EXODUS data file
Tests/Input/ClaySeamG/num_curr.inp	SANTOS_Analysis	Numbers input file
bin/numbers.exe	ACCESS_Warthog	Calculates properties of an EXODUS data file (code)
Tests/Output/ClaySeamG/clayg.g	SANTOS_Analysis	
Tests/Input/ClaySeamG /poro_void_wast.awk	SANTOS_Analysis	gawk input file
bin/santos.exe.o	ACCESS_Warthog	SANTOS object file
Tests/Input/ClaySeamG/clayg.i	SANTOS_Analysis	Santos input file

Table A-9. The libraries used in Part 1 were:

File		Comment
ACCESS_Warthog		
SANTOS_Analysis		

Table A-10. The log file used in Part 1 was:

File	Repository	Comment
Tests/RunControl/LogFiles/ClaySeamG /RS_Santos_Part1.log	SANTOS_Analysis	ReadScript.py log file

Table A-11. The output files used in Part 1 were:

File	Repository	Comment
Tests/Output/ClaySeamG/poro_void_0p2.dat	SANTOS_Analysis	Data file of results
Tests/Output/ClaySeamG/clayg0p2.o	SANTOS_Analysis	Output file from numbers
Tests/Output/ClaySeamG/poro_void_0p0.dat	SANTOS_Analysis	Data file of results
Tests/RunControl/LogFiles/ClaySeamG /RS_Santos_Part1.rtf	SANTOS_Analysis	Formatted version of ReadScript.py log file
Tests/Output/ClaySeamG/clayg0p0.o	SANTOS_Analysis	Output file from numbers
Tests/Output/ClaySeamG/clayg0p1.o	SANTOS_Analysis	Output file from numbers
Tests/Output/ClaySeamG/poro_void_0p1.dat	SANTOS_Analysis	Data file of results

Table A-12. The executable file used in Part 1 was:

File	Repository	Comment
etc/numbers	ACCESS_Warthog	The NUMBERS script

Summary of Files Used in Part 2

Table A-13. The command input file used in Part 2 was:

File	Repository	Comment
Tests/RunControl/ClaySeamG/RS_Santos_Part2.inp	SANTOS_Analysis	

Table A-14. The input files used in Part 2 were:

File	Repository	Comment
None		Exported in Part 1

Table A-15. The libraries used in Part 2 were:

File		Comment
SANTOS_Analysis		

Table A-16. The log file used in Part 2 was:

File	Repository	Comment
Tests/RunControl/LogFiles/ClaySeamG /RS_Santos_Part2.log	SANTOS_Analysis	ReadScript.py log file

Table A-17. The output files used in Part 2 were:

File	Repository	Comment
Tests/Output/ClaySeamG/clayg0p6.o	SANTOS_Analysis	Output file from numbers
Tests/RunControl/LogFiles/ClaySeamG /RS_Santos_Part2.rtf	SANTOS_Analysis	Formatted version of ReadScript.py log file
Tests/Output/ClaySeamG/poro_void_0p6.dat	SANTOS_Analysis	Data file of results
Tests/Output/ClaySeamG/poro_void_0p8.dat	SANTOS_Analysis	Data file of results
Tests/Output/ClaySeamG/clayg0p8.o	SANTOS_Analysis	Output file from numbers
Tests/Output/ClaySeamG/poro_void_0p4.dat	SANTOS_Analysis	Data file of results
Tests/Output/ClaySeamG/clayg0p4.o	SANTOS_Analysis	Output file from numbers

Table A-18. The executable files used in Part 2 were:

File	Repository	Comment
None		

Summary of Files Used in Part 3

Table A-19. The command input file used in Part 3 was:

File	Repository	Comment
Tests/RunControl/ClaySeamG /RS_Santos_Part3.inp	SANTOS_Analysis	Input file to ReadScript.py

Table A-20. The input files used in Part 3 were:

File	Repository	Comment
None		

Table A-21. The libraries used in Part 3 were:

File		Comment
SANTOS_Analysis		

Table A-22. The log file used in Part 3 was:

File	Repository	Comment
Tests/RunControl/LogFiles/ClaySeamG /RS_Santos_Part3.log	SANTOS_Analysis	ReadScript.py log file

Table A-23. The output files used in Part 3 were:

File	Repository	Comment
Tests/Output/ClaySeamG/clayg1p2.o	SANTOS_Analysis	Output file from numbers
Tests/Output/ClaySeamG/poro_void_1p2.dat	SANTOS_Analysis	Data file of results
Tests/Output/ClaySeamG/clayg1p0.o	SANTOS_Analysis	Output file from numbers
Tests/Output/ClaySeamG/poro_void_1p0.dat	SANTOS_Analysis	Data file of results
Tests/RunControl/LogFiles/ClaySeamG /RS_Santos_Part3.rtf	SANTOS_Analysis	Formatted version of ReadScript.py log file

Table A-24. The executable files used in Part 3 were:

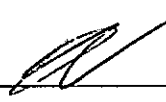| File	Repository	Comment
None		

APPENDIX B: Maximum Gas Generation Factor

Drum $\qquad$ $drum := 1$

Gas production potential
from anoxic corrosion: $\qquad$ $p_c := 1050 \dfrac{mole}{drum}$ $\qquad$ Butcher 1997, p. 19-20

Gas production potential
from microbial activity $\qquad$ $p_m := 550 \dfrac{mole}{drum}$ $\qquad$ Butcher 1997, p. 19-20

Total gas production potential $\qquad$ $p_t := p_c + p_m$ $\qquad$ $p_t = 1.6 \times 10^3 \dfrac{mole}{drum}$

Maximum moles of gas produced from PABC BRAGFLO results $\qquad$ Clayton 2007

In the entire repository $\qquad$ $m_{r.max} := 1.1586 \cdot 10^9 \, mole$

In a panel $\qquad$ $m_{p.max} := 1.5466 \cdot 10^8 \, mole$

Number of drums in room, ideal packing $\qquad$ $N_{D.r} := 6.804 \cdot 10^3$ $\qquad$ REFCON : DRROOM

Volume of a room $\qquad$ $V_{rm} := 3.644378 \cdot 10^3 \, m^3$ $\qquad$ REFCON : VROOM

Volume of a panel $\qquad$ $V_p := 4.609765 \cdot 10^4 \, m^3$ $\qquad$ REFCON : VPANLEX

Volume of repository $\qquad$ $V_{res} := 4.3840608 \cdot 10^5 \, m^3$ $\qquad$ REFCON : VREPOS

Number of rooms per panel $\qquad$ $N_{rm.p} := \dfrac{V_p}{V_{rm}}$ $\qquad$ $N_{rm.p} = 12.649$

Number of rooms in repository $\qquad$ $N_{rm.res} := \dfrac{V_{res}}{V_{rm}}$ $\qquad$ $N_{rm.res} = 120.297$

Number of drums in a panel $\qquad$ $ND_p := N_{rm.p} \cdot N_{D.r}$ $\qquad$ $ND_p = 8.606 \times 10^4 \, drum$

Number of drums in repository $\qquad$ $ND_{res} := N_{rm.res} \cdot N_{D.r}$ $\qquad$ $ND_{res} = 8.185 \times 10^5 \, drum$

Max gas generation factor in panel $\qquad$ $f_{max.p} := \dfrac{\dfrac{m_{p.max}}{ND_p}}{p_t}$ $\qquad$ $f_{max.p} = 1.123$

Max gas generation factor in repository $\qquad$ $f_{max.r} := \dfrac{\dfrac{m_{r.max}}{ND_{res}}}{p_t}$ $\qquad$ $f_{max.r} = 0.885$

Vugrin, Eric D 5/1/07

From:	Riggins, Michael
Sent:	Friday, April 27, 2007 7:22 AM
To:	Vugrin, Eric D
Cc:	Herrick, Courtney Grant; Lee, Moo; Chavez, Mario Joseph
Subject:	RE: Signature authority
Importance:	High

Eric,

I give signature authority to Eric Vugrin for documents pertaining to the paper "Recommendations for the Lower Limit of the Waste Shear Strength (Parameter BOREHOLE : TAUFAIL)".

Mike Riggins, PhD
Sandia Nat'l Labs
Org 6711 - WIPP PA
(505) 234-0066 Carlsbad
(512) 482-0008 Austin
(505) 284-2730 Albuquerque
mriggi@sandia.gov

From: Herrick, Courtney Grant
Sent: Thursday, April 26, 2007 3:56 PM
To: Riggins, Michael
Subject: Signature authority

Mike,

We you to send someone here signature authority for the paper we wrote: "Recommendation for the Lower Limit of the Waste Shear Strength (Parameter BOREHOLE : TAUFAIL)"

Courtney G Herrick
SNL - Carlsbad Programs Group
4100 National Parks Highway
Carlsbad, NM 88220
Telephone: (505) 234-0176
Fax: (505) 234-0061
e-mail: cgherri@sandia.gov

5/1/2007